AD-A033 067 NEVADA UNIV RENO LAB OF ATMOSPHERIC PHYSICS F/G 4/2
MEASUREMENT OF SIZE, CONCENTRATION AND STRUCTURE OF ATMOSPHERIC--ETC(U)
JUL 76 J HALLETT F19628-72-C-0280
UNCLASSIFIED AFGL-TR-76-0149 NL

1 OF 2
AD
A033067

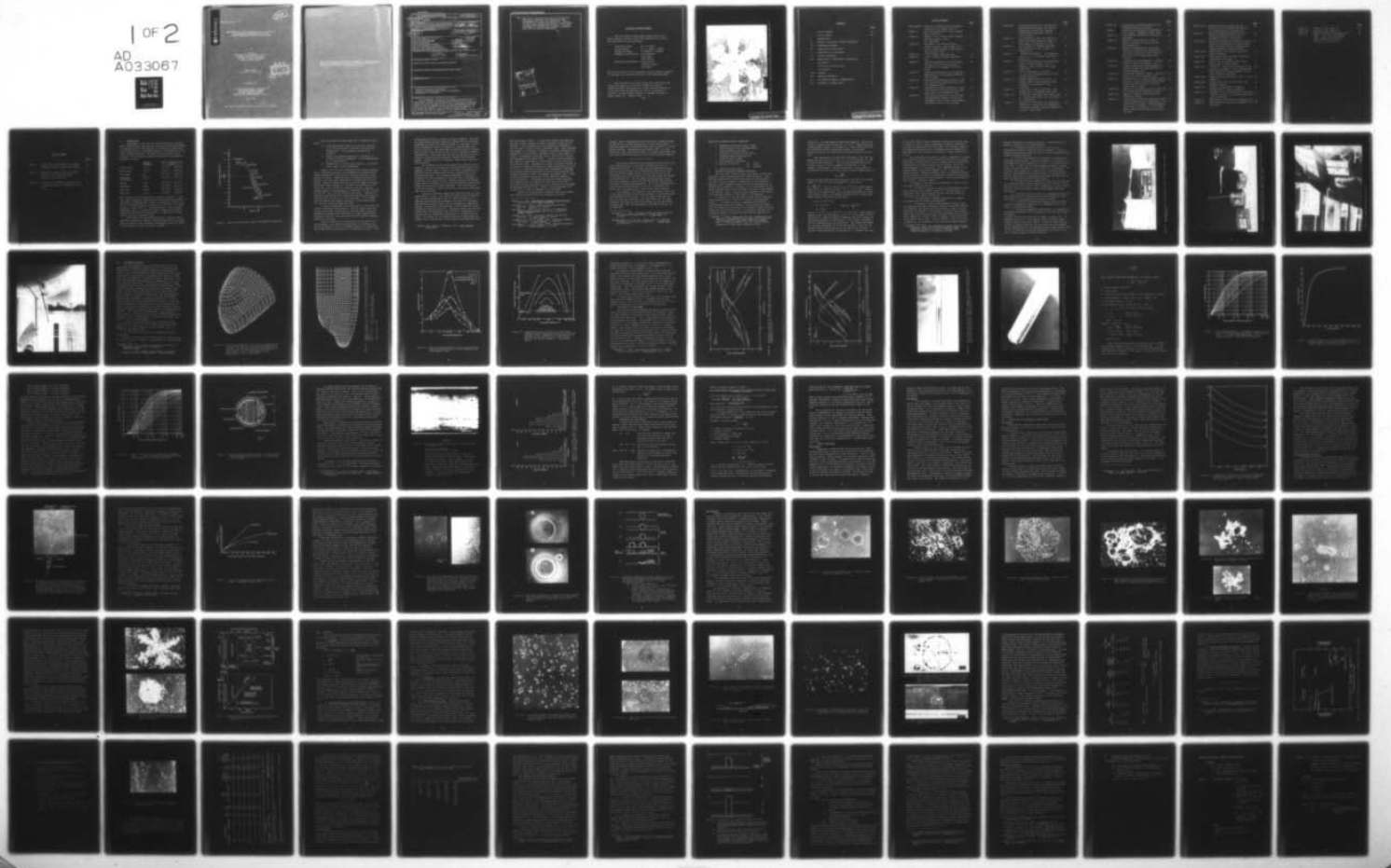

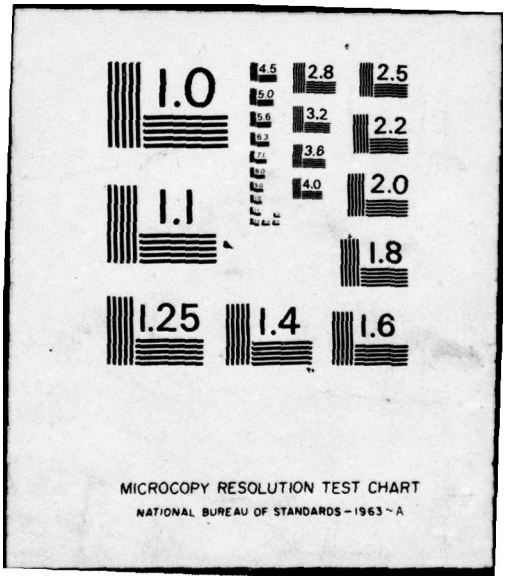
1.0
1.1
1.25
1.4
1.6
1.8
2.0
2.2
2.5
2.8
3.2
3.6
4.0
4.5
5.0
5.6
6.3
MICROCOPY RESOLUTION TEST CHART
NATIONAL BUREAU OF STANDARDS - 1963 - A

AD A033067

AFGL-TR-76-0149

MEASUREMENT OF SIZE, CONCENTRATION AND STRUCTURE OF ATMOSPHERIC PARTICULATES BY THE AIRBORNE CONTINUOUS PARTICLE REPLICATOR

by

J. Hallett
Laboratory of Atmospheric Physics
Desert Research Institute
University of Nevada System
Reno, Nevada 89507

DDC
RECEIVED
DEC 7 1976
C

FINAL REPORT
April 1972 - July 1976

Prepared For:

AIR FORCE GEOPHYSICS LABORATORY
AIR FORCE SYSTEMS COMMAND
UNITED STATES AIR FORCE
HANSCOM AFB, MASSACHUSETTS 01731

July 1976

Approved for public release; distribution unlimited

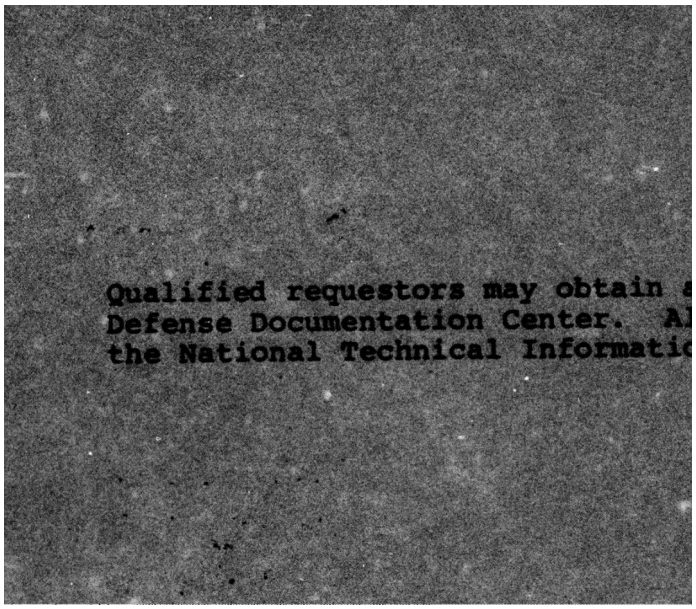
Qualified requestors may obtain
Defense Documentation Center.
the National Technical Informati

Unclassified

SECURITY CLASSIFICATION OF THIS PAGE (When Data Entered)

(19) REPORT DOCUMENTATION PAGE

READ INSTRUCTIONS BEFORE COMPLETING FORM

(18) 1. REPORT NUMBER: AFGL-TR-76-0149

2. GOVT ACCESSION NO.

3. RECIPIENT'S CATALOG NUMBER

(6) 4. TITLE (and Subtitle): MEASUREMENT OF SIZE, CONCENTRATION AND STRUCTURE OF ATMOSPHERIC PARTICULATES BY THE AIRBORNE CONTINUOUS PARTICLE REPLICATOR

(9) 5. TYPE OF REPORT & PERIOD COVERED: Final rept. Apr 72 - Jul 76

6. PERFORMING ORG. REPORT NUMBER

(10) 7. AUTHOR(s): J. Hallett

(15) 8. CONTRACT OR GRANT NUMBER(s): F19628-72-C-0280 New

9. PERFORMING ORGANIZATION NAME AND ADDRESS: University of Nevada Univ., Rano. Desert Research Institute Reno, Nevada 89507

(16) 10. PROGRAM ELEMENT, PROJECT, TASK AREA & WORK UNIT NUMBERS: 61102H 627A0001 (17) PP

11. CONTROLLING OFFICE NAME AND ADDRESS: Air Force Geophysics Laboratory Hanscom AFB, Massachusetts 01731 Contractor Monitor/Wilbur Paulsen/LYC

(11) 12. REPORT DATE: Jul 76

13. NUMBER OF PAGES: 106

14. MONITORING AGENCY NAME & ADDRESS (if different from Controlling Office)

(12) 105 p.

15. SECURITY CLASS. (of this report): Unclassified

15a. DECLASSIFICATION/DOWNGRADING SCHEDULE

16. DISTRIBUTION STATEMENT (of this Report)

Approved for public release; distribution unlimited.

17. DISTRIBUTION STATEMENT (of the abstract entered in Block 20, if different from Report)

6331F P13

18. SUPPLEMENTARY NOTES

19. KEY WORDS (Continue on reverse side if necessary and identify by block number)

Airborne Continuous Replicator
Cloud and Precipitation Particle Measurement
Atmospheric Ice Crystals

20. ABSTRACT (Continue on reverse side if necessary and identify by block number)

An assessment is made of the design characteristics of a continuous formvar cloud particle replicator for use on a pressurized aircraft such as the C130. Correction of measured replica particle concentrations is required depending on the siting of the instrument on the aircraft and the geometry of the collecting probe, to give free air concentration. A correction may also be required to the replica size to give → next page

DD FORM 1 JAN 73 1473 EDITION OF 1 NOV 65 IS OBSOLETE

Unclassified 407 747

SECURITY CLASSIFICATION OF THIS PAGE (When Data Entered)

20. the size of the particles prior to collection. Microscopy techniques for examination and photography of replica are described. Replica artifact results from coagulation, bounce, break-up and direct condensation of vapor. A simple technique is described for estimate of particle mass from the replica dimensions.

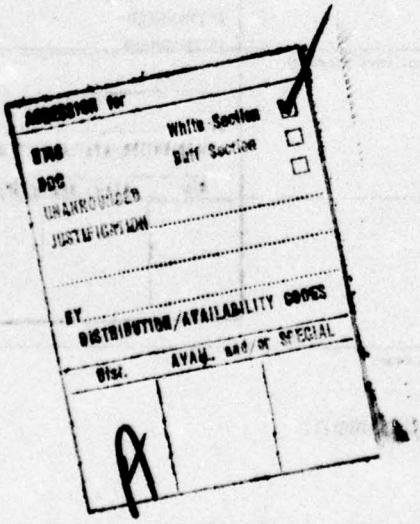

PERSONNEL ACKNOWLEDGEMENT

Over the course of this project many staff of the Desert Research Institute have been associated with design and construction of the instrument.

Electronic Design	- Dr. P. Wagner
Deicing Design	- Dr. D. Lamb, K. Gamara
Mechanical Design	- G. Keyser, R. Hanaway
Mechanical Construction	- Joe Calabrese
	John McKay
	Russ Sheltra
Electronic Construction	- Joe Dettling
	Clarence Fought
	Ted Spring

The overall success of the instrument and the projects in which it was used lies very much with their skill and enthusiasm.

Work relating to the early design of a continuous replicator was carried out in 1970-72 under Contract No. F19268-70-C-0279, and reported in "Design and Construction of a New Cloud Particle Replicator for use on a Pressurized Aircraft", by John Hallett, Richard W. Hanaway and Peter B. Wagner, Report No. AFCRL-72-0410.

753091

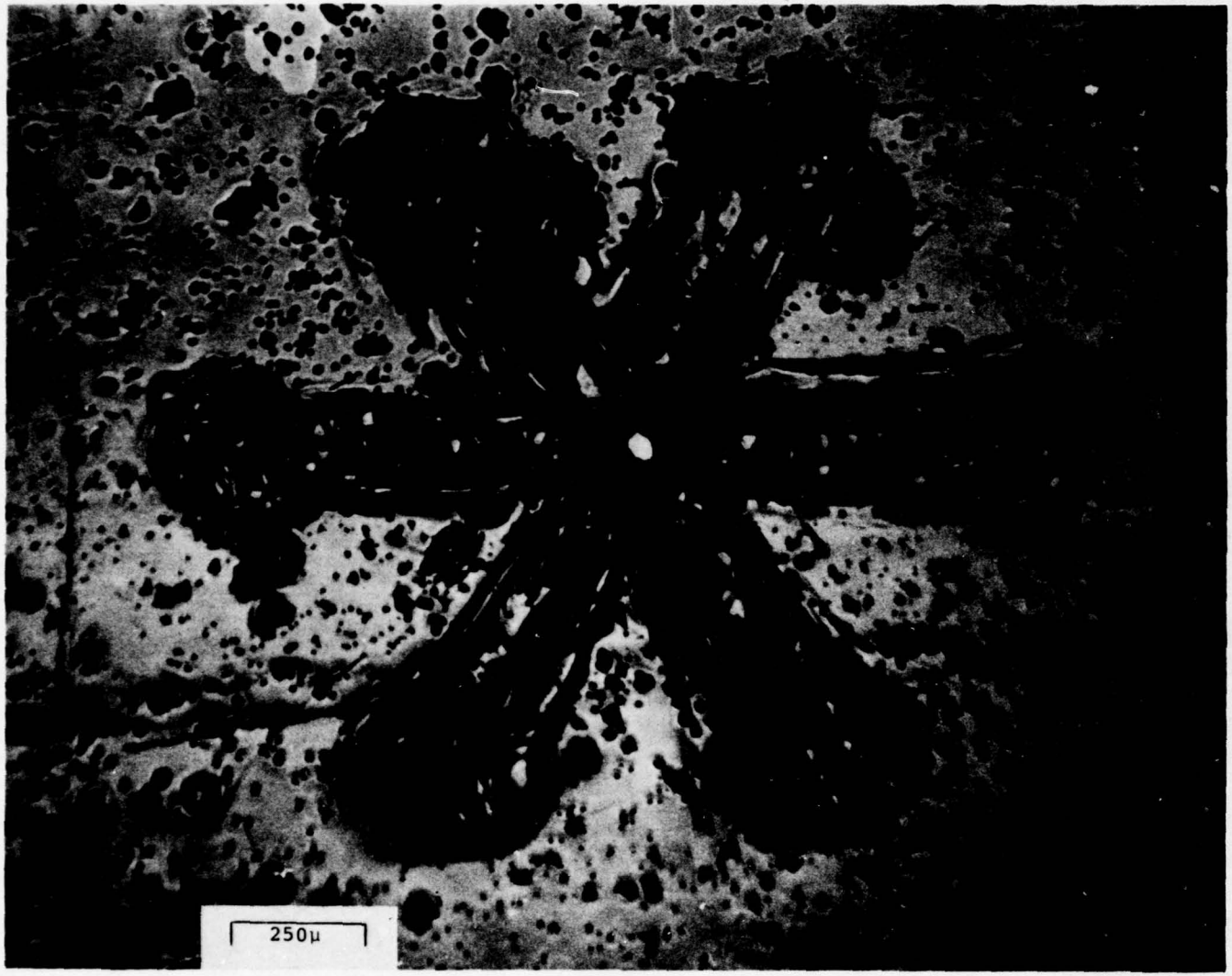

Frontispiece: Replica of a dendrite with end plates collected at air speed 120 m s^{-1}.

PRECEDING PAGE BLANK-NOT FILMED

CONTENTS

		Page
	LIST OF FIGURES	viii
	LIST OF TABLES	xiii
I.	INTRODUCTION	1
II.	DESIGN OF CONTINUOUS FORMVAR REPLICATOR	7
III.	INSTRUMENT EXPOSURE	15
IV.	COLLECTION OR CLOUD DROPS	20
V.	COLLECTION OF ICE CRYSTALS	34
VI.	OPTICAL TECHNIQUES	36
VII.	REPLICATION OF ATMOSPHERIC PARTICULATES	38
	The Replica	38
	Cloud Drops and Calibration	41
	Ice Crystals	49
VIII.	ARTEFACT	59
IX.	SAMPLING STATISTICS	71
X.	ICE PARTICLE REPLICA INTERPRETATION	75
XI.	ESTIMATE OF CRYSTAL MASS	81

PRECEDING PAGE BLANK-NOT FILMED

LIST OF FIGURES

		Page
Frontispiece.	Replica of a dendrite with end plates collected at air speed 120 m s^{-1}.	v
Figure 1.	Size and concentration range of atmospheric particles.	2
Figure 2a.	Replica (left), control panel (center) and power supply (right). "A" replicator.	11
Figure 2b.	Replicator (D,E) with TV camera linked to optics (right chassis top) and TV display mounted in same rack as control panel (left).	12
Figure 3a.	C-130A showing replicator arm.	13
Figure 3b.	C-130E showing extended replicator arm.	14
Figure 4a.	Computer-prepared plot of the digital description of the nose and cabin sections of the Lockheed C-130A airplane.	16
Figure 4b.	Computer-prepared plot of the digital description of the Lockheed C-130E forward fuselage.	17
Figure 5a.	Water drop concentration factors at and near the particle replicator slit from the Lockheed C-130A.	18
Figure 5b.	Concentration factor contours vs. water drop diameter along the particle replicator arm on the Lockheed C-130E.	19
Figure 6a.	Concentration factor vs. particle mass and melted drop diameter for various hydrometeor types at the C-130A formvar replicator slit at 5 kft altitude.	21

		Page
Figure 6b.	Concentration factor vs. particle mass and melted drop diameter for various hydrometeor types at the Lockheed C-130E formvar replicator slit at 5 kft altitude.	22
Figure 7a.	Ice accretion on rod 1 cm diameter exposed just behind observers' seat in front cabin, C-130A, May 12, 1970.	23
Figure 7b.	Ice collected on unheated replicator arm installed in C-130, flight 17, February 1971.	24
Figure 8.	ollection efficiency at stagnation point, $\theta = 0$, on cylinders with ideal fluid flow.	26
Figure 9.	Collection efficiency at the stagnation point of ideal cylinder, 3.5 cm diameter, under typical C-130 flight conditions.	27
Figure 10.	Total collection on a cylinder. $\phi = 1000$ to 3000 approximates to C-130 flight conditions.	29
Figure 11.	Section through collection slot. A slight inward airflow enables smaller droplets (5 μm diameter) to be collected.	30
Figure 12.	Collection of small cloud drops, wind tunnel test - 23 February 1973, AFGL.	32
Figure 13.	Collection of droplets, AFGL tunnel test. a. replica edge (about 10° half angle). b. Film center.	33
Figure 14.	Variation of viscosity of a mixture of formvar and chloroform with indicated % by weight of formvar and with temperature (after K. Pocs, AFGL).	40

		Page
Figure 15.	Interference microscope examination of thickness profile of replica.	42
Figure 16.	Distortion calibration with aspergillus niger spores. (MacReady & Todd, 1964).	44
Figure 17.	Drop replicas examined by interference microscopy.	46
Figure 18.	Spherical cloud drops in a layer of formvar solution (a) and the replica after drying (b).	47
Figure 19.	Schematic representation (from transmission and interference microscope) of the drying process of a 100 μm drop in a thick film of 5% formvar-chloroform solution.	48
Figure 20.	A cracked and uncracked plate. Cracking becomes evident for diameter > 100 μm.	50
Figure 21a.	A sector plate prior to development to a dendrite cracked on impact parallel to crystallographic axes.	51
Figure 21b.	Large plate cracked on impact. Cracks are parallel to crystallographic axes.	52
Figure 22.	Impact crater of a large irregular graupel particle. Particles showing flat crystal facets show some evidence of crystal growth from the vapor.	53
Figure 23a.	Replica of two dendrites grown on each end of a column which collapsed on impact.	54
Figure 23b.	Replica of spatial column formed by collapse on impact.	54
Figure 23c.	Interference microscope analysis of column replica showing that the center part is almost devoid of replica. The surrounding walls rise to a height of ∿ 20 μm, estimated from the fringe position on top of the wall.	55

		Page
Figure 24a,b.	Rimed dendrite and graupel particle. Drop size can be inferred from the size of irregularities on each particle.	57
Figure 25.	Replica characteristics for solid and liquid precipitation particles at collection velocity $\sim$ 120 m s^{-1}.	58
Figure 26a.	Ice crystal growth from solution on frozen droplets and fractured ice crystal particles; some drops did not freeze and show complete absence of crystal growth.	61
Figure 26b,c.	Other forms of ice crystal growth from formvar solution.	62
Figure 27a.	Bounce crater left by column revealed by interference microscopy.	63
Figure 27b.	Shape of an ice crystal bounce crater, showing gently sloping walls.	63
Figure 28.	Occasional association of drop pairs or triplets of diameter $\sim$ 30 μm suggests that they formed from a drop diameter $\sim$ 40 μm which divided on impaction.	64
Figure 29a.	Radial splash pattern from a drop $\sim$ 1.0 mm diameter.	65
Figure 29b.	Higher impact velocity gives more catastrophic breakup.	65
Figure 30.	Summary of crater/drop calibration. Deformed drop or replica diameter.	69
Figure 31.	Fragments of an ice crystal and cloud drops "rafting" by motion in a thick formvar film after collection.	71
Figure 32.	Replication of particles of different sizes.	77
Figure 33.	Mass-diameter relation for atmospheric ice particles.	85

		Page
Figure 34.	Overlay (1) for Figure 33.	86
Figure 35.	Overlay (2) for Figure 33.	87
Figure 36.	Mass-size relation from Wyoming and Japan data (R.C. Cunningham, AFGL, private communication). Overlay (3) for Figure 33.	89

LIST OF TABLES

		Page
TABLE I.	Splash Index (Weber Number) and Impact Reynolds' Number for water and formvar.	67
TABLE II.	Approximate sample volume and flight path per 16 mm film frame under typical flight conditions.	72
TABLE III.	Probability of finding n particles with the average number of particles, a, per frame.	74

I. INTRODUCTION

Measurement of the size and mass distribution of atmospheric particulates, their spatial concentration and their shape is required both for understanding of precipitation mechanisms and for application to problems relating to the operation of aircraft and space vehicles. The spatial concentration of particles in the atmosphere extends over many orders of magnitude depending on size:

	Typical Diameter	Typical Concentration in Air	
Aitken nuclei	.01 μm	10^{3} cm^{-3}	(10^{9} m^{-3})
Cloud drops	20 μm	10^{2} cm^{-3}	(10^{8} m^{-3})
Rain drops	mm	10^{-4} cm^{-3}	(10^{2} m^{-3})
Individual Ice Crystals	100 μm	10^{-2} cm^{-3}	(10^{4} m^{-3})
Graupel	2 mm	10^{-4} cm^{-3}	(10^{2} m^{-3})
Snowflakes	5 mm	10^{-4} cm^{-3}	(10^{2} m^{-3})
Small Hail	10 mm	10^{-9} cm^{-3}	($10^{-3}m^{-3}$)
Large Hail	10 cm	$10^{-12}cm^{-3}$	($10^{-6}m^{-3}$)

The variabilities of concentration is shown in Figure 1. This wide range of particle concentrations highlights the problems of measurement instrumentation. There is a practical limit in observing a concentration of one particle in 10^{-9} m^{-3} - an Aitken nucleus, to one in 10^{6} m^{3} - a large hailstone - with a single instrument; there is a practical limit in sampling sufficient numbers of particles over the whole size range to give a meaningful statistical representation.

The solution of this problem has been to employ several different instruments capable of sampling particles in a limited range of volumes, each instrument overlapping in part the range of that measuring larger and smaller volumes.

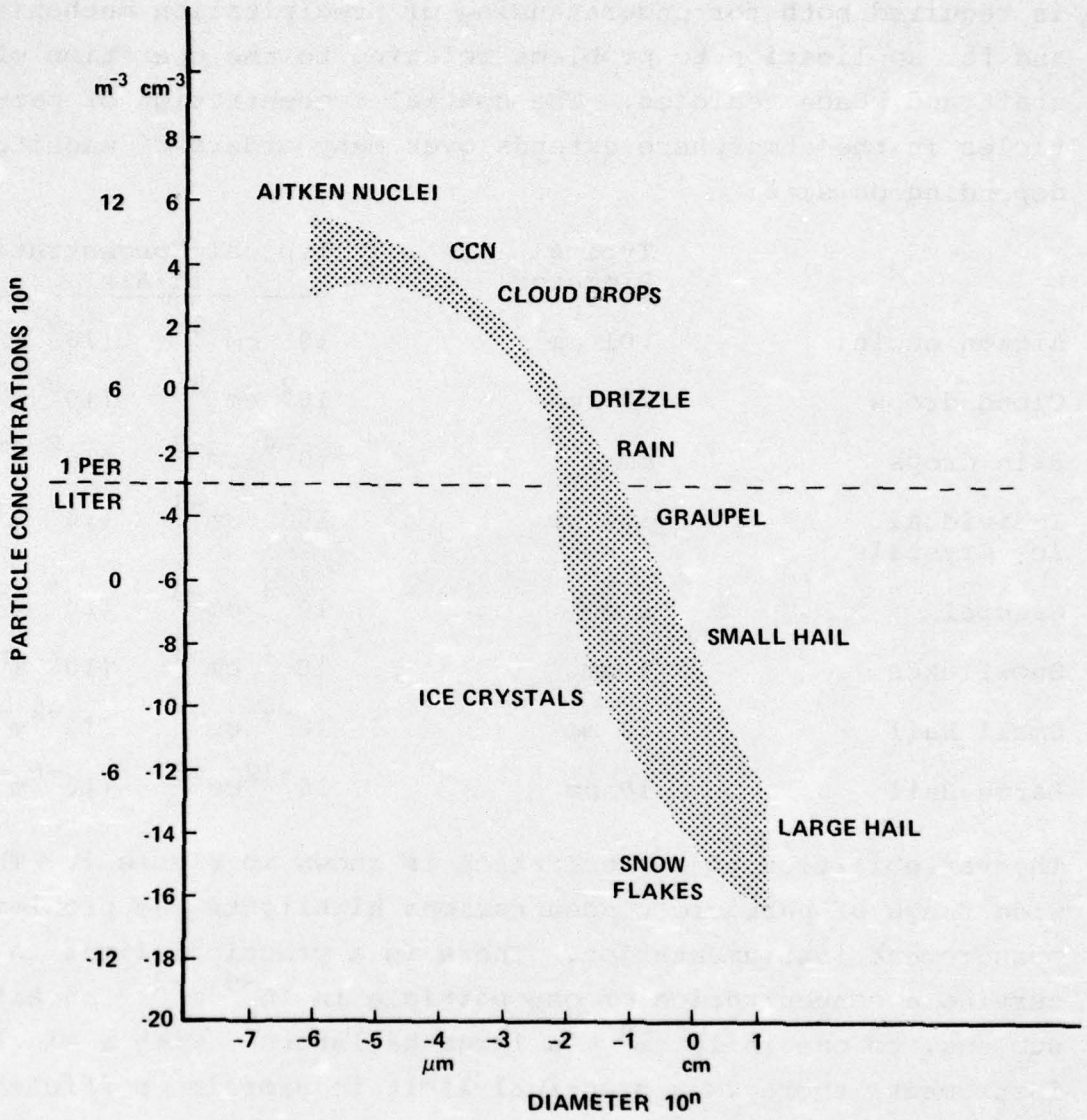

Figure 1. Size and concentration range of atmospheric particles.

Three principles have been employed in sampling instruments:

(1) Instruments which sweep out a definite volume of air in the horizontal, collecting all particles sequentially - as an impactor carried by an aircraft.

(2) Almost instantaneous sampling of a sequence of volumes by optical techniques - direct photography, or an optical array.

(3) Sedimentation on a horizontal surface - an exposed filter paper collects raindrops.

Ideally, the first two techniques give volume concentration of particles directly; the sedimentation technique gives volume concentration only when the terminal velocity of each particle is known. Sampling areas or volumes are selected depending on the size and concentration of particles to be examined. Impactor systems carried at aircraft speeds have used microscope slides, areas 10 to 100 mm^2, for collecting cloud drops; foil areas 10^4 mm^2 for graupel particles. Optical systems examine, instantaneously, volumes mm^3, 10^3 mm^3, 10^5 mm^3 for aerosol, cloud and precipitation particles. Sedimentation systems, at ground surface, collect precipitation particles on areas 100 mm^2 (drizzle) to 1.0 m^2 (hail pad). It is evident that the spatial and temporal resolution required must enter the choice of areas and sampling times.

A further fundamental difference exists in the detail obtained in recording each particle. Optical systems give concentration and some information on size and shape; collection systems give concentration and detail of shape together with permanent retention of non-volatile materials should subsequent analysis be required.

From the viewpoint of investigation of ice particles in the atmosphere, the significant advantage of collection over optical techniques is that a permanent replica of the particle may be made which gives detail of its physical structure. This

is much more difficult to obtain by optical methods. The optical array sensors produce electrical signals which are readily processed and reduce the analysis effort to a minimum; in contrast considerable effort is required in reducing data from direct collection. The techniques of optical detection systems and continuous replication of particles are therefore somewhat complementary in the sense that the bulk of the optical data is subject to rapid digital processing, whereas the continuous replica, although tedious in analysis, gives crystal and calibration detail.

The information which is obtained from collection techniques is limited by two practical considerations which will be examined in detail later. First, the volume concentration of particles must be deduced from the area concentration of the collected particles - this requires knowledge of collection efficiency of both instrument and aircraft and a knowledge of airspeed at the collection site. Second, particles may change shape, break or coalesce in the collecting medium; spurious particles may grow whilst others evaporate. The utility of the collection system is related to the skill with which these problems can be overcome.

The early collecting medium for cloud drops was oil, magnesium oxide, or soot. Oil coating suffered from the disadvantage that drops dissolved in the oil after collection, so immediate photography was necessary; the other two techniques gave permanent records which could be subsequently examined at leisure. Collection of ice particles in the atmosphere posed a considerably greater difficulty. Obviously melting must be prevented prior to examination; more difficult, metamorphosis of the particles by preferential evaporation or condensation may occur. For studies at the surface direct micro-photography of freshly fallen crystals was used by Bentley and Humphries (1931)[1]

[1] Bentley, W.A., and W.J. Humphries, 1931: Snow Crystals. McGraw-Hill.

and later Nakaya (1954)[2]. A significant advance was made with the use of formvar replica to give a permanent record of ice crystals. This technique was first developed by Schaefer in 1941 and used in Project Cirrus (Schaefer, 1941)[3] where crystals were caught in a solution of formvar in ethylene dichloride; on evaporation of the solvent a permanent cast of the crystal remained. A comparable technique, using a quick drying varnish, was developed by Weickmann (1944)[4]. Initially these techniques were used for investigation of particles at a few sites along the aircraft track. Instruments to enable continuous records to be obtained, together with data on volume concentration and particle flux at the earth's surface were subsequently developed. A continuous formvar replicator for use at the surface was developed by Hindman (1964)[5] and Hindman and Rinker (1967)[6] using 35 mm film moving horizontally past an aperture exposed to falling particles. A knowledge of particle volume concentration required the fall velocity of each size of particle. A continuous formvar replicator for use on aircraft was developed by MacCready and Todd (1964)[7] using a 16 mm film moving vertically past an aperture exposed to the airstream.

Details of the replication technique used under different conditions differed as more experience was gained.

---

[2] Nakaya, U., 1954: Snow Crystals, Natural and Artificial. Harvard University Press, Cambridge.

[3] Schaefer, V.J., 1941: A Method for Making Snowflake Replicas. Science, 93, 239-240.

[4] Weickmann, H., 1944: The Ice Phase in the Atmosphere. Translation Volkenrade, 716, 95 pp., Ministry of Supply, London.

[5] Hindman, E.E., 1964: Continuous Sampler for Settling Particles. J. Rech. Atmos., 1, 29-35.

[6] Hindman, E.E., and R.L. Rinker, 1967: Continuous Snowfall Replicator. J. Appl. Meteor., 6, 126-133.

[7] MacCready, P.V., and C.J. Todd, 1964: Continuous Particle Sampler. J. Appl. Meteor., 3, 450-460.

Schaefer (1962)[8] subsequently found that better replicas could be obtained by collecting crystals on a pre-coated formvar slide and exposing to chloroform vapor from a source at -5°C for several minutes. Speyers-Duran and Braham (1967)[9], on the other hand, used a chloroform spray on a formvar pre-coated 16mm film; this dried more quickly to give a better quality replica.

o——————————o

This report describes the principles and practice of particle replication by an instrument designed for use on a pressurized aircraft. It surveys those problems which arise from the change in particle concentration around the aircraft and collection problems arising from the finite size of the collecting probe, and the nature of the flow around and through the collecting slot. It also examines problems which arise from the impaction of particles with the drying replica which can lead to breakup and coalescence. The aim is interpretation of the replica record so that, as far as is possible, the properties of the particles in the free air may be deduced.

For purposes of illustration, two replicators, operating on the same principle but differing somewhat in detailed design, are discussed in this report. The "A" model replicator was built in 1970 and installed on the AFGL C130A; the "E" model replicator was built in 1973 and installed on the AFGL C130E. A similar unit ("D") was subsequently modified to operate on the NOAA DC6.

---

[8] Schaefer, V.J., 1962: The Vapor Method for Making Replicas of Liquid and Solid Aerosols. J. Appl. Met., 1, 413-418.

[9] Speyers-Duran, P.A., and R.R. Braham, 1967: An Airborne Continuous Cloud Particle Replicator. J. Appl. Met., 6, 1108-1113.

Analytical procedures may be summarized:

1. Assessment of particle type: drops, crystal graupel, etc. and approximate size; presence of artefact.
2. Influence of aircraft on collection enhanced/reduced concentration, enhanced local airflow.
3. Arm collection efficiency.
4. Replica calibration for drops
   for graupel.
5. Mass-size relationship.

II. DESIGN OF CONTINUOUS FORMVAR REPLICATOR

The replicator system on which this report is based was designed to give optimum operational characteristics - both from the viewpoint of installation and use in the aircraft - and also from the viewpoint of simplicity in the collection process so that subsequent uncertainties of interpretation of the data were reduced to a minimum. A full description of the design and operation of the instrument is given in AFGL Reports I, II (Hallett, 1976)[10]; here is given a summary of the design criteria which becomes of importance in data analysis.

An aircraft of the type used in cloud physics research travels through the air with an air speed of approximately 100 m s^{-1}. In order to obtain a representative spectrum, a statistically significant number of particles must be caught - this can evidently be achieved by an appropriate choice of sampling area and collection time. In continuous operation the collecting medium - a formvar solution freshly applied on a

---

[10] Hallett, J., 1976: Measurement of Size, Concentration and Structure of Atmospheric Particulates by the Airborne Continuous Particle Replicator, AFGL Final Report. Part I - Operating Manual, Part II - Service Manual. Supplement to Final Report #AFGL-TR-76-0149.

16 mm film - is moved behind a collecting aperture. With a convenient transport rate for film of ~ 0.5 m s^{-1}, typical particle concentrations dictate a slit width of ~ 2 mm to give collection of cloud drops without significant overlap. This width necessarily limits the collection of particles larger than this size.

The concentration of particles collected on the film (N_f) depends on the width of the slit (b), on the film speed (R) and on the aircraft speed (V). If N_a is the concentration of particles in the air, the slit sweeps a volume Vbh (h = slit height) in each second. Particles from this volume N_aVbh, are collected on a film of area Rh to give a surface concentration of

$$N_f = \frac{N_a Vb}{R} .$$

Taking typical values for cloud drops $N_a = 500$ cm^{-3}, an aircraft speed, $V = 10^2$ m s^{-1} and slit width, b = 2 mm, gives

$N_f = \frac{10^6}{R}$ cm^{-2}. If R is 1 cm s^{-1}, $N_f = 10^6$ cm^{-2}, a mean separation of 10 μm. With R = 50 cm s^{-1}, $N_f = 2 \times 10^4$ cm^{-2}, a separation of 70 μm which would still give some overlapping in clouds from tropical cumuli, with higher concentrations of large drops. Taking typical values for ice particles

$N_a = 5 \times 10^{-2}$ cm^{-3}

$V = 10^2$ m s^{-1} gives $N_f = \frac{10^2}{R}$ cm^{-2}

b = 2 mm

With R = 1 cm s^{-1}, $N_f = 10^2$ cm^{-2}, i.e., 100 cm^{-2}, a mean particle separation of 1 mm, and with R = 50 cm s^{-1}, gives about 2 particles per cm^2. With ice crystal dimensions 100 μm or larger, and drop median diameter in cold clouds ~ 20 μm, these film speeds and slit dimensions are not unrealistic. The higher film speeds are certainly necessary for cloud drop studies; a slit of 1 mm dimension would also be practical and improve this further, giving a lower probability of overlapping. A narrower slit will,

on the other hand, prevent collection of particles of size 1 mm or larger and give a higher probability of partial collection of particles impinging on the slit edge. For tropical clouds at low temperatures this forces a compromise since a reduction of slit width to 1 mm limits the collection of larger graupel particles.

The collecting arm diameter is also a compromise; it needs to be narrow to ensure a high collection efficiency for smaller particles, yet sufficiently large to enable the 16 mm film to be transported, the formvar solution to be applied, and any deicing equipment to be installed. This compromise gives, in the present design, a cylinder diameter 3.5 cm. A cylinder was chosen as being a simple aerodynamic shape for assessing collection efficiency, for ease of construction, and for the stability of the stagnation point during changes in the flight attitude of the aircraft. (Nielsen, 1969)[11].

The design of the system was undertaken in order to satisfy the following criteria:

a. To achieve a system to work on a pressurized aircraft and to maintain the internal pressure of the replicator at a value other than cabin pressure, so that airflow through the collecting slit could be controlled.

b. To incorporate a variable speed drive to examine cloud particles of variable concentration.

c. To achieve a formvar coating whose thickness could be controlled and whose uniformity could be maintained constant for different film speeds and under as wide a range of flight conditions as possible. This enables a coating to be applied which would be sufficiently thin to prevent drops moving around after capture and "rafting" prior to drying; a thin coat also gives quicker drying time. Quality control of the coat is also necessary if, at a subsequent time, we wish to apply automatic

---

[11] Nielsen, K.W., 1969: An Experimental Inquiry into the Flow Around Two Continuous Particle Replicator Heads. Desert Research Institute, University of Nevada, Reno, Technical Report No. 4, Physical Sciences.

optical techniques for counting replicas. Quality control of drying is inherent in this consideration.

d. To achieve in-flight viewing of the replica: monitoring of particle concentration is necessary in order to decide on optimum film speed and adjust coating thickness during changing flight conditions.

e. To have the capability of stopping and starting the replicator during flight. This is necessary as, although on a slow speed with film transport of 1 1/2" s^{-1} a 1350 foot roll of film lasts $\sim$ 3 hours, at the higher speeds necessary in water cloud, the time available at 24" s^{-1} falls to $\sim$ 10 minutes. In practice, this capability is achieved by a chloroform flush system, which replaces the formvar solution in the applicator head, so that solution evaporation during idle periods does not clog the applicator head with dried formvar.

f. To have de-icing capability so that the slit does not ice up during flight through supercooled cloud, and also to prevent the arm icing up for at least 3 diameters on either side of the slit, since any change in shape would change collection efficiency.

g. To maintain the replicator at a temperature below 0°C when replicating ice crystals so that melting shall not take place prior to the drying of the formvar solution.

h. To achieve a system which reduces pre-flight operations to a minimum and results in an instrument which can be used on an operational basis.

i. To maintain component accessibility at a maximum for maintenance simplicity and to provide room for any future modifications.

A general view of the replicator is shown in Figure 2a,b. It comprises three units - the control panel, the power supply chassis, and the replicator itself. In the "A" model the replicator is mounted such that the collecting arm is horizontal and is perpendicular to the fuselage symmetry plane (Figure 3a,b) In the "E" model the arm slopes downwards at an angle 10 1/2° and is almost normal to the aircraft skin.

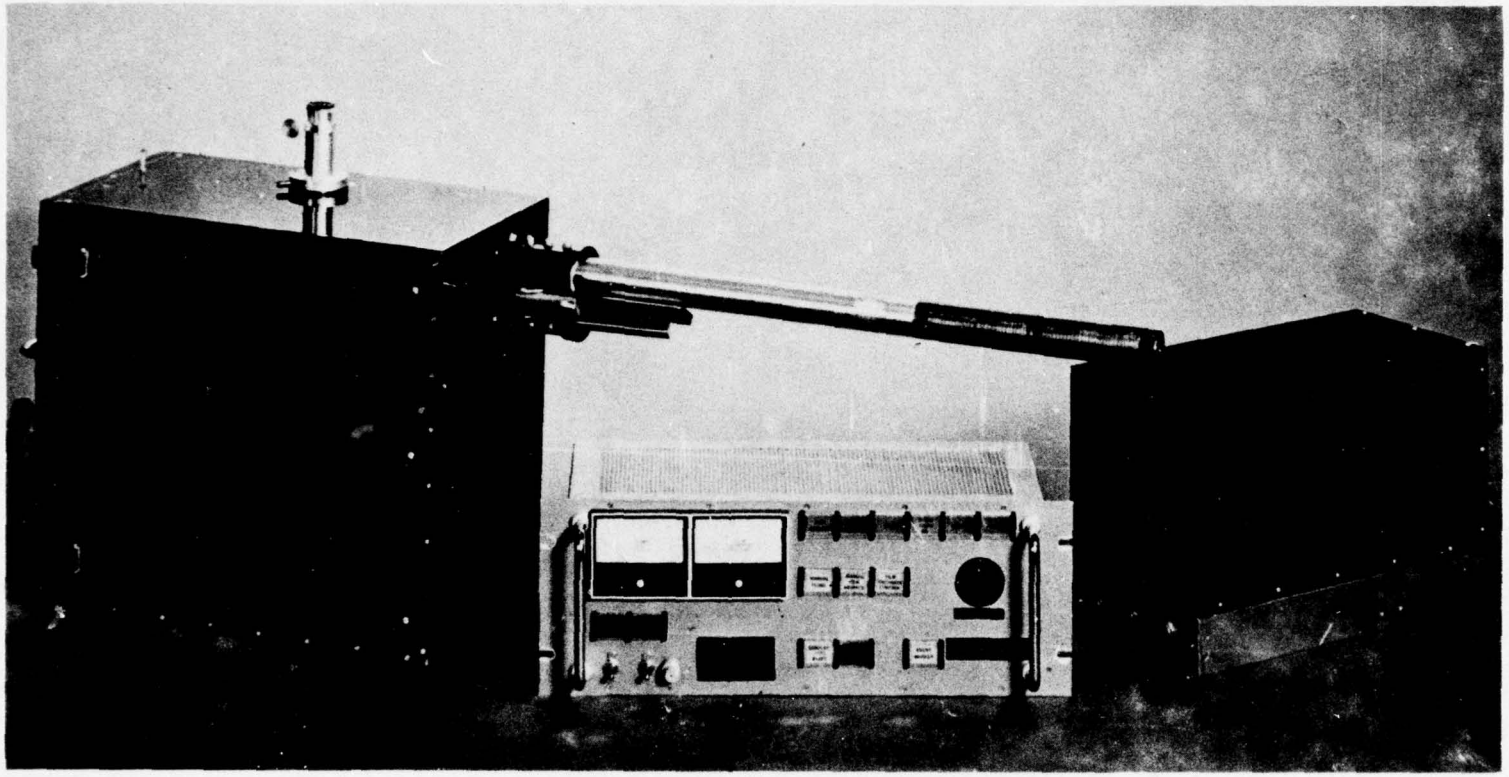

Figure 2a. Replicator (left), control panel (center) and power supply (right). "A" replicator.

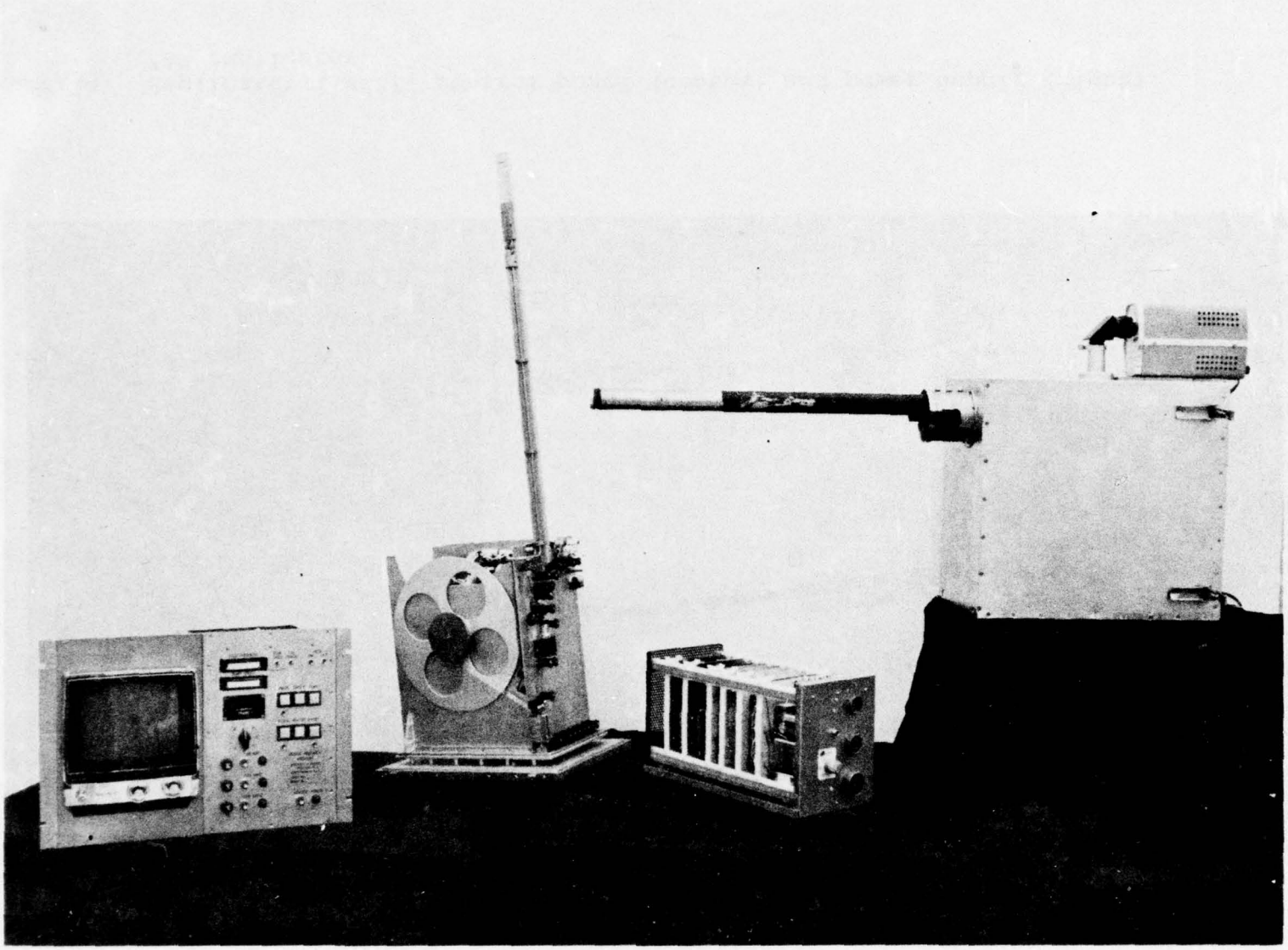

Figure 2b. Replicator (D,E) with TV camera linked to optics (right chassis, top) and TV display mounted in same rack as control panel (left).

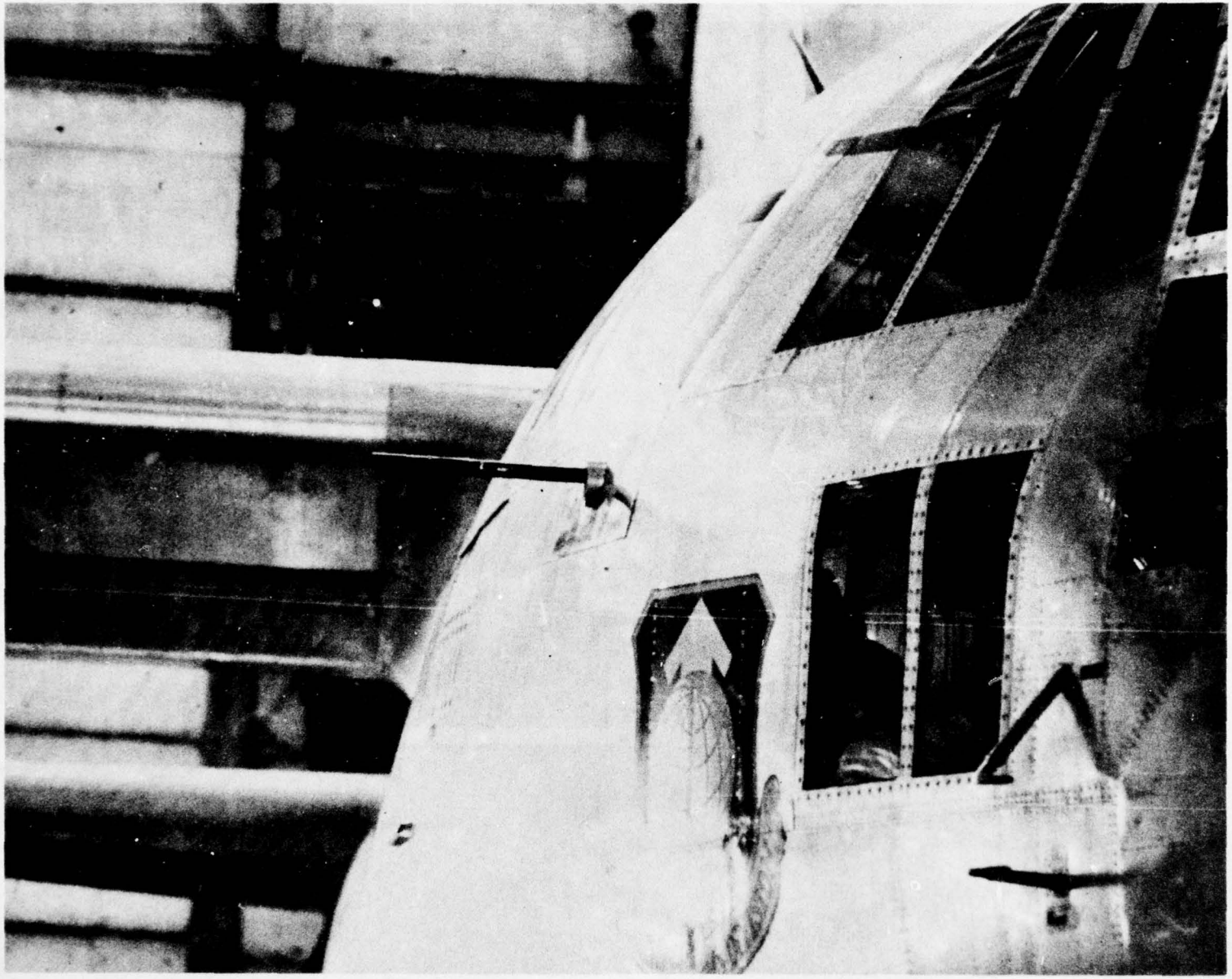

Figure 3a. C-130A showing replicator arm.

Figure 3b. C-130E showing extended replicator arm.

III. INSTRUMENT EXPOSURE

An ideal exposure site on a moving aircraft for the assessment of atmospheric properties is at a sufficient distance from the aircraft such that there is no disturbance of airflow. For various practical reasons mounting sites are less than ideal and the airflow is disturbed to a greater or lesser extent by the proximity of aircraft surfaces. Particles in the air cross such deflected streamlines - depending on their inertia and drag coefficient. This results in regions of higher or sometimes lower concentration particle concentrations. This problem has been investigated theoretically by Norment (1974, 1975)[12], with specific reference to the Air Force C130A and C130E aircraft. A computer prepared plot with each replicator site is shown in Figure 4. He points out that the aircraft boundary layer extends to a maximum thickness of 3 1/2" at a point well beyond the replicator mounting position. Since the sampling position for each replicator is well beyond this distance, its presence is unimportant. Norment develops a three-dimensional model of potential flow around the fuselage of each aircraft. The trajectory of hydrometeors - water drops and different habit ice particles-as they move across streamlines to the sampling site is calculated by an iterative process. Two effects are to be distinguished:

(1) The streamlines become closer together as they follow around the wider part of aircraft from free air; this results in a velocity increase of 1.102 (C130A), and 1.04 (C130E) at the sampling slot.

(2) The particle concentration changes by crossing streamlines.

Results of calculations for water drops for each aircraft are shown in Figure 5; results of calculations for ice particles

---

[12] Norment, H.G., 1974: Effects of Airplane Flow Fields on Hydrometeor Concentration Measurements. AFCRL-TR-74-0602.

_____, 1975: Effects of Airplane Flow Fields on Cloud Water Content Measurements. AFCRL-TR-75-0231.

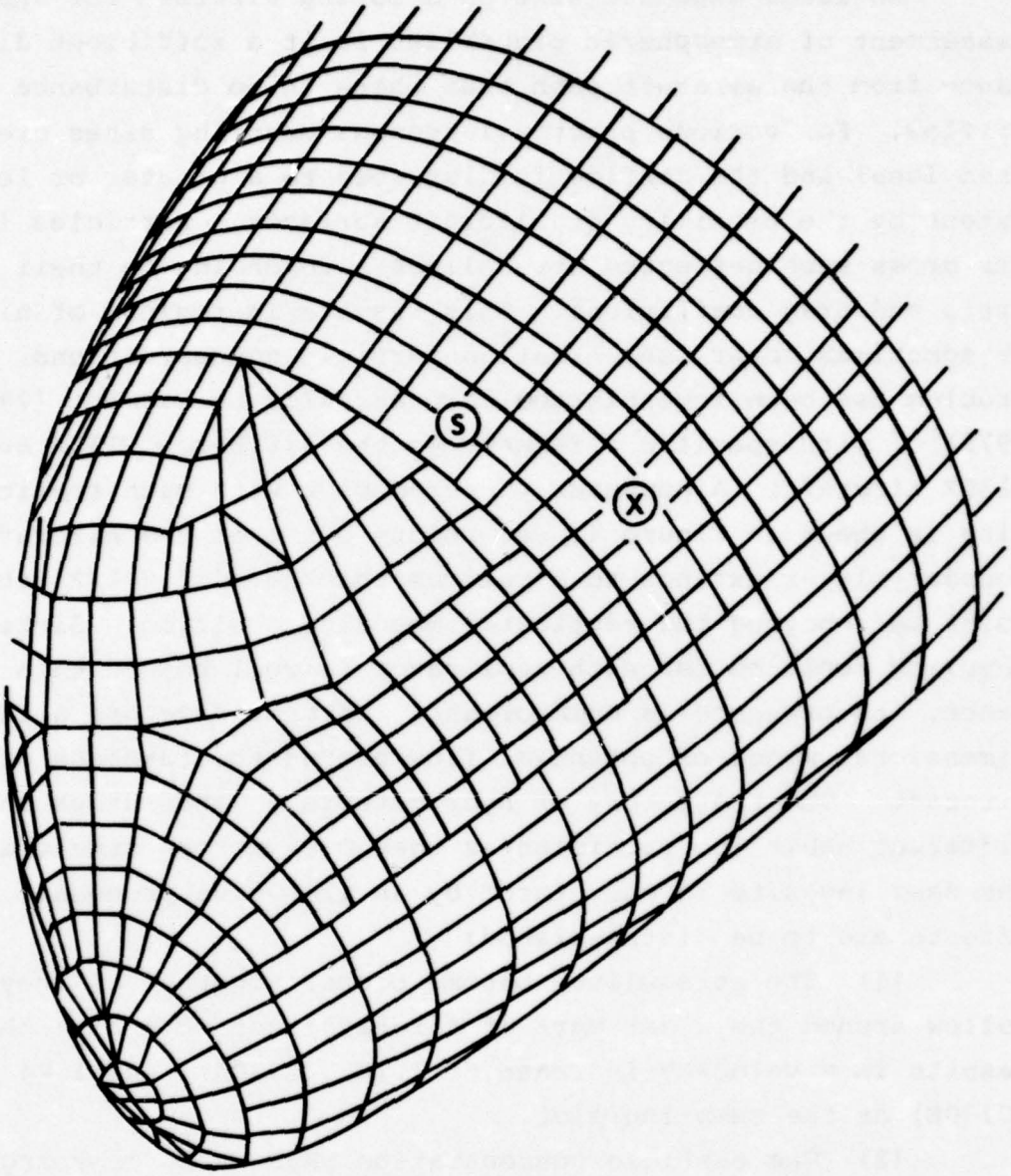

Figure 4a. Computer-prepared plot of the digital description of the nose and cabin sections of the Lockheed C-130A airplane. X marks the location of the particle replicator (RHS). S marks the position of the ice stick sampler (LHS). (From Norment, 1974). Sampling Site: 13.75" from skin.

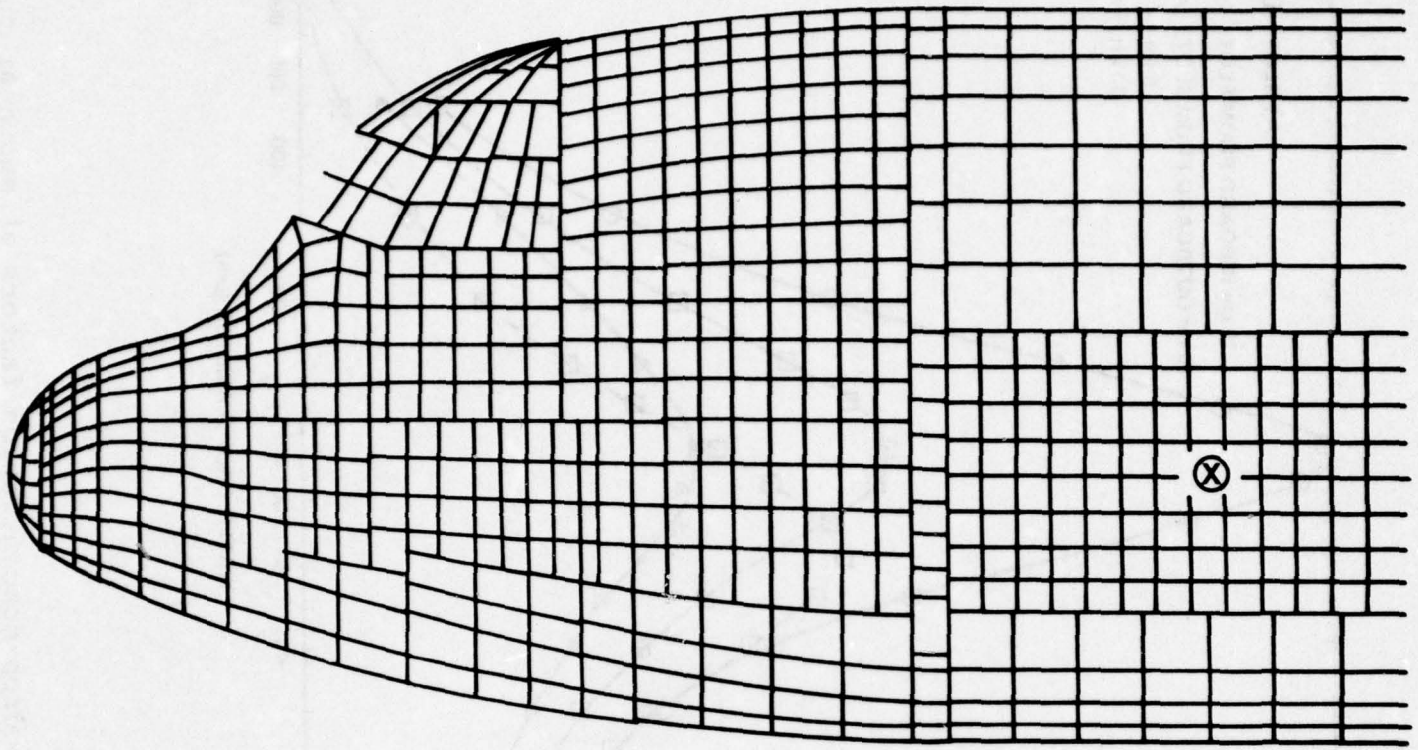

Figure 4b. Computer-prepared plot of the digital description of the Lockheed C-130E forward fuselage to FS 350". X marks the location of the particle replicator.

Sampling Site: 13.75" from skin (short arm)
21.75" from skin (extended arm)

(From Norment, 1974)

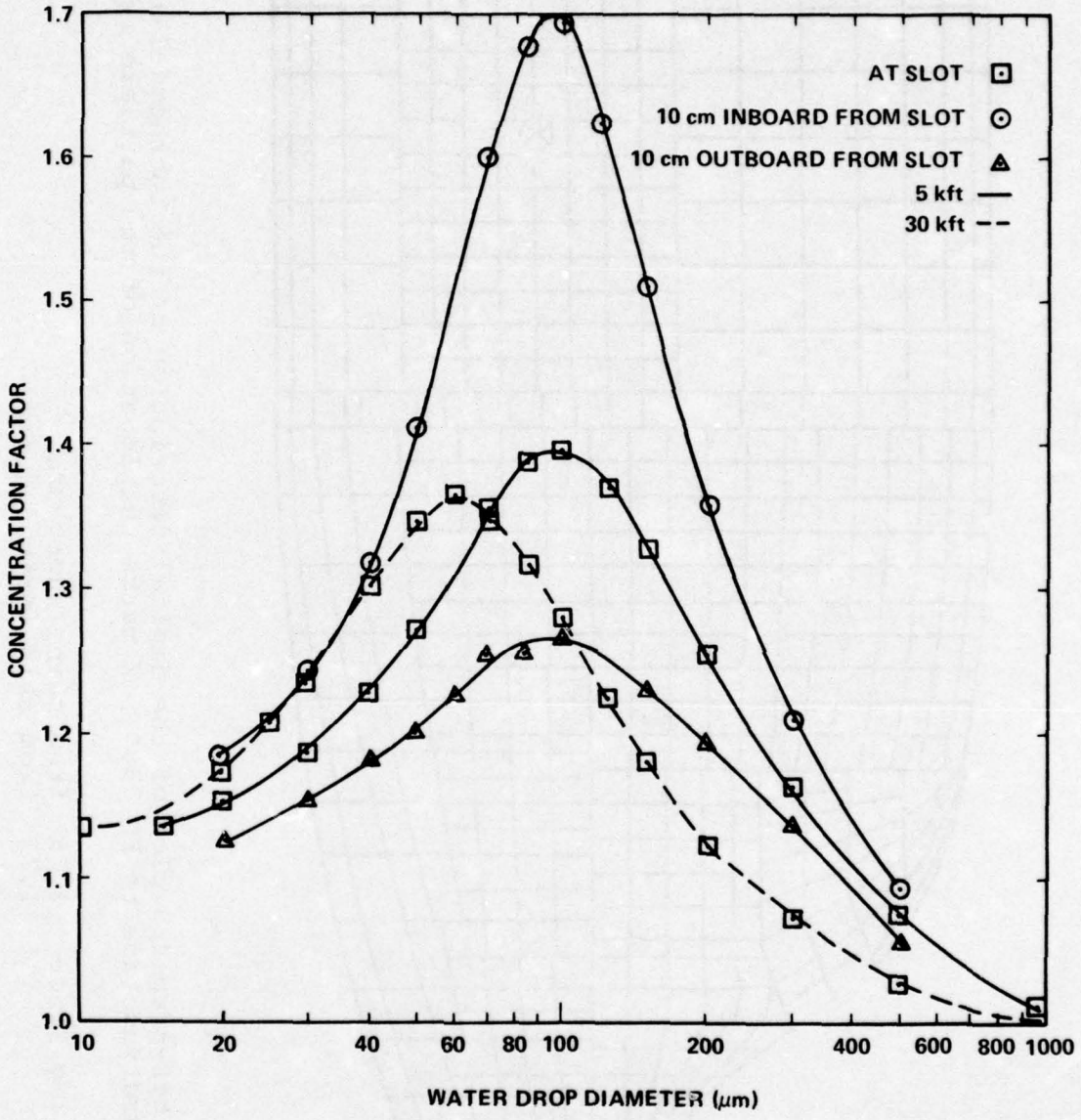

Figure 5a. Water drop concentration factors at and near the particle replicator slit on the Lockheed C-130A. (From Norment, 1974).

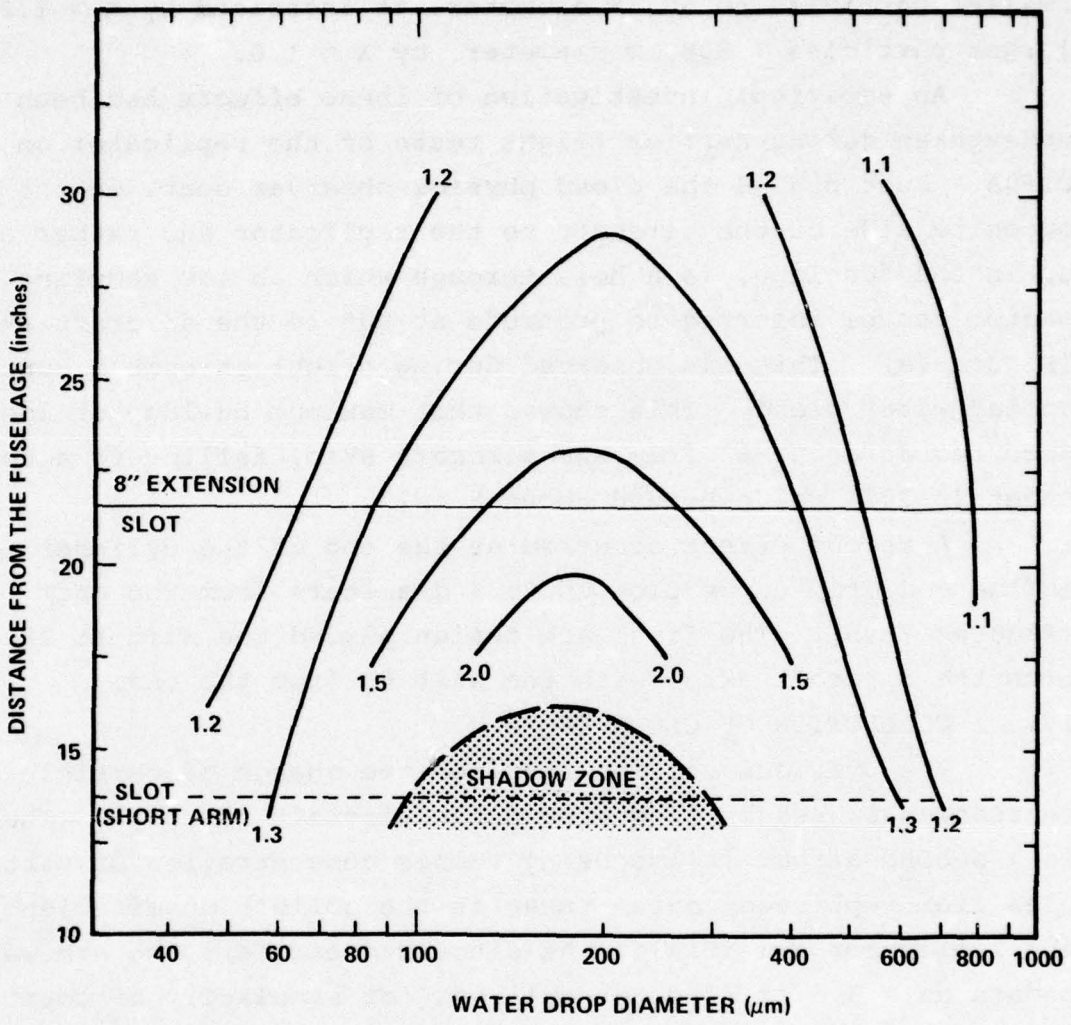

Figure 5b. Concentration factor contours vs. water drop diameter along the particle replicator arm on the Lockheed C-130E. Dashed line is the position of the slit in the short arm; full line is the position for the 8" extension. (From Norment, 1974).

are shown in Figure 6. It is evident that concentration of smaller particles to 50 μm diameter, is increased by X ∿ 1.2; larger particles ∿ 200 μm diameter, by X ∿ 1.6.

An empirical investigation of these effects had been undertaken during earlier flight tests of the replicator on the C130A. Just behind the cloud physics observer seat, on the opposite side of the aircraft to the replicator and rather high up in the fuselage, is a hole through which an ice sampling impactor can be inserted to protrude at 90° to the aircraft skin (Figure 4a). This was observed during flight through a supercooled water cloud. This showed that maximum buildup of ice occurred at about 6" from the aircraft skin, falling to a constant (± 20%) value beyond about 8 1/2".

A second effect occurred at the end of the cylinder; this influenced drop deposition up to 3 diameters from the end (Figures 7a,b). The final arm design placed the slit at 18.75" from the aircraft skin, with the slit 6" from the end.

IV. COLLECTION OF CLOUD DROPS

The previous section examined the change of particle concentration caused by flow around the aircraft fuselage. There is a second effect in assessing volume concentration of particles from replicator data - that is the collection efficiency of the replicator arm itself. As discussed earlier, the arm was chosen as a 3.5 cm diameter cylinder for simplicity of construction and for ease of assessing droplet collection. Langmuir (1961)[13] has estimated the collection efficiency of a cylinder for spherical cloud droplets of different size. Flow around the cylinder is computed from potential flow theory; the cloud droplet trajectories cross streamlines depending on their inertia and drag coefficient. Langmuir expressed his results in the form of two dimensionless numbers - the Stokes number (K) to be interpreted as the ratio of particle stopping distance (assuming Stokes fluid resistance) to collector radius:

---

[13] Langmuir, I., 1961: Mathematical Investigation of Water Droplet Trajectories. Collected Works, 11, 335-393.

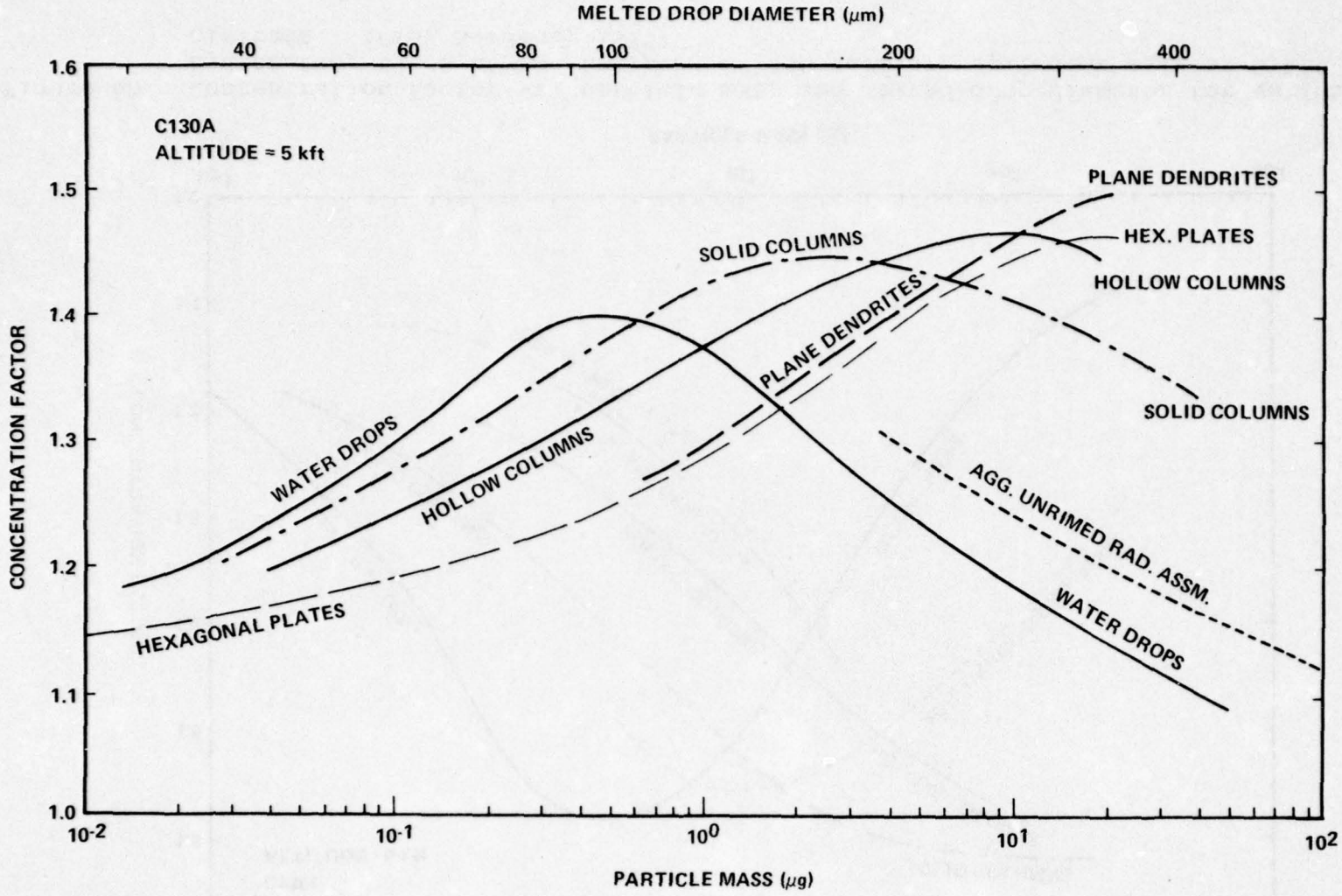

Figure 6a. Concentration factor vs. particle mass and melted drop diameter for various hydrometeor types at the C-130A formvar replicator slit at 5 kft altitude. (From Norment, 1975).

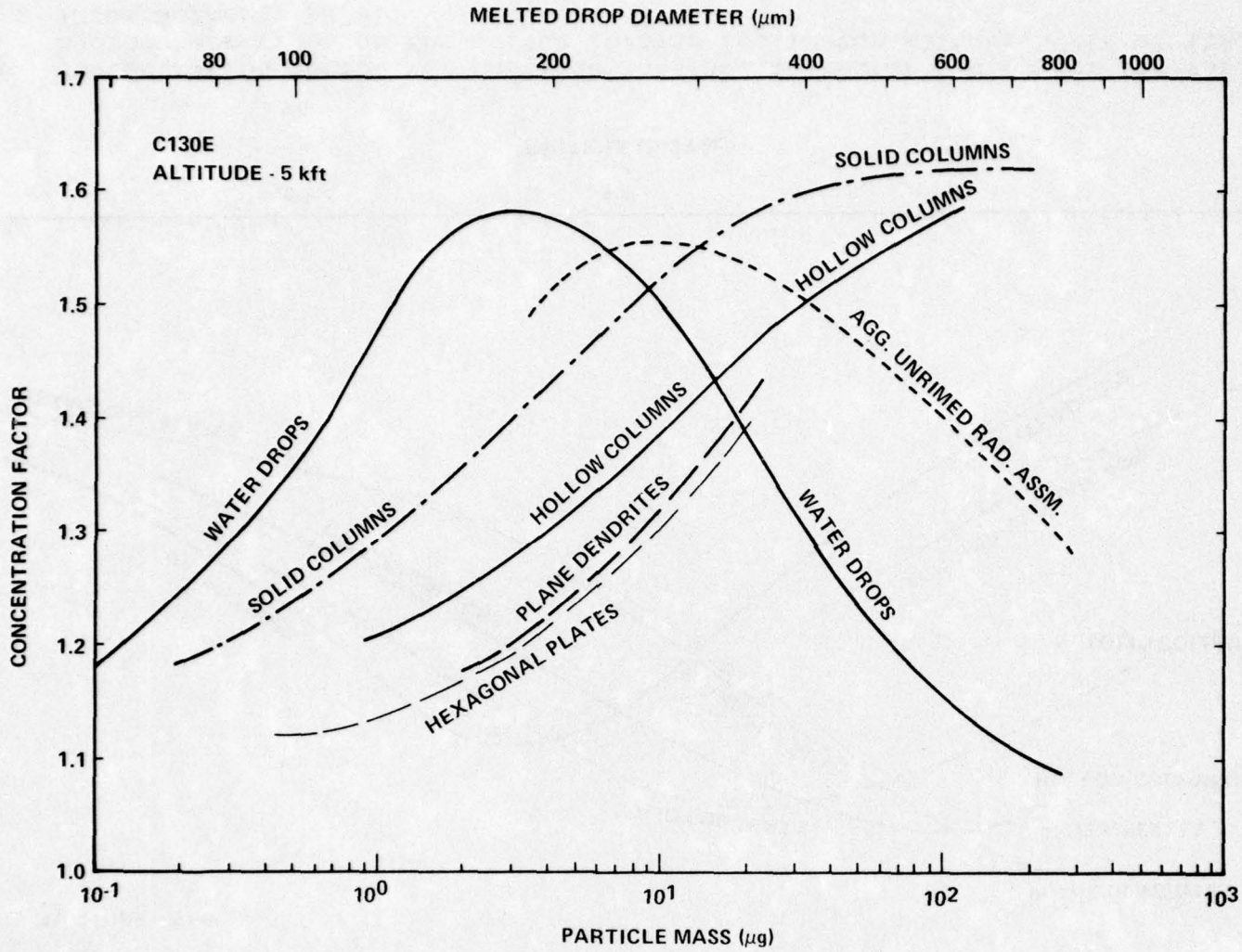

Figure 6b. Concentration factor vs. particle mass and melted drop diameter for various hydrometeor types at the Lockheed C-130E formvar replicator slit at 5 kft altitude. (From Norment, 1975).

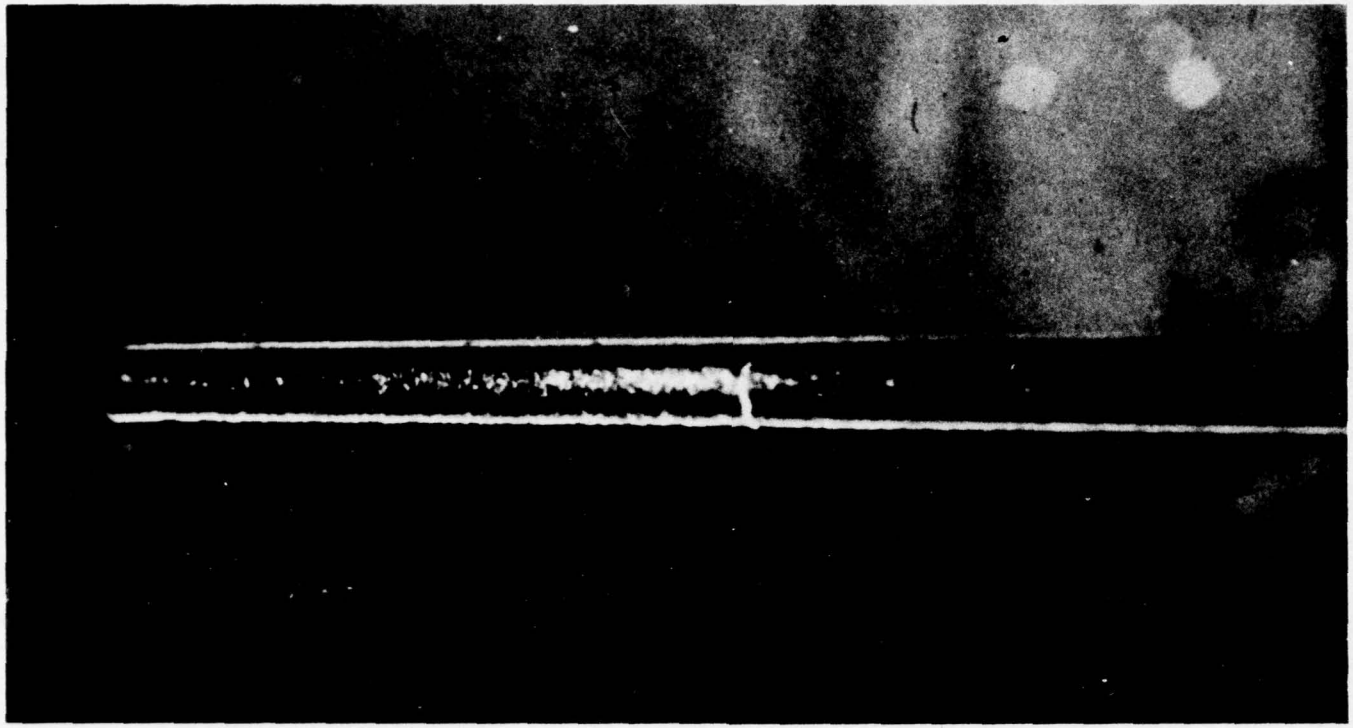

Figure 7a. Ice accretion on rod 1 cm diameter exposed just behind observers' seat in front cabin, C-130, May 12, 1970. Enhanced accretion can be seen at a position 6" from the skin (indicated by ring).

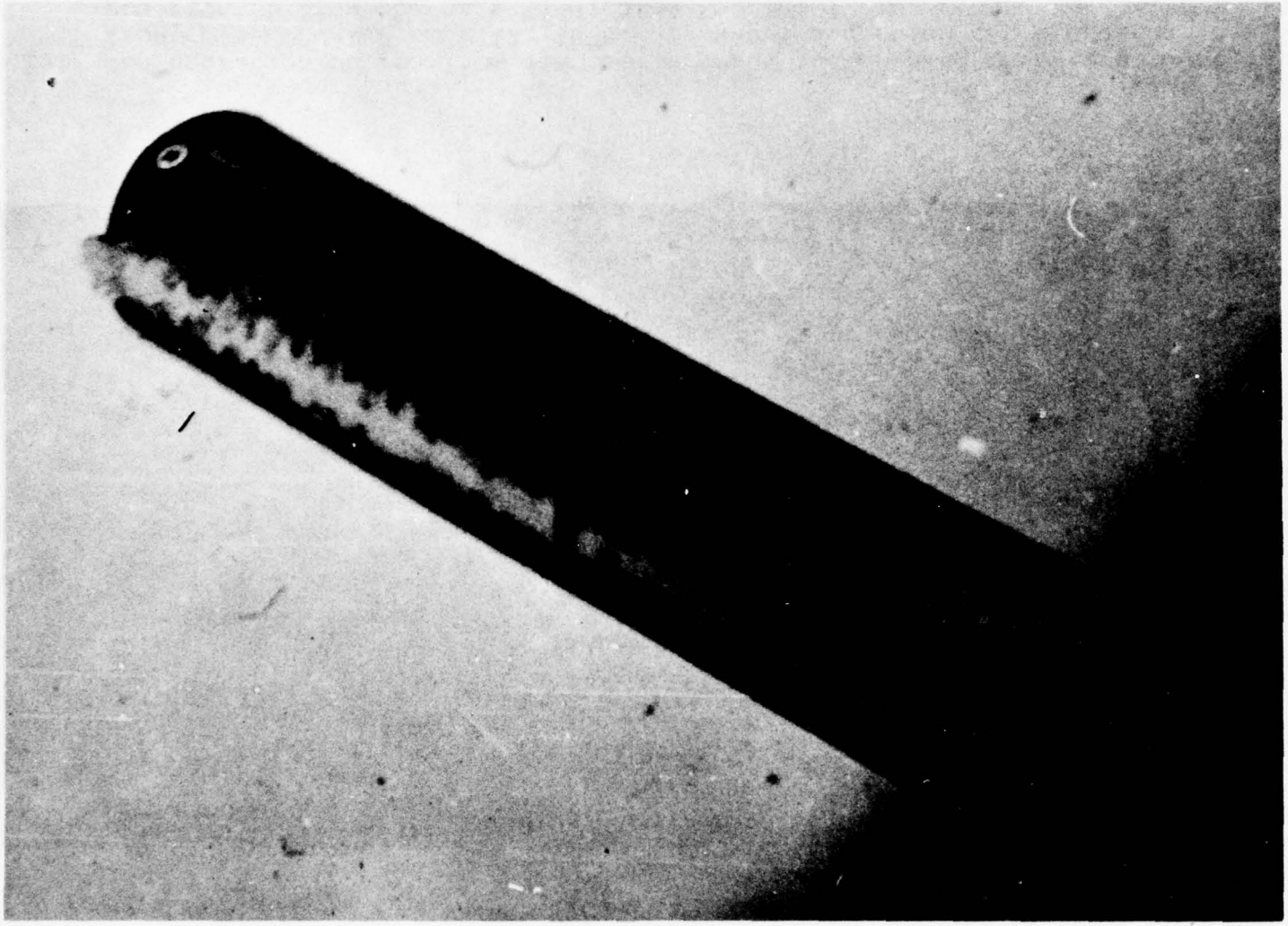

Figure 7b. Ice collected on unheated replicator arm installed in C-130, flight 17, February 1971. Note enhanced accretion at the end; the slit is just visible near the center.

$$K = \frac{2\rho_w a^2 V}{9\ \eta\ c}$$

and a number formed from the Reynolds' and Stokes' number,

$$\phi = \frac{R_e^{\ 2}}{K} = \frac{18\ \rho_a^{\ 2}\ cV}{\eta\ \rho_w}$$

ρ_w = water density 1.0g cm^{-3}

a = drop radius

V = velocity of drop with respect to the collector at infinity

η = air viscosity, (0.00017, 0°C, c.g.s. .00016, -20°C)

c = cylinder radius = 1.75 cm

ρ_a = air density, 1.29 x 10^{-3}g cm^{-3} 0°C, 1 atm.

0.69 x 10^{-3}g cm^{-3} -20°C, 0.5 atm.

$K \sim 7.5\ a^2V$

$\phi \sim 3V$ (0°C, 1 atm.)

$\phi \sim 9.4V$ (-20°C, 0.5 atm.)

with V in m s^{-1}.

Taking V = 100 m s^{-1}, gives

$\phi\ C_{130} \sim \begin{matrix} 3000 \\ 936 \end{matrix}$ $\begin{matrix} (0°C,\ 1\ atm.) \\ (-20°C,\ 0.5\ atm.) \end{matrix}$

$K = 7.47 \times 10^6\ a^2$ (0°C, 1 atm.)

$7.94 \times 10^6\ a^2$ (-20°C, 0.5 atm.)

with a in cm.

The collection efficiency for different sizes of drops at the cylinder stagnation point is given by Figure 8. $\phi \sim 2000$ represent C130 flight conditions to sufficient approximation; drop diameter are marked on this curve. A direct plot of collection is given in Figure 9.

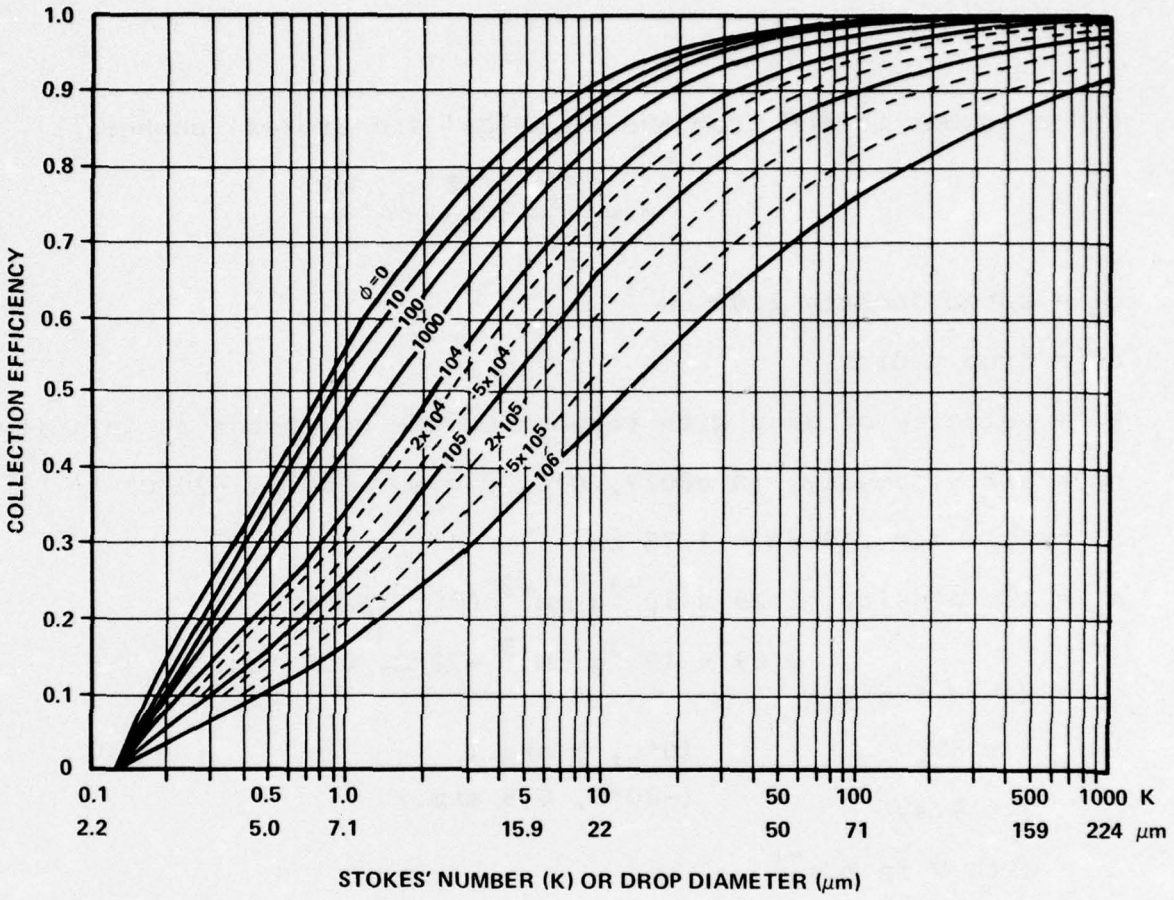

Figure 8. Collection efficiency at stagnation point, $\theta = 0$, on cylinders with ideal fluid flow. (after Langmuir, 1961). ϕ = 1000 to 3000 approximate to C-130 flight conditions and indicated drop sizes.

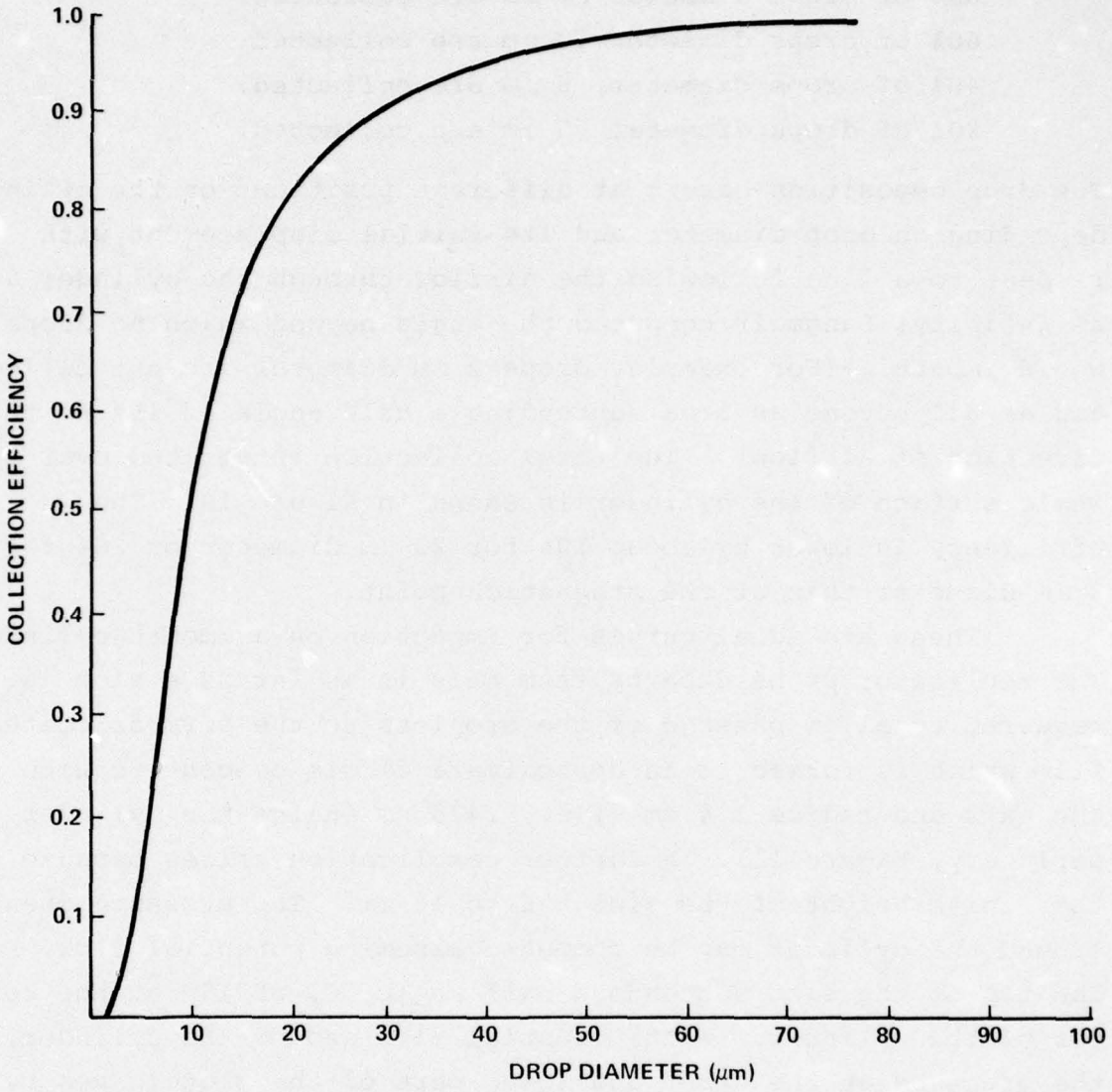

Figure 9. Collection efficiency at the stagnation point of ideal cylinder, 3.5 cm diameter under typical C-130 flight conditions (100 m s^{-1}, 500 mb).

80% of drops diameter 22 μm are collected.
60% of drops diameter 10 μm are collected.
40% of drops diameter 8 μm are collected.
20% of drops diameter 5 μm are collected.

The drop deposition occurs at different positions on the cylinder depending on drop diameter and its initial displacement with respect to a line following the airflow through the cylinder axis at infinity; Langmuir computed the angle beyond which no drops would impact. (For example, drops 2 μm diameter are not collected at all beyond an area subtending a half angle of 15° to the direction of airflow). The total collection integrated over the whole surface of the cylinder is shown in Figure 10. The efficiency is lower by about 10% for 22 μm diameter or 20% for 8 μm diameter than at the stagnation point.

These are ideal curves for impaction on a smooth cylinder. The replicator probe departs from this in as far as a slot is required to allow passage of the droplets to the formvar coated film which is formed to an approximate circle concentric with the axis and radius 1.4 cm (i.e., .475 cm inside the cylinder periphery, Figure 11). A further complication arises because of the finite height of the slot - 6 to 10 mm. The pressure change around the cylinder may be computed assuming potential flow. The top of the slot subtends a half angle, θ, of 15° at the center of the cylinder. With potential flow around the cylinder, the pressure at the upper and lower part of the slot (given by $1-4 \sin^2 \theta$) has dropped to 0.73 of the stagnation pressure. Some circulation in the slot itself may result from this. In practice, the dynamic pressure is influenced by the detailed motion of the aircraft - its angle of attack and the rate of change of angle of attack, besides the air velocity itself. Whilst flying through a turbulent cloud, these quantities evidently vary significantly so that the instantaneous dynamic pressure at the slot is subject to appreciable variation - which in practice would probably dominate any local flow resulting fr the pressure change over the slot height.

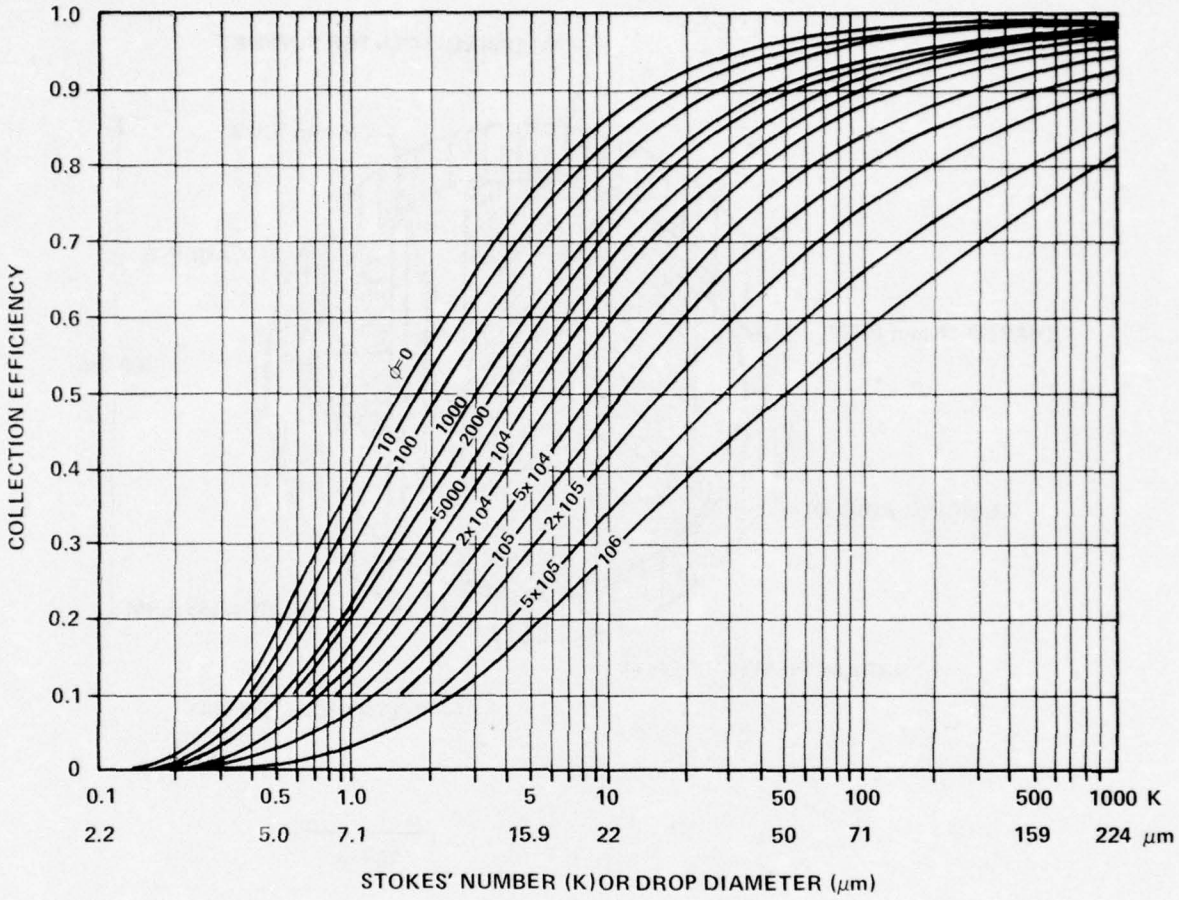

Figure 10. Total collection on a cylinder (after Langmuir, 1961). ϕ = 1000 to 3000 and indicated drop sizes approximate to C-130 flight conditions.

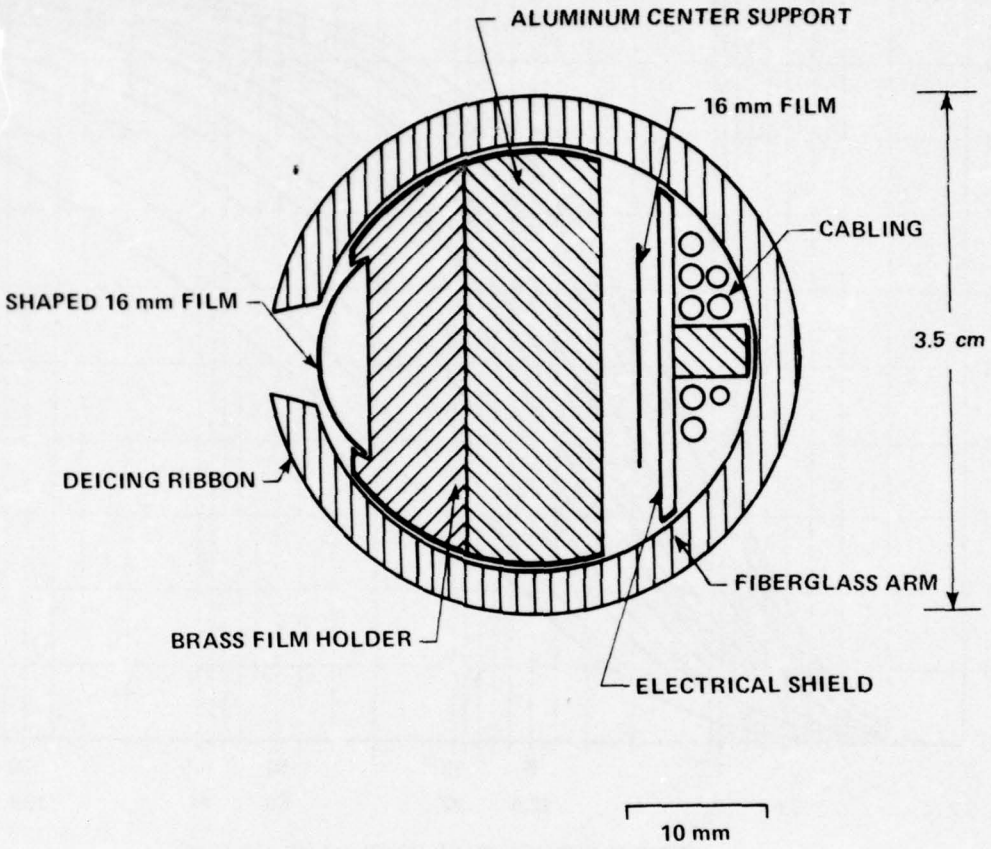

Figure 11. Section through collection slot. A slight inward airflow enables smaller droplets (5 μm diameter) to be collected.

Air flows through the slot depending on the mean air pressure differential between the external dynamic pressure and the internal replicator pressure. This can be controlled by flow rate of the drying air into the replicator and its exit through a controlled leak (Part I , page 9). This situation was simulated on tests on the C130A replicator in the AFGL wind tunnel in 1973. Collection of drops produced by a steam jet (5 μm diameter) was examined with different pressure differentials. With internal pressure greater than external pressure, that is airflow out of the slot, no drops at all were collected. With flow into the slot with pressure differential of ∿ 1" H_2O, these drops were caught, but only at the sides of the formvar - towards top and bottom of the slit, subtending a half angle Θ of about 10° (Figure 12).

This result is opposite to that which collection calculations would predict - preferential collection at the stagnation point - and implies that the drops, although probably collected towards the center,were swept towards the edge before entering the replica. With pressure differential ∿ 2" H_2O, collection over the replica was more uniform with some tendency for larger drops to be absent from the edges (Figure 13).

Braham and Speyers-Duran (1967)[14] found that a slight inflow into their replicator slot was desirable to prevent Helmholtz resonance during flight; it also appears that slight inflow is necessary to ensure collection of the small cloud droplets. An excessive internal pressure leading to flow out of the slot, on the other hand, prevents collection of smaller cloud drops but permits collection of larger drops and ice particles.

In summary, with the probe geometry used, droplets of diameter down to 5 μm are replicated. The ideal collection efficiency at the center of the cylinder exceeds 80% for drops

---

[14] Speyers-Duran, P.A., and R.R. Braham, 1967: An Airborne Continuous Cloud Particle Replicator. J. Appl. Meteor., 6, 1108-1113.

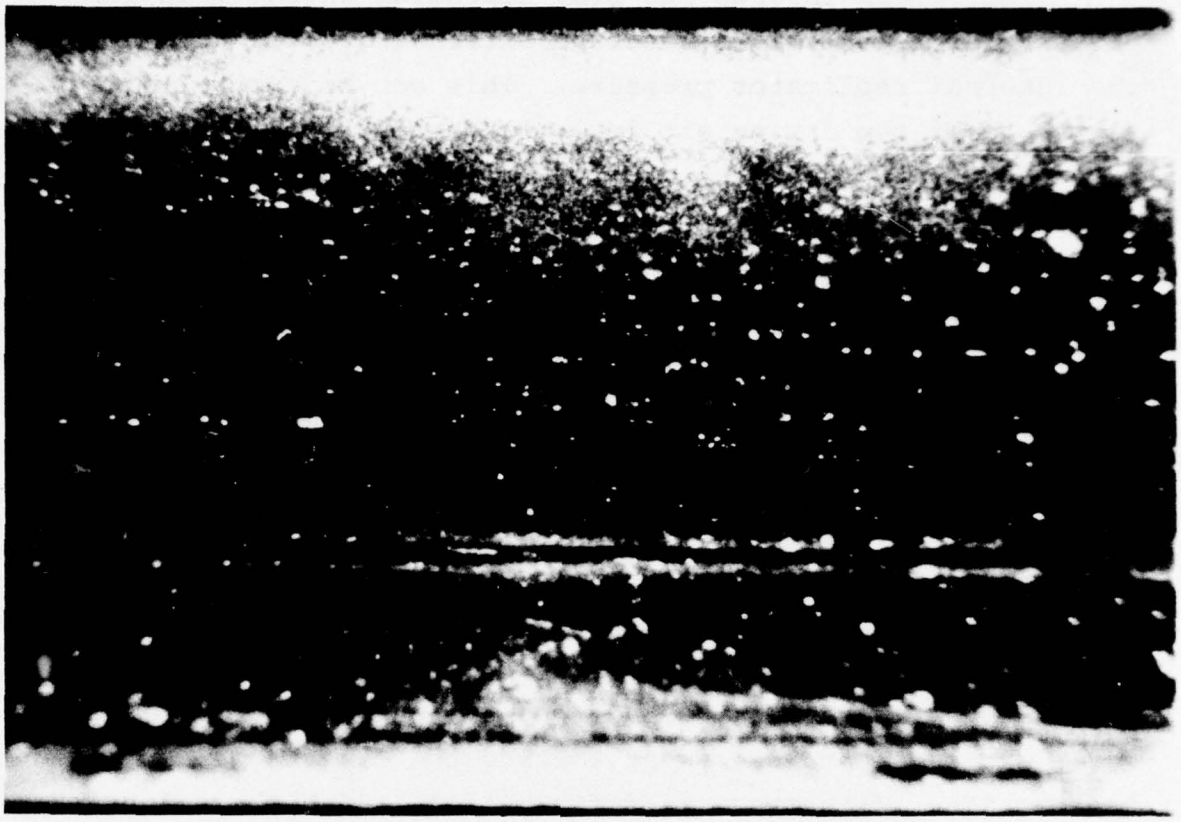

Figure 12. Collection of Small Cloud Drops. Wind tunnel test - 23 February, 1973.

12 in s^{-1}, film speed 8.
Tunnel Speed, 14½" H_2O = 148 kts.

Replicator pressure differential Δp = 1¼" H_2O
Water drops produced by steam inlet. This shows collection of drops, largest diameter ∿ 5 μm, at the edge of the film. This implies that drops move over the replica surface to be caught near the edge. Drops are also caught where the replica is slightly thicker - near the scratch marks in the formvar. A few larger drops are also caught uniformly across the film.

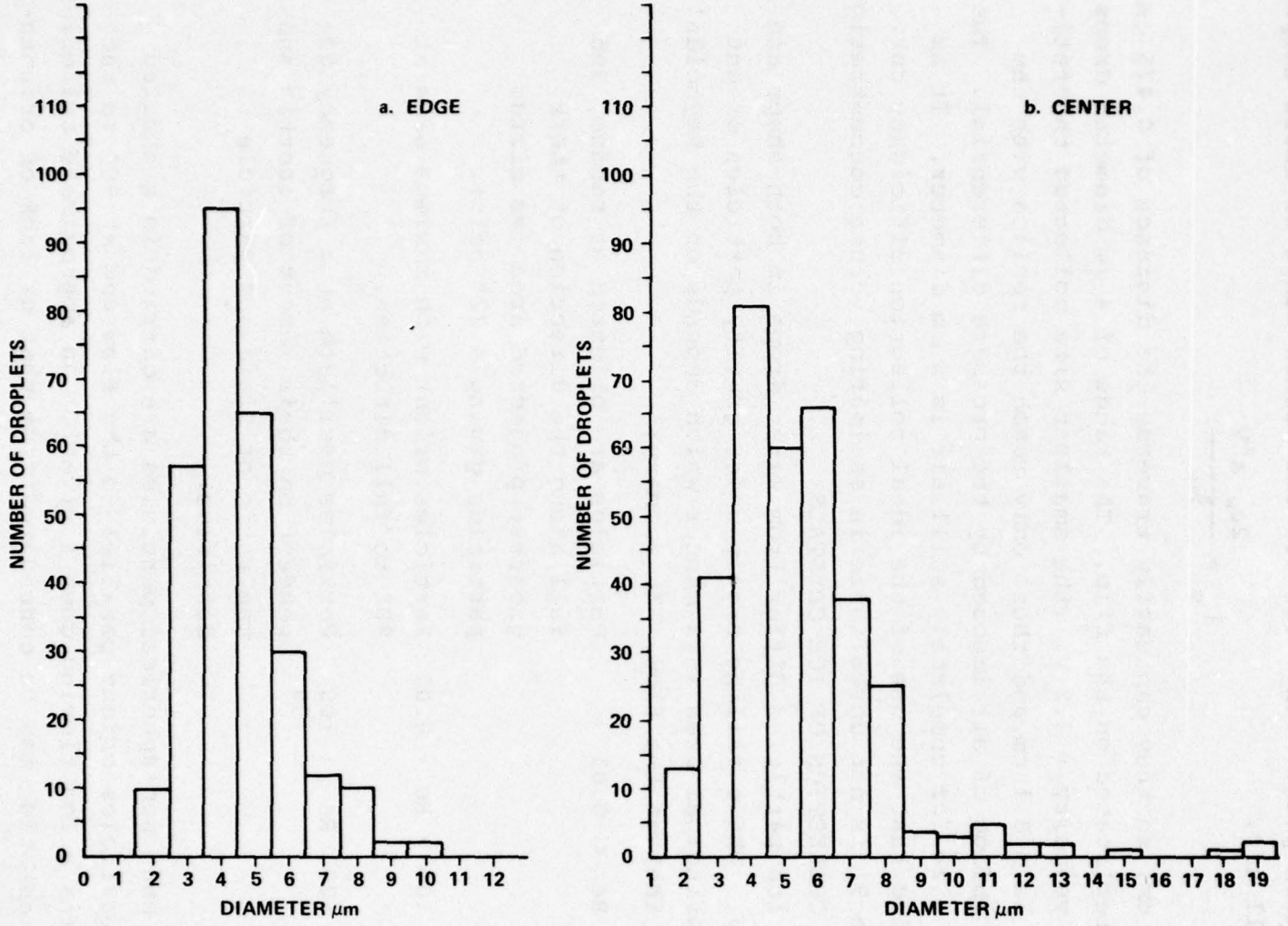

Figure 13a,b. Collection of droplets, AFGL tunnel test. Dynamic pressure: 14½" H_2O, 149 kts. Internal replicator pressure: 13½" H_2O. a. replica edge (about 10^o half angle). b. Replica center.

15 μm diameter; drops of this size impact on the cylinder at the stagnation point with ∿ 0.5 V. The Stokes range of these drops in still air,

$$\lambda_s = \frac{2\rho_w a^2 V}{9\eta}$$

is ∿ 4 cm, so they can easily traverse the distance of 0.475 cm to be replicated on the film. The range of 4 μm diameter drops, impact velocity ∿ 0.2 V, (the smallest size collected theoretically) is ∿ 0.1 cm and these only reach the replica with the slight inflow of air imposed by the pressure differential. The cutoff size for completely still air is 3 μm diameter. It is concluded that the use of the ideal collection efficiency curve (Figure 9) is not unrealistic in estimating volume concentration.

V. COLLECTION OF ICE CRYSTALS

Ice particles differ from water drops in both shape and density. While falling freely under gravity particles orient their principal axes in a manner which depends on the Reynolds' Number (Re) of the flow. In summary:

$Re < 0.01$	Particles are oriented at random, and fall along the direction of their greatest projected area (as cirrus particles giving a 22° halo).
$100 > Re > 0.01$	Particles orient with maximum area at 90° to fall direction.
$1000 \pm 500 > Re > 100 \pm 50$	Particles oscillate at a frequency dependent on their moment of inertia and the ratio of fluid and particle densities.

When non-spherical particles are carried in a sheared flow, particles orient parallel to the flow and at 90° to the shear (as a log flowing down a river). An approximate criterion for orientation may be considered from that of lack of orientation of particles $Re < 0.01$ in free fall. Reynolds' Number in excess of 0.01 would be expected to give a significant turning torque to the crystal.

Define a Reynolds' Number in shear:

$$\frac{\text{Vel. differential across particle oriented at 90° to flow x dia.}}{\text{Kinematic Viscosity}}$$

e.g., ice crystal 200 μm across, in air $\nu = 0.2\ cm^2 s^{-1}$

in shear $\frac{100\ m\ s^{-1}}{5\ cm}$ (aircraft speed) / (1½ probe diameter)

This gives Re $\sim \frac{.02 \times 10^4 \times 0.02}{5 \times 0.2} \sim 4$

i.e., the fluid forces on the particle will be sufficient to turn it and orient it along the flow.

A second question is - will there be time for this orientation to occur? A typical time is given by the flow of the air around the probe - $\frac{5\ cm}{100\ m\ s^{-1}} \sim 0.5$ m s.

Consider a viscous torque,

$$I\ \Theta = \mu A \frac{du}{dz}\ \ell$$

I - moment of inertia of crystal, 0.25 m x^2

Θ - angular velocity

μ - air viscosity = .00016 cgs

A - projected area of crystal

ℓ - crystal length

Take a crystal 200 (ℓ) x 50 x 50 μm^3; density 0.5 g cm^{-3}

$$m \sim 2.5 \times 10^{-7}\ gm$$

$$I = 0.25 \times 10^{-11}\ cgs$$

$$A = 10^{-4}\ cm^2$$

$$\frac{du}{dz} \sim \frac{100\ m\ s^{-1}}{5\ cm}$$

$$\Theta = 1.3 \times 10^4\ rad\ s^{-1}$$

i.e., to orient $\frac{\pi}{4}$ takes 0.06 m s. Comparing these two times shows that this particle size has time to orient parallel to the flow (i.e., perpendicular to the shear) on approach to the replicator slot. The behavior of these particles on passing through the slot to the film requires more detailed

study and has not been attempted. The time taken for larger particles with $\lambda_s > 0.475$ cm is $\sim \frac{0.475 \text{ cm}}{0.5 \times 100 \text{ m s}^{-1}}$

~ 0.1 m s which is of the same order as the rotation time calculated above; evidently it is possible that plate or needle ice particles orient their widest dimension parallel to the film on approaching the slot, and retain this orientation as they cross the short region to the film.

The calculation of collection efficiency for the probe could be undertaken as in Langmuir's original work with appropriate values of drag coefficient and particle density. With particle density 0.2, and a viscosity enhancement (through drag coefficient) of x 10, K values increase by x 50, so the particle diameter for collection efficiencies $\sim$ 0.5 increases by x 10 from 16 μm for drops to $\sim$ 80 μm for ice particles. Under water cloud growth conditions particle sizes are often well in excess of these values. It is of interest that freshly nucleated particles size $\sim$ 30 μm are *sometimes almost* equiaxed and would therefore be collected in a way comparable to water drops; small thin (few μm) plates would probably have a significantly lower collection.

VI. OPTICAL TECHNIQUES

Projection

Examination of replica data must be carried out under optimum conditions to ensure full utilization of the technique. For continuous examination of larger particles, $\sim$ 500 μm, a stop motion projector (Kodak analyst or L & W Photo Analytical) with standard 2" lens is ideal. For examination of smaller particles and cloud drops, larger magnification is necessary. A 1/2" lens enables this to be carried out by projection in a small room for visual examination. An alternate technique is to mount a mirror at 45° and project the image on a horizontal desk. This technique is convenient for manual counting. Care should be taken to ensure that the projector beam is horizontal, otherwise

excessive image distortion will occur. The image may be calibrated by a thin mm graticule inserted into the projector; it is convenient to adjust the distance to give a x 10^n enlargement of the replica.

Microscopy

It is convenient to locate the frames to be examined in detail, mark the frame in the projector with a felt color pen and run forward the film a few hundred frames to insert in the microscope stage. It is convenient to construct a small film holder which enables the film to be held in place in the X-Y microscope movement. Vertical illumination (as in a metallurgical microscope with internal reflector) gives surface detail; transmitted illumination enables any internal replica features to be seen. In the latter case, it is best to illuminate a white card about 2" below the replica to obtain good contrast. In practice objectives x5 and x 10 and x 20 combined with x5 and x10 eyepieces are convenient. Lower magnification (x2, x1) objectives are sometimes necessary for the larger particles. Photography is straightforward in either case - polaroid photographs are readily obtainable. It is well to include a mm scale in each photograph for reference purposes. An eyepiece should always be used in photography - if it is not used troublesome internal reflections sometimes occur.

Vertical detail of the replica can be obtained by use of depth of field technique with a high power objective and a microscope which has a vertical calibration. Whilst this gives some information on replica thickness, by far the most convenient technique is interference microscopy. This uses the replica as one surface of a Michelson Interferometer. The optical system is set up to give parallel fringes for a flat surface in white light. The fringe pattern is deflected laterally by variations in vertical height of the replica. This gives some 10 to 20 fringes, where fringe order can readily be seen from their complementary color. Monochromatic light gives sharper fringes, but there is considerable difficulty in distinguishing between the order of the fringes. The number and separation of the

fringes can be selected by tilt of the reference mirror. For light wavelength 0.5 μm, each fringe displacement is equivalent to a depth difference of 0.25 μm. This enables vertical height differences of the replica to be estimated to ∿ 0.1 fringe width or ± 0.05 μm. Each fringe displacement corresponds to a height difference of quarter a wavelength. (sodium yellow, .59 μm; mercury green, 0.55 μm). This is a powerful tool in assessing the formation mechanism of the replica imprint and in differentiating between particle and artefact. A convenient interference objective to use is the Watson 16 or 8 mm (Ealing Corporation, Cambridge, MA), which can be adapted for use on any microscope.

VII. REPLICATION OF ATMOSPHERIC PARTICULATES

The Replica

The detailed interaction of particles with the solution and the formation of the crater as the solution dries is a complicated process.

A particle small compared with the solution depth becomes totally immersed. A particle large compared with the solution depth, becomes covered with a thin layer as the solution spreads over the emergent surface. A liquid drop deforms somewhat under surface tension forces to a shape which becomes permanent as the solution dries and its viscosity becomes sufficiently large. A solid particle on the other hand, is unchanged by the drying process. Once the solution has hardened, vapor diffuses out through small holes or through the formvar itself to leave a hollow cast of the particle. In some cases the upper layer of formvar is sufficiently thin and fragile that it is easily moved or lost during collection as the film is wound up on the take-up spool.

Formvar solution is applied to the moving film from a series of small holes in a brass applicator, fed from a reservoir by a controlled speed gear pump. As film speed is changed the supply of solution is increased proportionately. The solution is fed at approximately 0.05 cm^3 per centimeter length of

film to cover a 0.8 cm width. This gives a depth of solution of 60 μm. This dries to a thickness of about 3 μm. The flow rate can be varied by a factor of ten by a potentiometer in the control chassis; the solution thickness and width can be varied (± 100%) by changing the position of the film with respect to the applicator (see I, page 29). For a constant flow, a thicker, narrower coat forms as the film is moved further from the applicator -- and conversely. In the present system this thin solution coat is used to reduce problems of drying and particle motion in the film after collection. It also reduces the tendency for the drying film to blow away under the turbulent conditions of convective cloud sampling. This coat is considerably thinner than that used by MacReady and Todd (1964)[15] where the solution thickness was 5 to 10 times greater.

Use of a solution of high viscosity also prevents particle motion. It may also inhibit particle breakup on impaction by viscous dissipation. The upper limit of solution viscosity is set by the pump delivery system. In practice, a 5% formvar solution worked satisfactorily at temperatures above -20°C; at lower temperatures a 4 1/2% solution was more satisfactory. The viscosity of the solution, influenced by temperature and formvar concentration, was measured at AFGL (Figure 14). The lower limit of viscosity for application is approximately 200 centistokes.

Particles enter the solution 0.1 to 3 seconds after the solution has been applied to the film; this interval depends on the film speed and arm configuration. Drying takes place mostly by the airflow through the drying chamber in that part of the instrument inside the aircraft.

---

[15] MacCready, P.V., and C.J. Todd, 1964: Continuous Particle Sampler, J. Appl. Meteor., 3, 450-460.

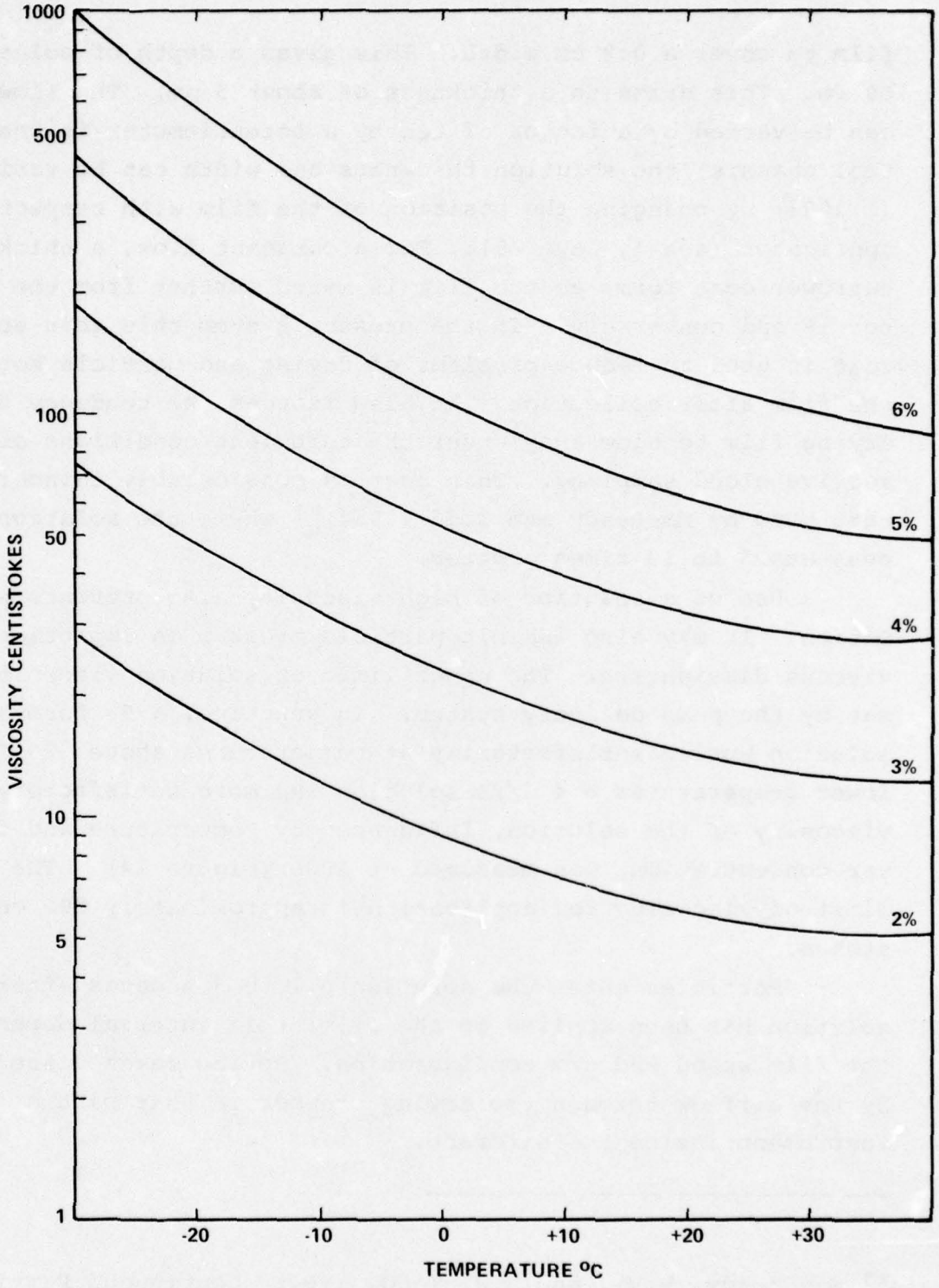

Figure 14. Variation of viscosity of a mixture of formvar and chloroform with indicated % by weight of formvar and with temperature. (after K. Pocs, AFGL).

The thickness of the formvar can be measured directly with a micrometer, or more accurately by a microscope with a vertical calibration. It is best to use a x20 objective to give a small depth of field, and focus on top of the formvar and the uncovered base. A more convenient technique employs an interference objective, with tungsten illumination. This enables the replica over the whole field of view to be examined at one time, and the thickness variations measured simply by moving the interference fringes across the field of view by slight change of focus. Typical variations are ± 10% for a given setting (Figure 15).

The object serves as one plate of an interferometer. Changes of height give rise to a lateral shift of each fringe with a height difference of d giving n fringe displacements, $2d = \frac{n\lambda}{2}$, where λ = wavelength of illumination. The central fringe can easily be located by its color and a monochromatic filter inserted for precise measurement of its position. Figure 15 shows the displacement of fringes at the edge of the formvar film. The bright fringe from the upper surface of the formvar is displaced to the left by about 3.5 fringes; this gives a height difference of $\sim$ 2 μm assuming a wavelength 0.5 μm. Formation of a second set of fringes also occurs by reflection from the base of the formvar; these give a displacement of 2.5 fringes and indicates a thickness d given by $2d(\mu-1)$ and gives a formvar refractive index of 1.4. Knowing this refractive index the formvar thickness may be computed from the separation of the two sets of fringes alone, $2\mu d = \frac{n\lambda}{2}$.

Cloud Drops and Calibration

Although this replicator was primarily designed for the detection of ice particles, it does collect cloud and rain drops. Calibration of drop replicas was undertaken to give a comparison of drop size spectrum from replica and from an instrument using direct optical technique. Uncertainties arise because of larger drop splash on impact and coalescence in the solution. A further complication arises because drops, on impact, even in the absence of breakup, distort and give a replica crater which is somewhat larger than the original size of the drop.

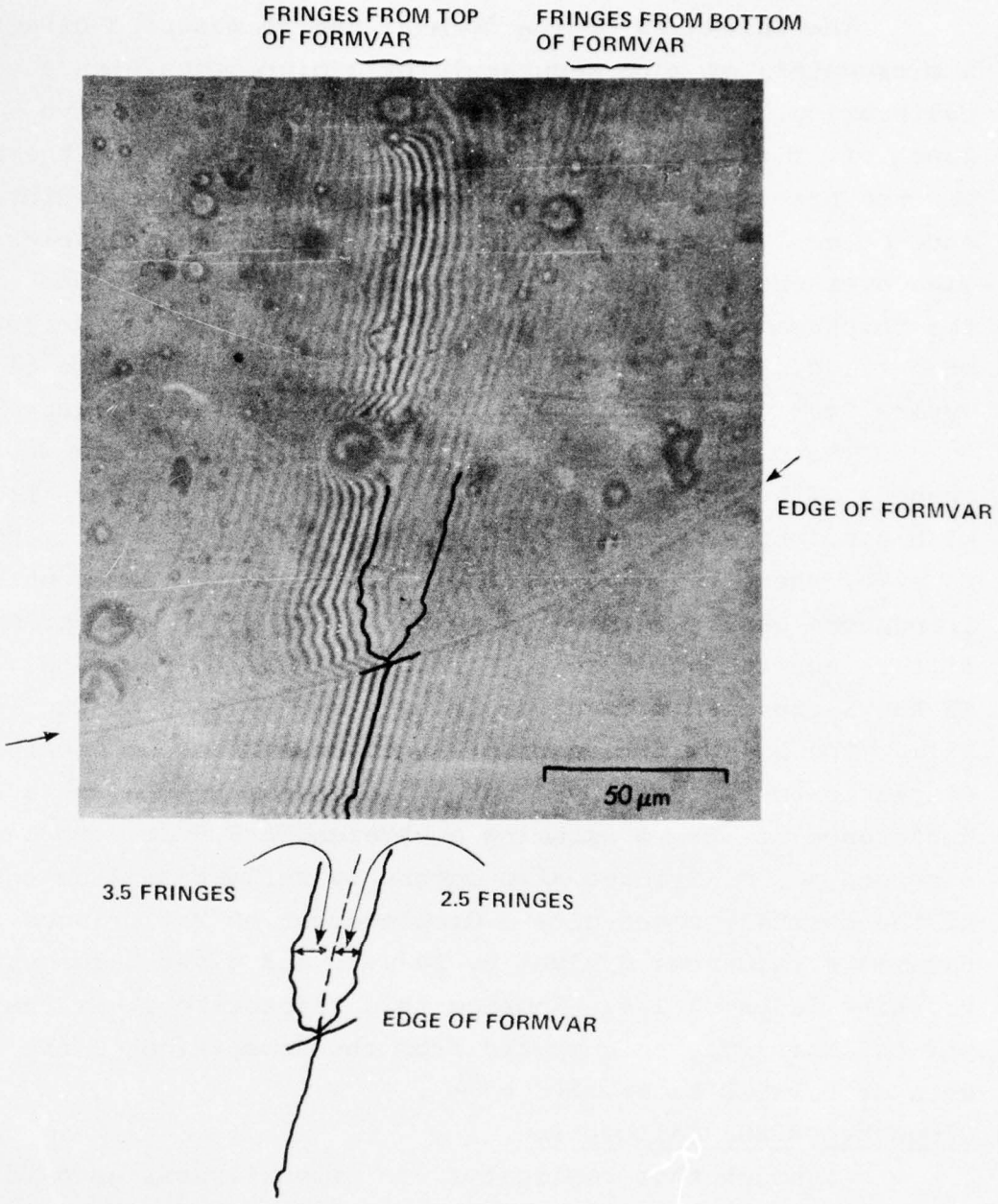

Figure 15. Interference microscope examination of thickness profile of replica. Formvar thickness is given by the number of fringes (n) displaced laterally as it traverses from the bare film to the formvar. The formvar upper profile is given by the bright fringes deflected to the left, $n\frac{\lambda}{2}$. Fringes also form at the formvar base-film boundary, displaced to the right. The thickness is then $n\ (\mu-1)\frac{\lambda}{2}$.

Calibration of this distortion was carried out by MacReady and Todd (1964)[15] who sprayed a suspension of aspergillus niger spore (diameter 3 μ) into their replicator. The number of spores associated with the crater was related to the size of the original drop. Figure 16 shows the calibration curves. Over the whole range of these curves, the solution thickness (200 μm to 400 μm) was greater than the drop diameter.

Significant departure from a direct relation of drop and crater size occurs when the drop diameter exceeds the dried replica thickness. Essentially, the drop size and crater size differ little up to a diameter of ∿ 40 μm; (about twice the dried replica thickness) thereafter the replica diameter is flattened by an amount which depends on the ratio of dry formvar thickness to drop size.

A liquid drop, impacting at sufficient velocity, in a layer of solution becomes immersed. As discussed earlier, very small drops < 5 μm diameter may fail to penetrate the surface on initial impact and be swept to the edge before becoming submerged. As the solution evaporates its depth decreases and two effects can occur. The drop can be flattened to an ellipsoid of revolution (as assumed by MacReady and Todd) until the solution viscosity is sufficient to prevent further shrinkage. Occasionally, the solution may shrink from the drop, to leave the water surface partly open at the top. This latter effect seems at first unlikely, particularly in view of the fact that chloroform on water has a positive spreading coefficient (S initial = +13, S final = +1.3 dynes, Davies and Rideal[16] page 22). However, the effect has been observed to occur in laboratory studies. The result leaves a crater with overhang and an open top, which is slightly deformed.

Interference microscopy provides a powerful tool for examining the detail of the replica. This technique shows that

---

[16] Davies, J.T., and E.K. Rideal, 1961: Interface Science, p. 22. Academic Press, New York.

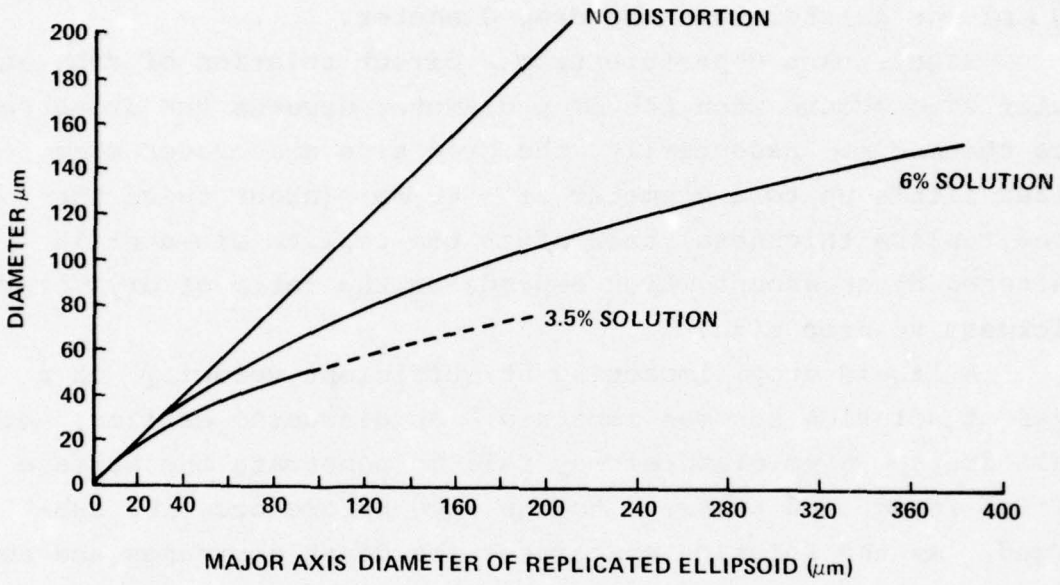

Figure 16. Distortion calibration with aspergillus niger spores. (MacReady & Todd, 1964).

usually drop replica only consists of a crater with side walls, which are vertical at the top of the crater. The thickness of the replica in and around the crater can be investigated by the interference technique. Figure 17 shows examples of drop replicas examined in this way. A cloud drop crater has a center almost devoid of replica with thickness $\sim$ 1/2 μm towards the edge. Outside the main crater the wall rises almost perpendicularly, to a height $\sim$ 10 μm for a 50 μm diameter crater. Preliminary laboratory studies showed that the width remained substantially unchanged during the whole drying procedure of the drop and its subsequent crater.

Drops were produced by an ultrasonic vibrator system and caught in a layer of solution on a microscope slide. Figure 18a shows the original underformed drop submerged in 5%formvar solution of depth somewhat greater than the drop diameter. After drying (Figure 18b) the crater diameter is greater by x 1.25. This ratio holds for the larger drop 200 μm diameter and the smaller drop $\sim$ 30 μm diameter and is at variance with the earlier results. Further work on this calibration as influenced by impact velocity for different solution depths is required.

Figure 19 gives a schematic representation of how the crater forms. The formvar solution layer dries and thins; a very thin layer of formvar covers the water. After a period of 1 to 10 seconds, following the drying of the formvar, the water suddenly begins to evaporate and the upper thin layer of plastic collapses to the base of the crater - often to be colored by interference effects. It is concluded from these studies that, in the absence of splashing, thinner formvar film gives craters with diameter in excess of the original drop by 1.25 ± 0.1 or a calibration factor of 0.8 ± 0.1 over the range 30 to 200 μm diameter. In practice, drops diameter $\gtrsim$ 40 μm will break up or splash on impact, so that calibration of original drop craters is only of importance up to diameter 40 μm. Drops diameter less than 20 μm changed little in diameter as the replica dried. Results are summarized in Figure 30.

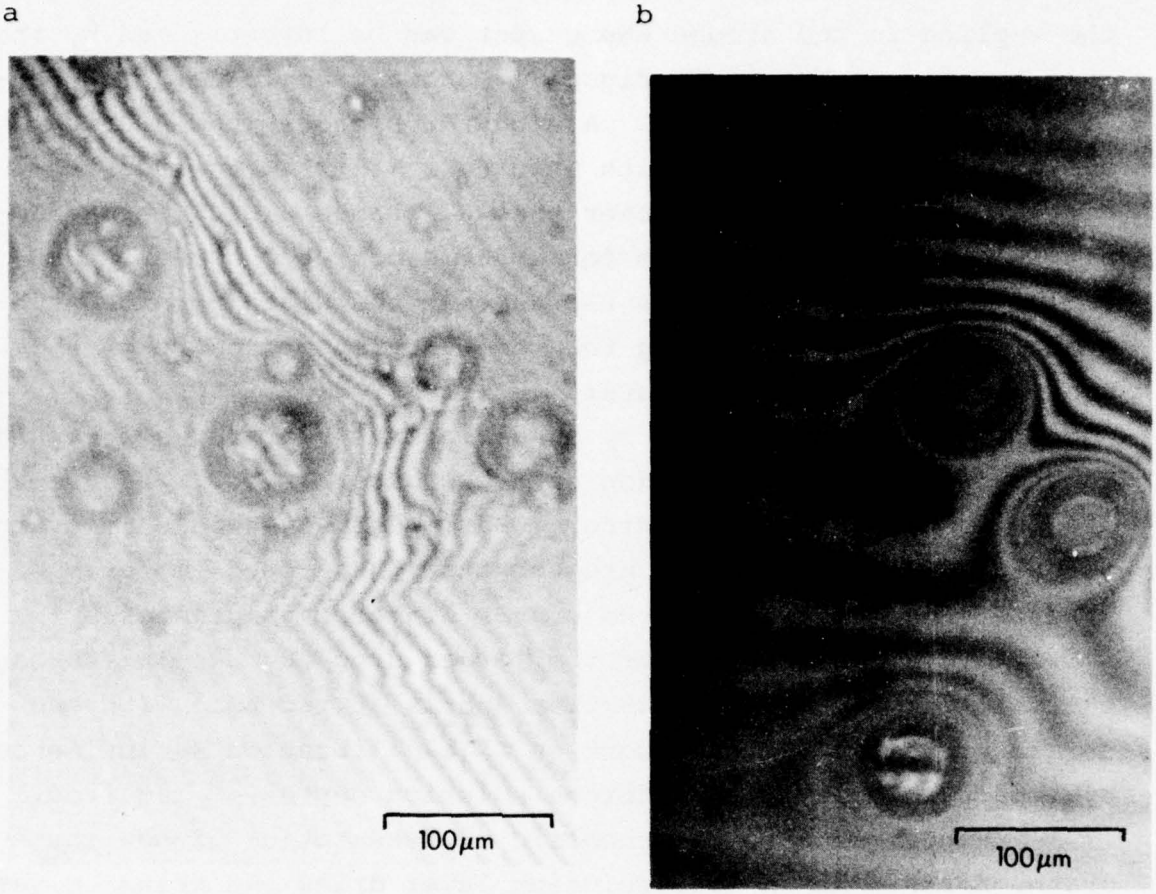

Figure 17. Drop replicas examined by interference microscopy. The central part of the crater is almost flat and consists of very thin replica. This can be seen from the presence of low order fringes (a) which are in line with the fringes external to the replica in the lower part of the picture. (b) shows the same thing for the lower drop. The distribution of fringes around the replica gives the shape (see Figure 19d).

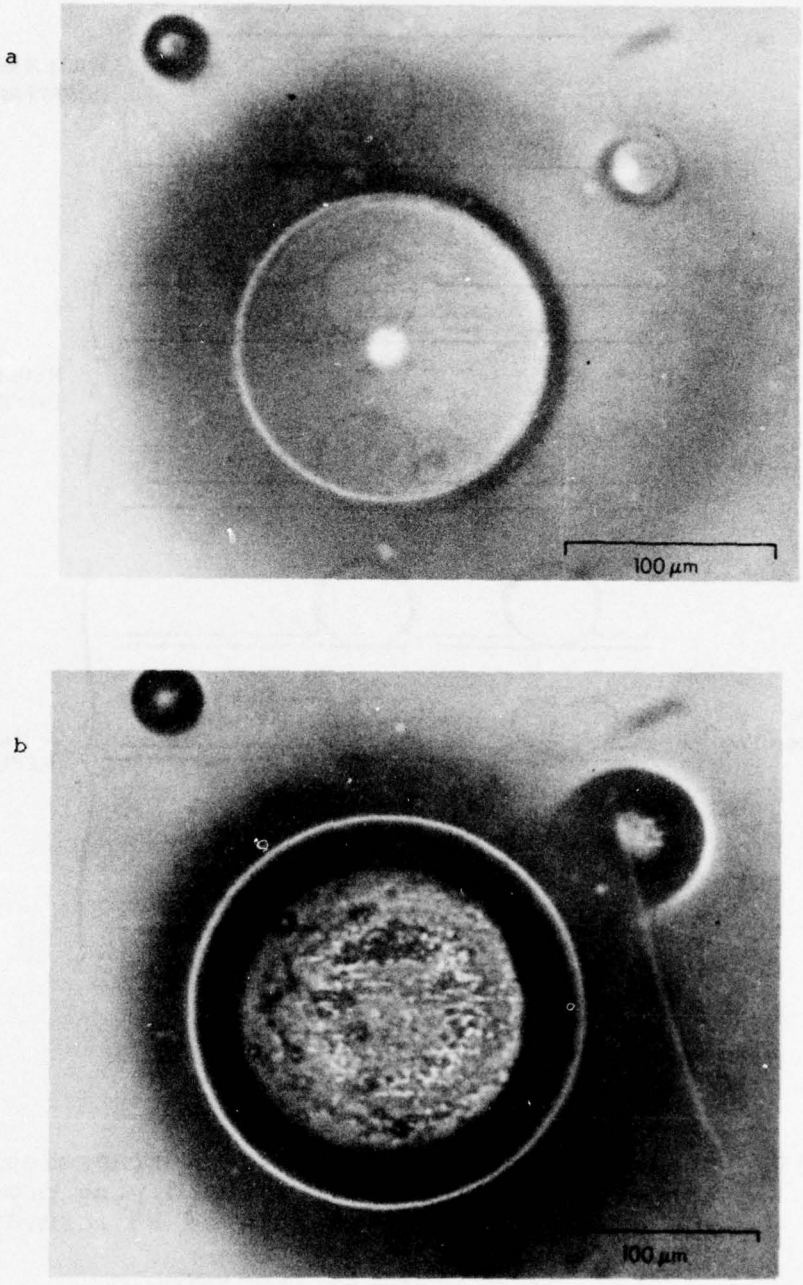

Figure 18. Spherical cloud drops in a layer of formvar solution (a) and the replica after drying (b). The replica crater is about 1.25 times the original drop diameter.

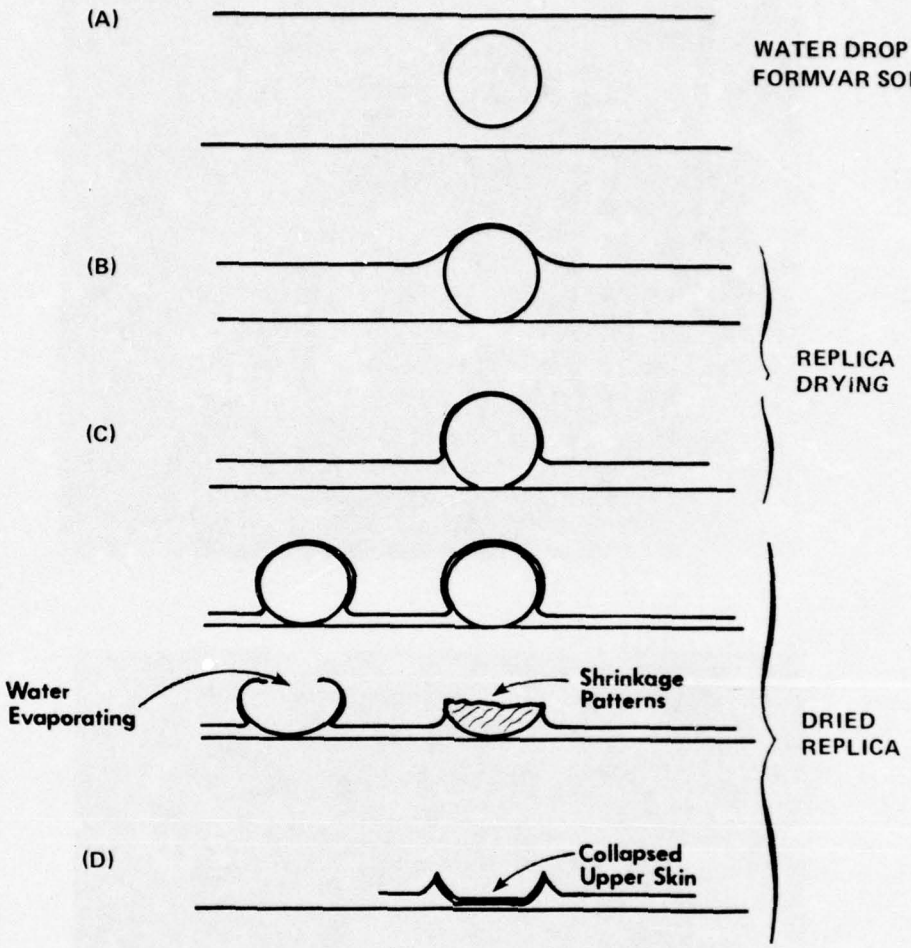

Figure 19. Schematic representation (from transmission and interference microscopy) of the drying process of a 100 μm drop in a thick film of 5% formvar - chloroform solution.

(a) initial total immersion.
(b) formvar partly dry with thin layer covering the protruding water drop.
(c) formvar completely dry. Sometimes the formvar fails to cover the drop completely (left) and leaves a hole for the water to evaporate. In either case the thin formvar layer collapses as the water evaporates.
(d) dry formvar shape after water has evaporated. The thin formvar layer has collapsed to the bottom of the crater.

Ice Crystals

Unbroken ice crystals leave craters which are almost identical to their original dimension; there appears to be a slight shrinkage (5%) of the formvar on complete drying. Replication of planar crystal surfaces is usually quite evident. Planar crystals less than 100 μm diameter are usually replicated in good condition. Larger planar crystals break on impact, but nevertheless retain their original shape. Cracks often run parallel to the crystallographic axes (Figure 20). Crystals of size exceeding 100 μm give cracked replicas (Figure 21a,b) which, nevertheless can easily be recognized as a single original particle. Larger particles and snow crystals which extend in three dimensions, are more liable to shatter on collection. This can give rise to many hundreds of particles. Each particle usually has a sharp edge, often with angles which do not bear any relation to simple crystallographic directions. Collision with the slot edge apparently gives a similar effect. With some imagination in interpretation, and particularly when particle density is low so that these fragmentation patterns do not overlap, it is possible to relate each pattern to a single particle. Often with these patterns, a central area is completely cleared of replica. This may be interpreted as the initial impact of the particle and taken as approximating its original diameter, as in the case of larger raindrops (page 52), (Figure 22); a spread of x2 to 3 of the graupel particle occurs on impact (Figure 30) and probably increases with impact velocity.

An intermediate situation exists when a three dimensional system - as spatial prisms or dendrites - impacts; these arms collapse on top of each other and give a two dimensional "projection" of its original shape (Figure 23a,b).

As described in the section, COLLECTION OF ICE CRYSTALS (page 35), ice crystals may orient themselves 90° to the shear and parallel to the film prior to impact. These crystals presumably are the ones which give the more perfect replicas. Figure 23c shows a column replica viewed by interference microscopy. The position of the fringes in the crater compared with

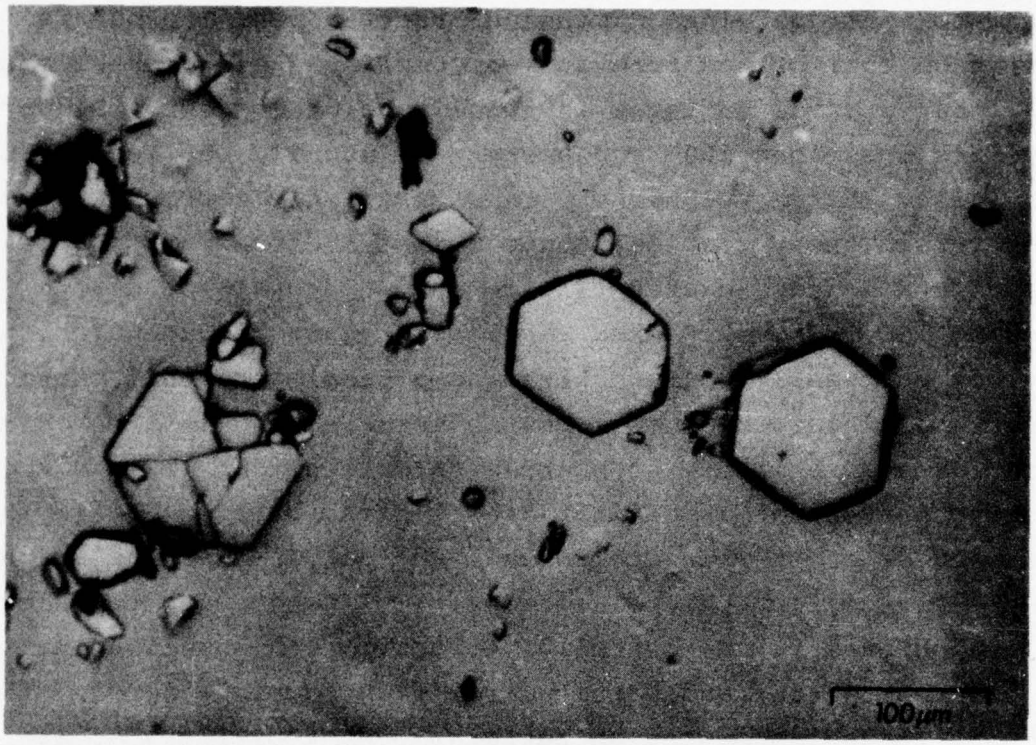

Figure 20. A cracked and uncracked plate. Cracking becomes evident for diameter $\gtrsim$ 100 μm.

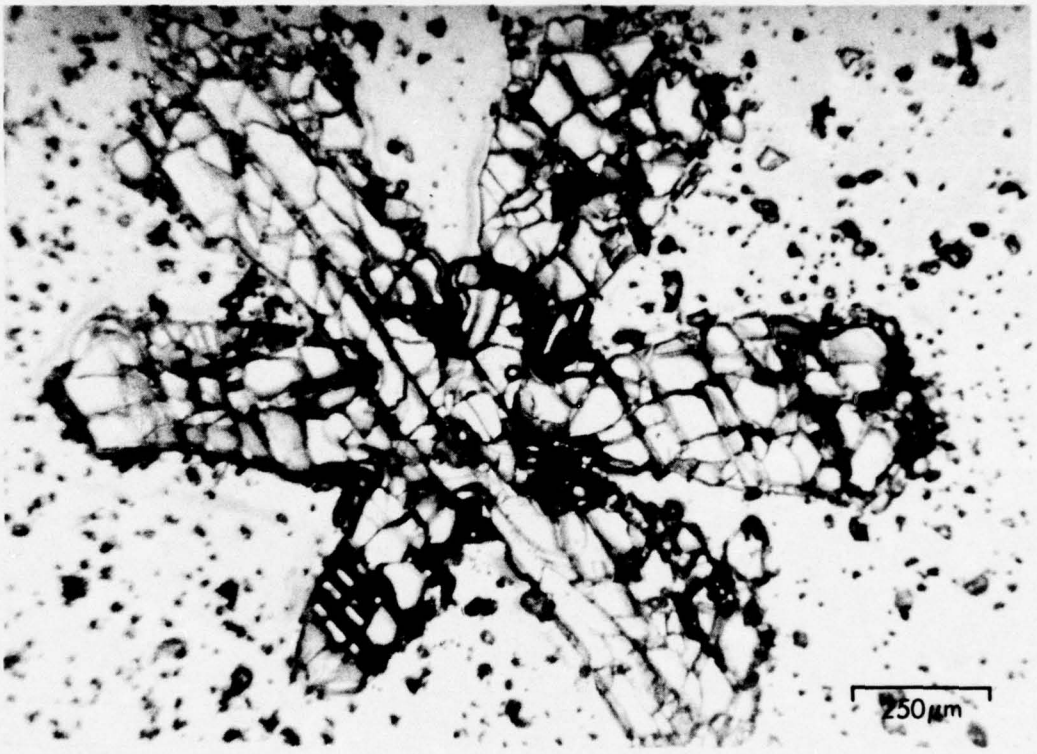

Figure 21a. A sector plate, just prior development to a dendrite, cracked on impact parallel to crystallographic axes.

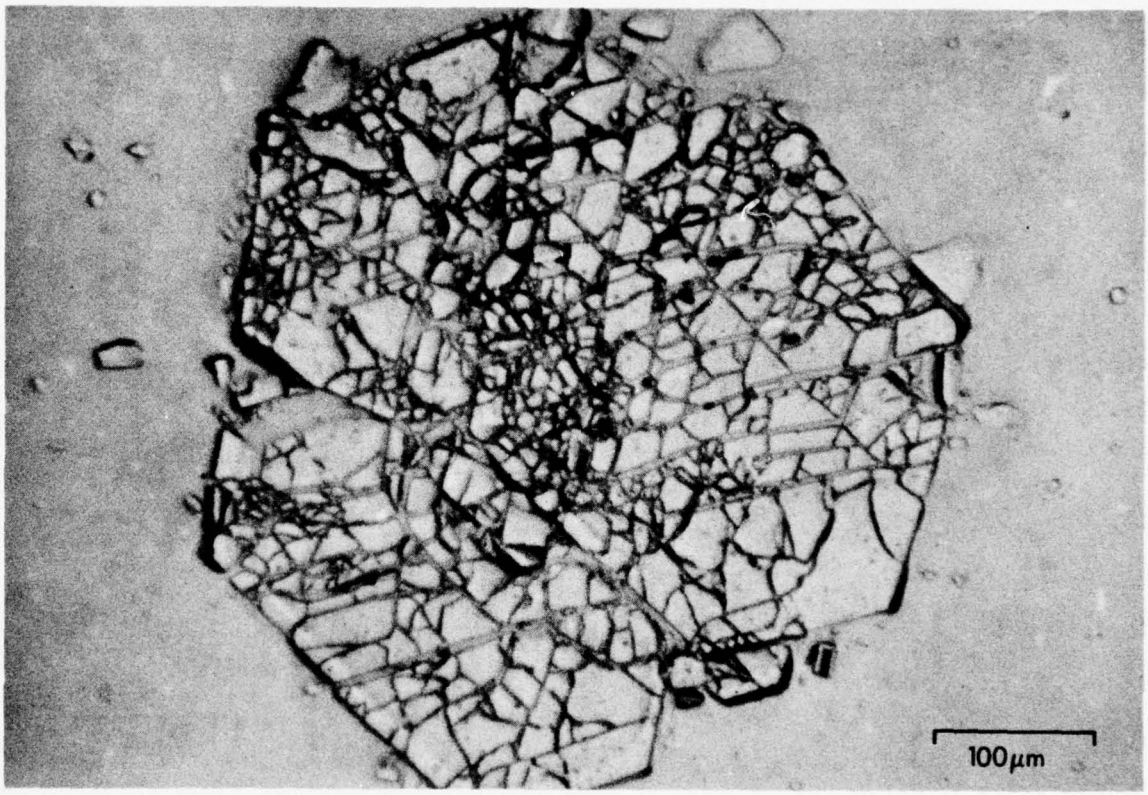

Figure 21b. Large plate cracked on impact. Cracks are parallel to crystallographic axes.

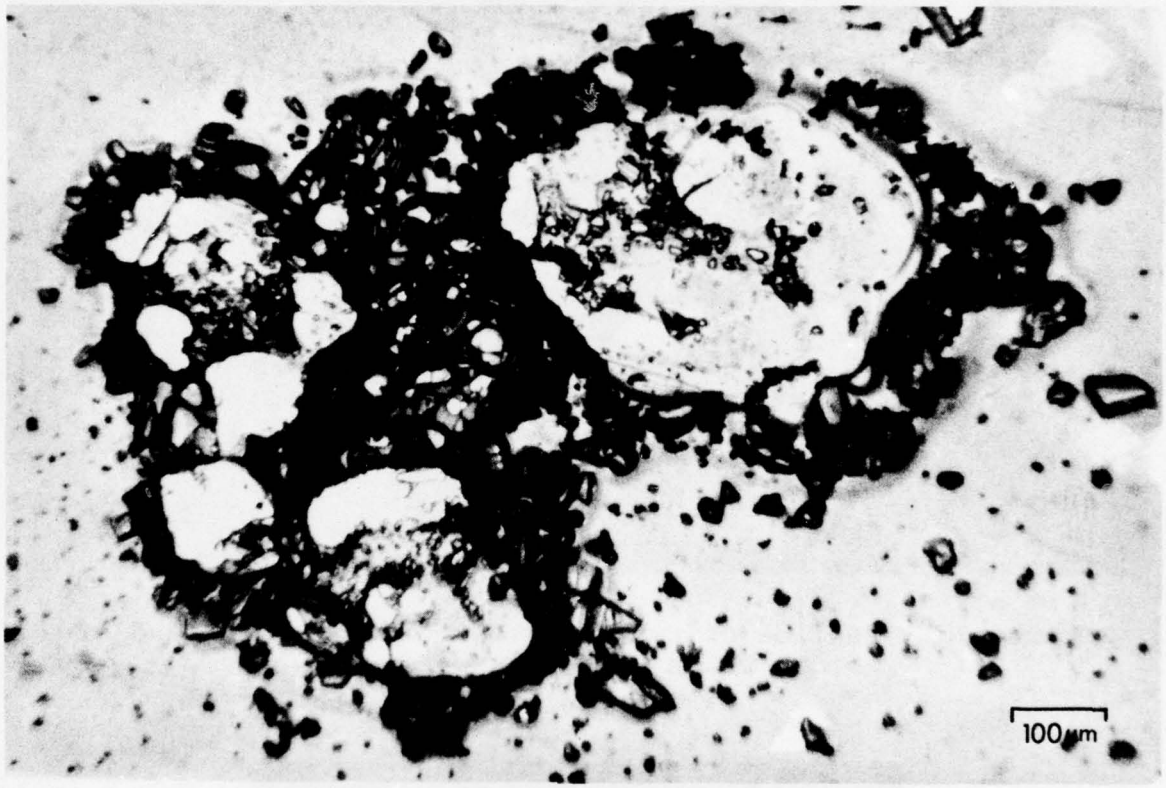

Figure 22. Impact crater of a large irregular graupel particle. Small particles which show flat crystal facets show evidence of some crystal growth from the vapor.

Figure 23a. Replica of two dendrites grown on each end of a column which collapsed on impact.

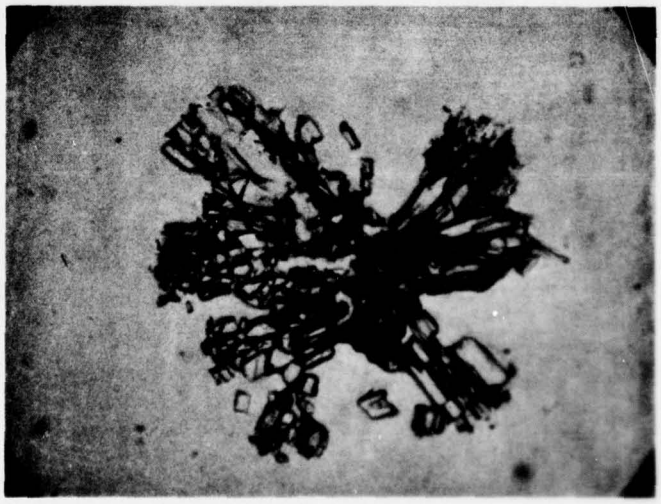

Figure 23b. Replica of spatial column formed by collapse on impact.

100 μm

Figure 23c. Interference microscope analysis of column replica showing that the center part is almost devoid of replica. The surrounding walls rise to a height of ∿ 20 μm, estimated from the fringe position on top of the wall.

fringes beyond the replica edge showed that the crater was almost devoid of replica. Examination of many column crystals of size $\sim$ 100-200 μm shows that the impact process may be more complex. In some cases (30%) crystals in this size range are associated with a depression in the formvar, about 500 μm distant. The shape of this depression may be investigated by interference microscopy (p. 63 , Figure 27a,b). This is quite different from any drop crater; it has smooth edges and no crater wall. The association of these crystals and depressions suggest that the crystal has bounced, without shattering and formed a good replica a short distance away. A further complication can arise for very small crystals - as for very small cloud drops. Laboratory studies have shown that crystals size $\lesssim$ 20 μm sometimes float above the solution surface presumably supported by the flux of evaporating chloroform. These may move to the edge of the solution and float away without being replicated. Since this only appears to happen for drops diameter $\sim$ 5 μm, it might be anticipated that only crystals $\gtrsim$ 10-20 μm dimensions would have sufficient momentum to enter the solution during aircraft collection. The possibility of loss in this way (in addition to the collection problem) for crystals of this size must always be borne in mind.

The replica detail readily gives information on the presence of flat crystal facets and the occurrence of riming; the replica size of drop should reproduce that in the ice particle - although the original size of the cloud drop, before accretion and deformation on the ice particle, must be inferred from the impact velocity on accretion (Figure 24a,b).

A summary of ice crystal and droplet replica characteristics is given in Figure 25. In all cases estimates of the original thickness, shape and density of ice particles is open to interpretation; this must put together all information available for its final reconstruction and is discussed later.

a

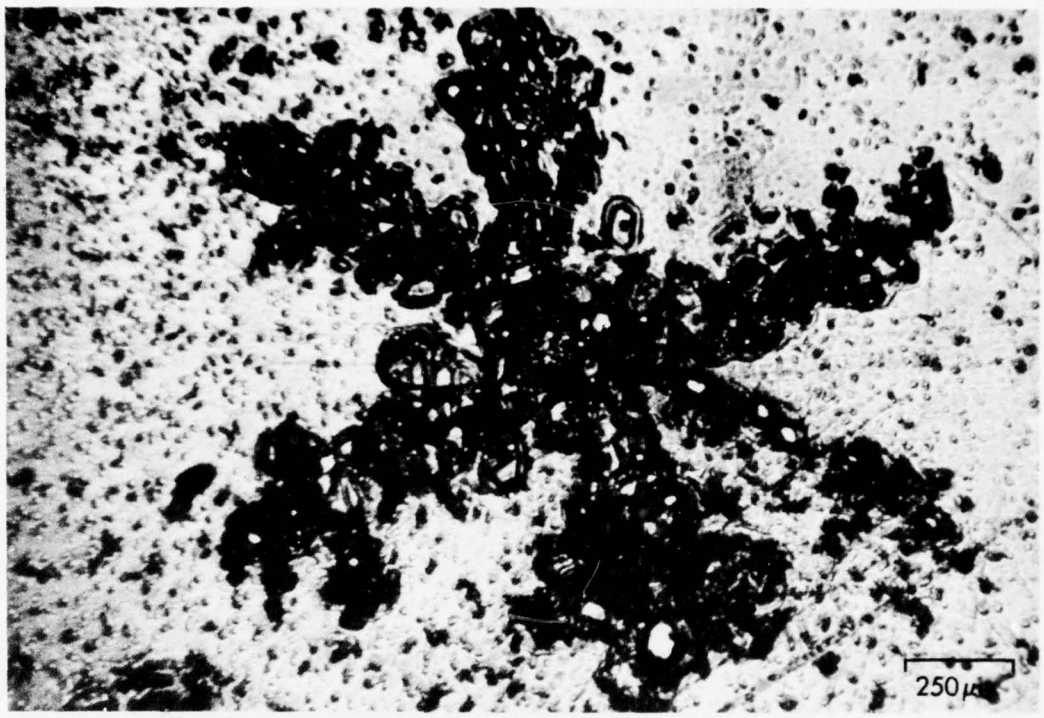

b

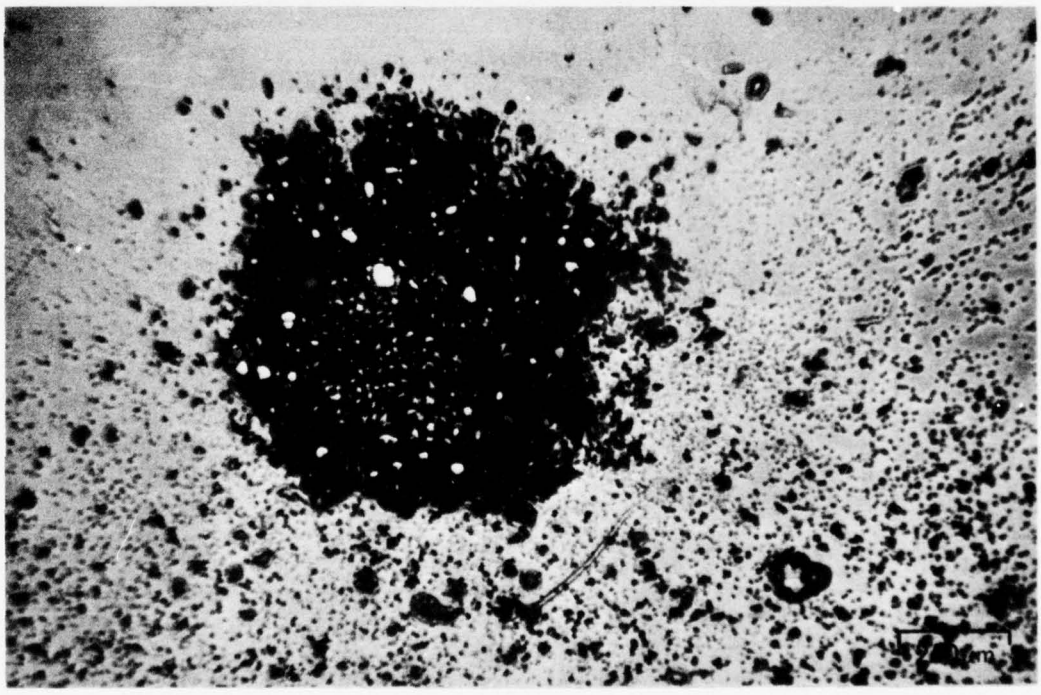

Figure 24a,b. Rimed dendrite and graupel particle. Drop size can be inferred from the size of irregularities on each particle.

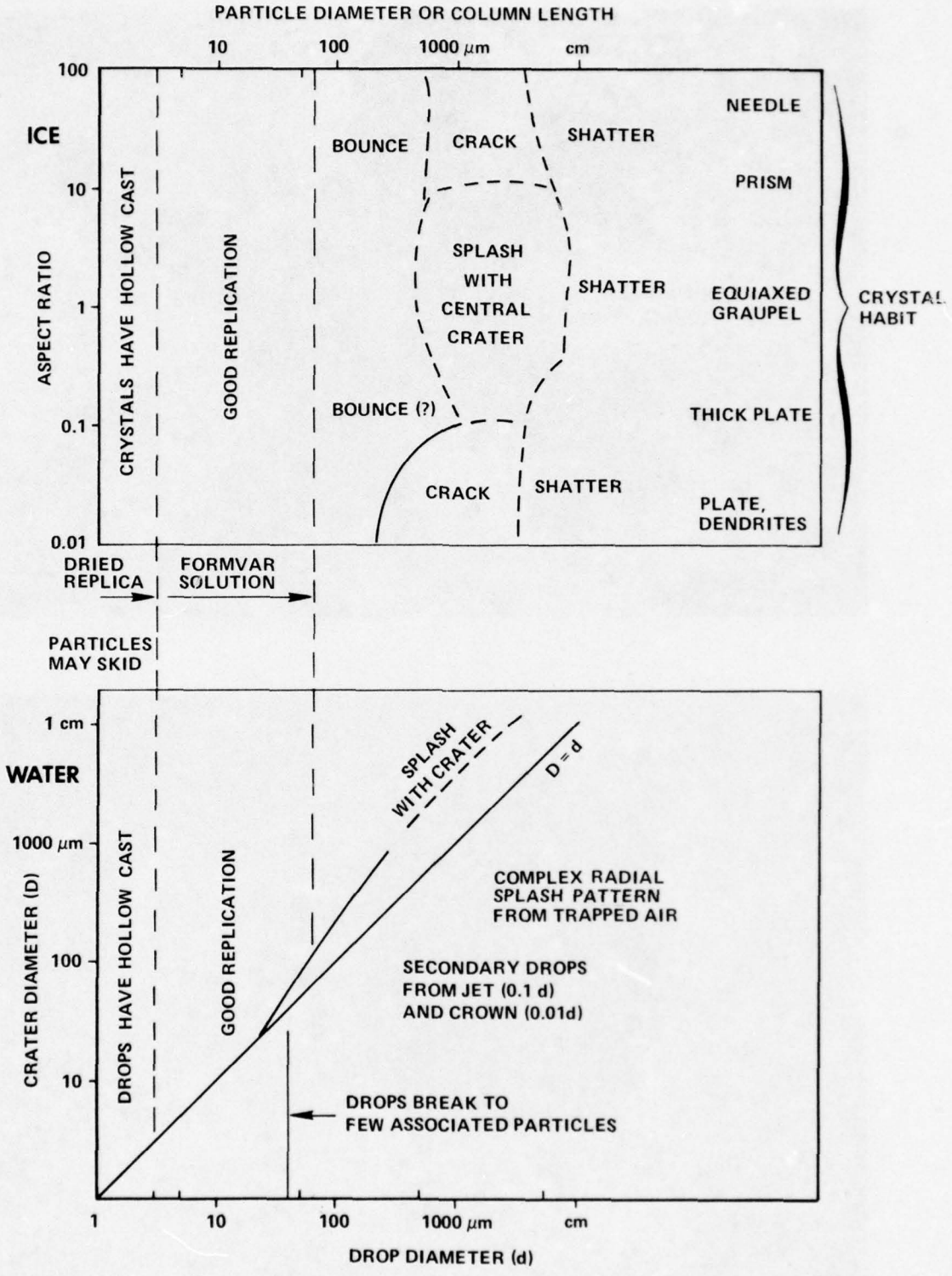

Figure 25. Replica characteristics for solid and liquid precipitation particles at collection velocity $\sim$ 100 m s^{-1}.

VIII. ARTEFACT

Ice crystal growth and drop condensation sometimes occur on the drying replica. The following possibilities arise:

(a) Blushing. The rapid evaporation of chloroform reduces the solution temperature below ambient dewpoint. Taking the wet bulb depression equation and substituting values for chloroform,

gives a depression $\Delta T = \frac{L\varepsilon\ \Delta e}{C_p P}$

$L = 58$ cal g^{-1},	Latent heat of evaporation of chloroform
$\varepsilon = \frac{119}{30}$,	Molecular weight ratio to air
$\Delta e = 10$ mb	Excess vapor pressure of chloroform over environment
$P \sim 500$ mb	Ambient air pressure
$C_p \sim 0.2$ x water	Specific heat

gives $\Delta T \sim 20°C$

This sometimes leads to condensation of water drops from the surrounding air. Typically diameter is 1-2 μm with separation of the same dimension. This is termed "blushing" by MacReady and Todd, 1964.[15] It gives the replica a brownish appearance, and occurs preferentially in those regions where the replica is thicker. This process tends to give brownish areas a few mm across which occur with some periodicity. Collected small drops on the other hand are replicated uniformly with respect to the slot.

(b) Drop Freezing and Ice Crystal Growth. As the temperature of the drying replica falls well below 0°C, selected drops - those containing appropriate nuclei - may freeze, and grow from the vapor at the expense of neighboring drops to form quite distinct ice crystals. These are often in the form of curved dendrites, as on a frosted window pane, and are quite different from natural snow crystals. These crystals grow directly from overlying moist air from neighboring unfrozen drops

or from water dissolved in chloroform. Figure 26a,b,c shows beginning growth of such crystals. To prevent problems of this kind, the formvar solution should not contain water or be exposed to a moist environment; if the air drying system is functioning correctly, these problems should not occur. The solubility of water in chloroform is ∿ 0.1% at 20°C lowering to .01% at -40°C which could alternatively lead to slight dissolution of ice or water drops. Should the temperature drop below -40°C, all drops freeze and give an appearance of small angular particles ∿ few micrometers across. Occasionally ice particles form where the replica rubs on a piece of grit. This gives a line of such crystals running along the film and is easily distinguished from collected crystals.

(c) Bounce. Ice particles size ∿ 100 μm sometimes bounce as they impact on the replica and re-enter it some few hundred micrometers away. Evidence for this comes from shallow depressions with gently sloping sides associated with these replicas (Figure 27a,b).

(d) Air Bubbles. Sometimes air bubbles are trapped in the replica and can be mistaken for drops. Air bubbles tend to be large - 50 to 200 μm and may form, as do some artefact ice crystals, with regularity caused by replica rubbing before it dries. Bubbles also may form should a leak occur in the formvar line, or a large piece of grit be lodged under the applicator. In all these cases, bubbles will occur with some periodicity and be lined up along the film. In analysis any periodic linear array should be regarded with suspicion.

(e) Drop Breakup and Splash. Drops with diameters greater than ∿ 40 μm break into several comparable size drops on impact which tend to remain together (Figure 28). Larger drops of 0.5 to 1.0 mm diameter give spectacular spoked splash patterns which can easily be recognized (Figure 29). The pattern diameter is 5 times the initial drop diameter (d) which is indicated by the central replica free area. The larger drops give rise to a number of smaller drops ∿ 0.01 d (d = initial drop diameter) by breakup of the splash edge, which may travel

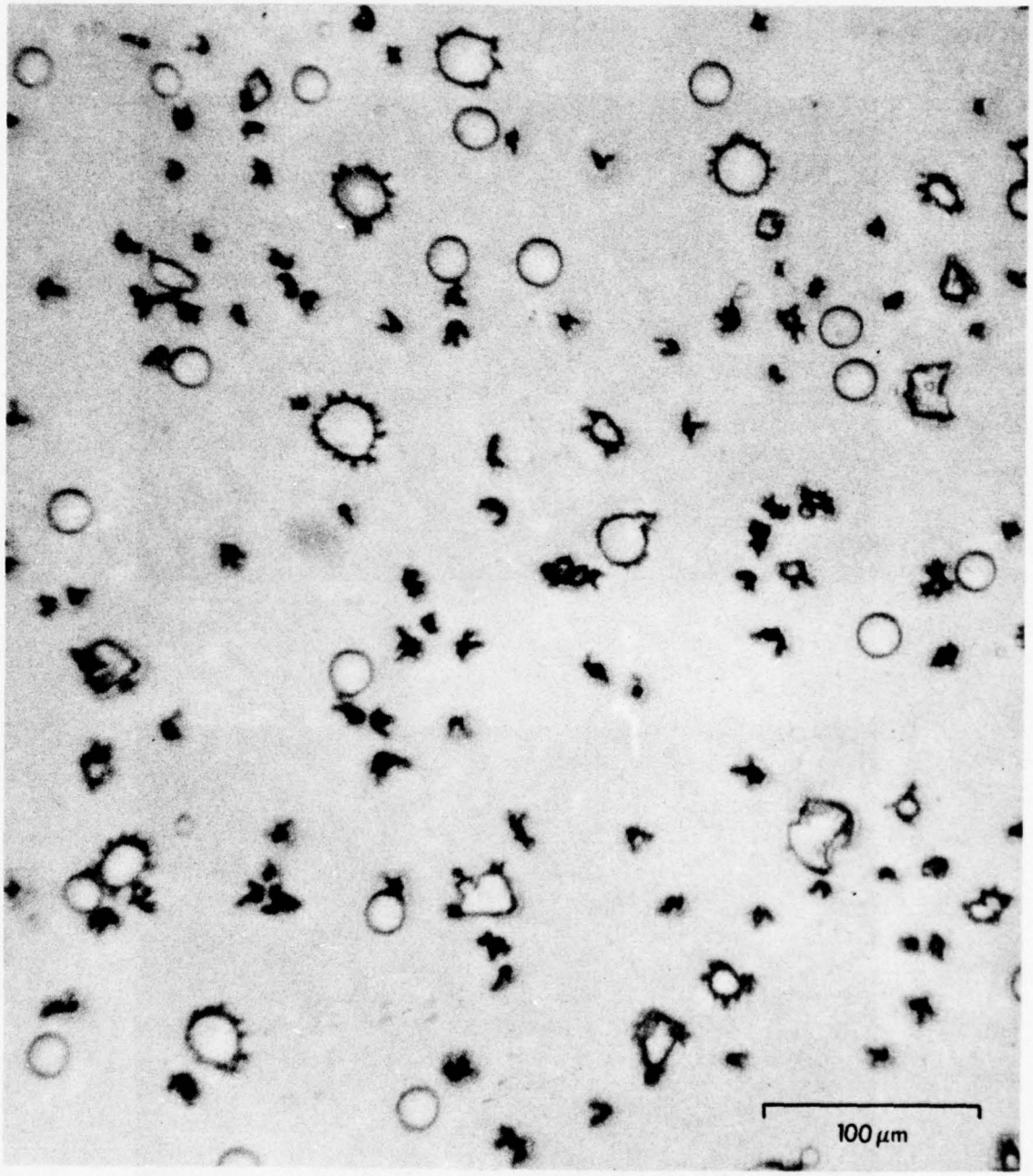

Figure 26a. Ice crystal growth from solution on frozen droplets and fractured ice crystal particles; some drops did not freeze and show complete absence of crystal growth.

b

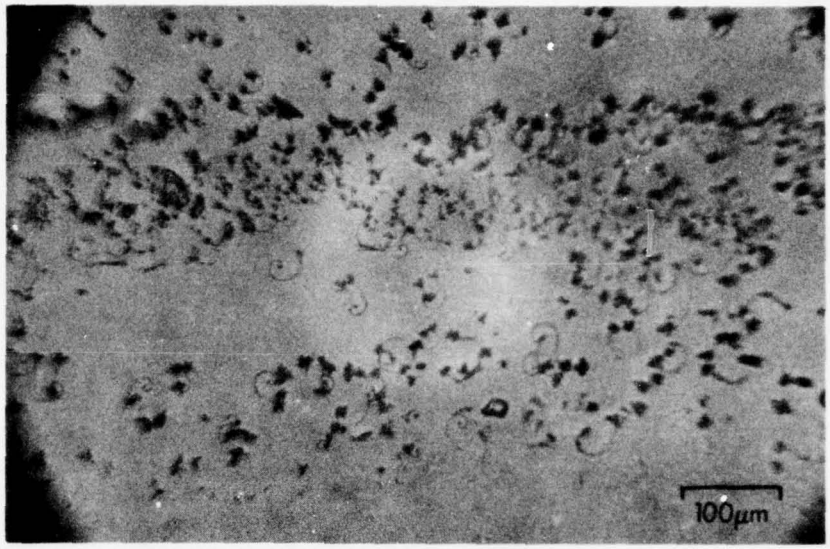

c

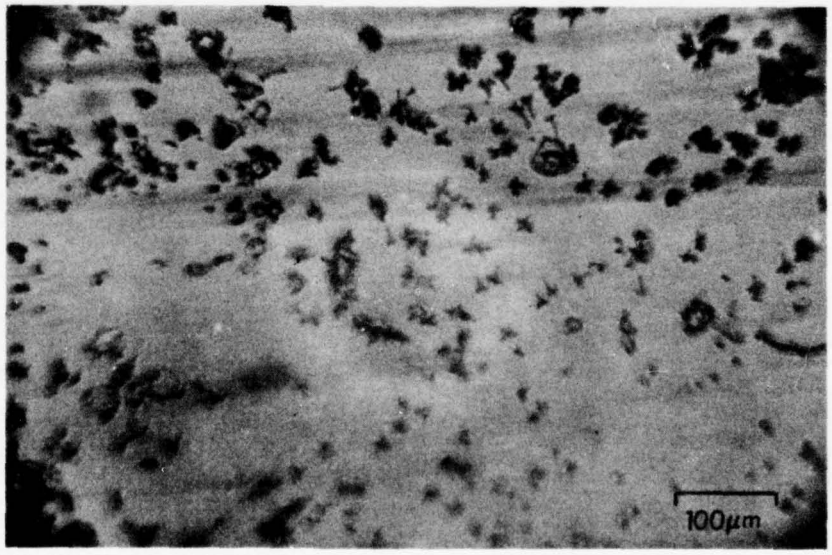

Figure 26b,c. Other forms of ice crystal growth from formvar solution.

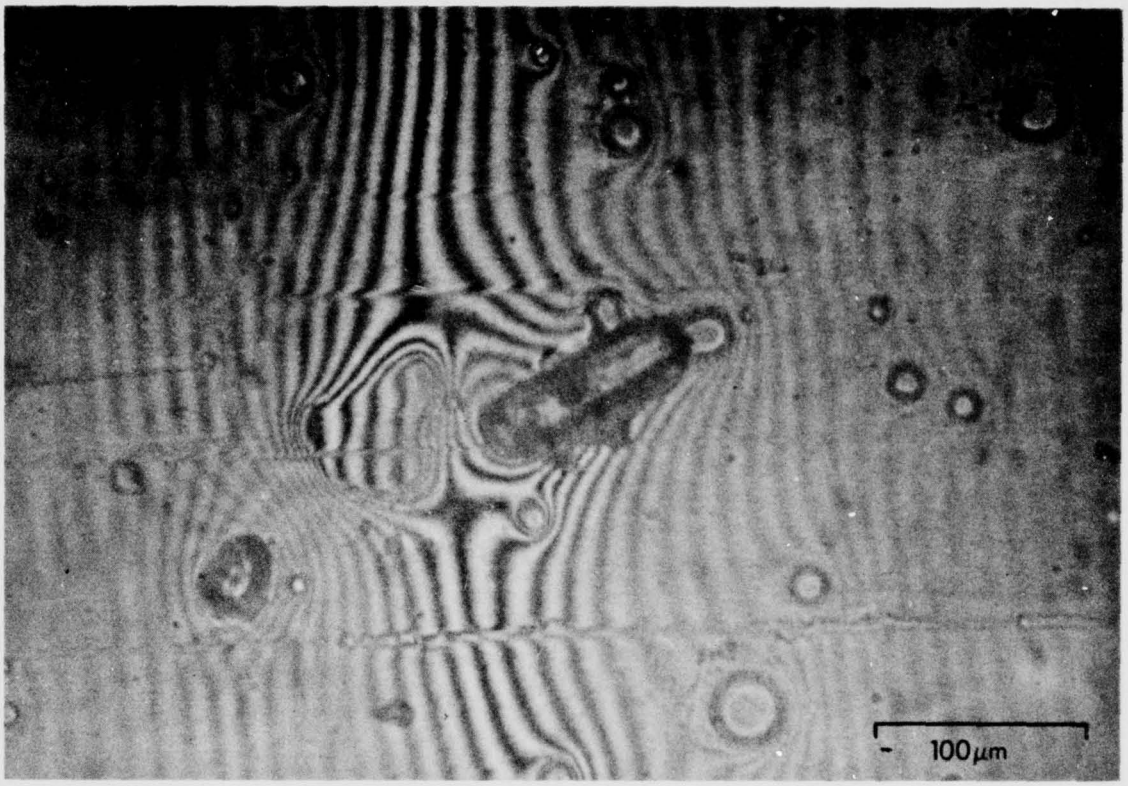

Figure 27a. Bounce crater left by column revealed, by interference microscopy. Arrows show crater. Column replica is in center.

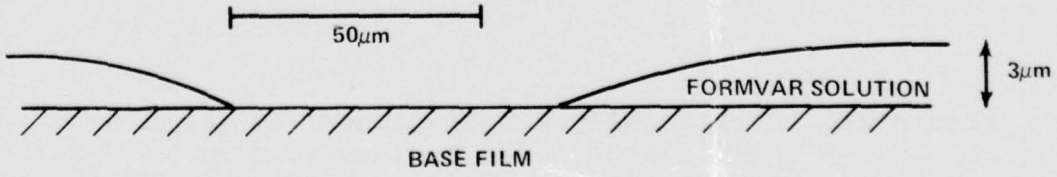

Figure 27b. Shape of an ice crystal bounce crater, showing gently sloping walls.

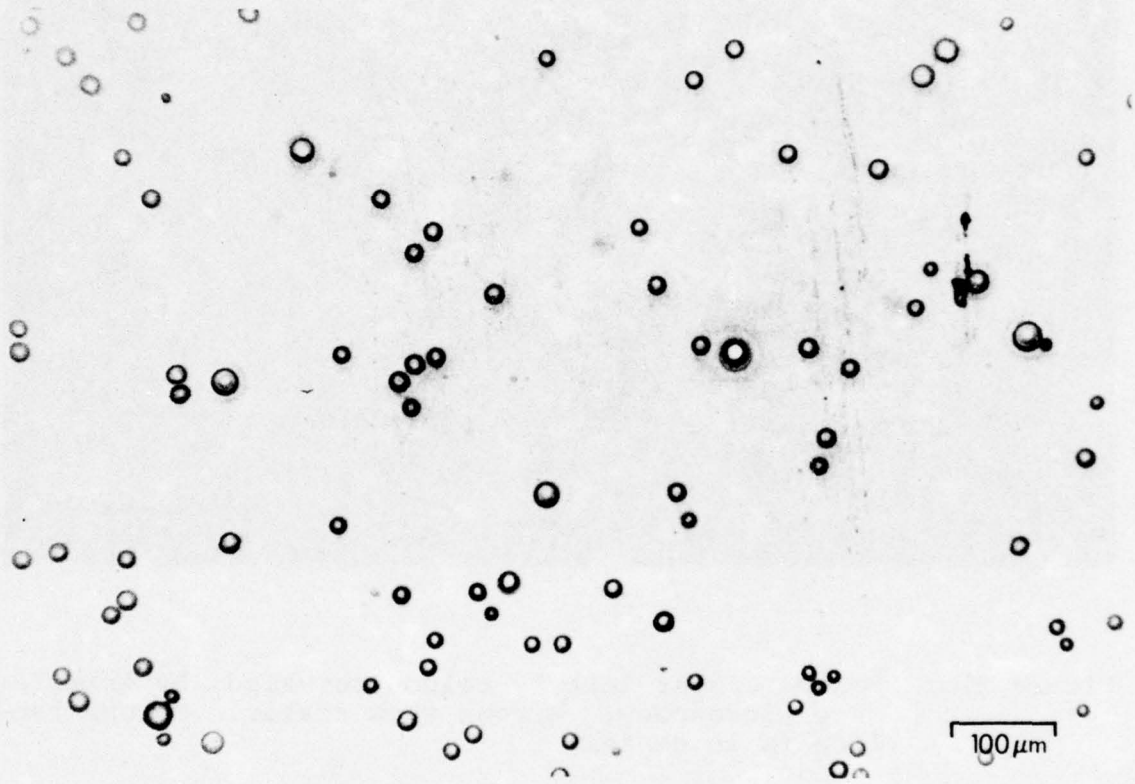

Figure 28. Occasionally association of drop pairs or triplets of diameter ∿ 30 μm suggests that they formed from a drop diameter ∿ 40 μm which divided on impaction.

(a)

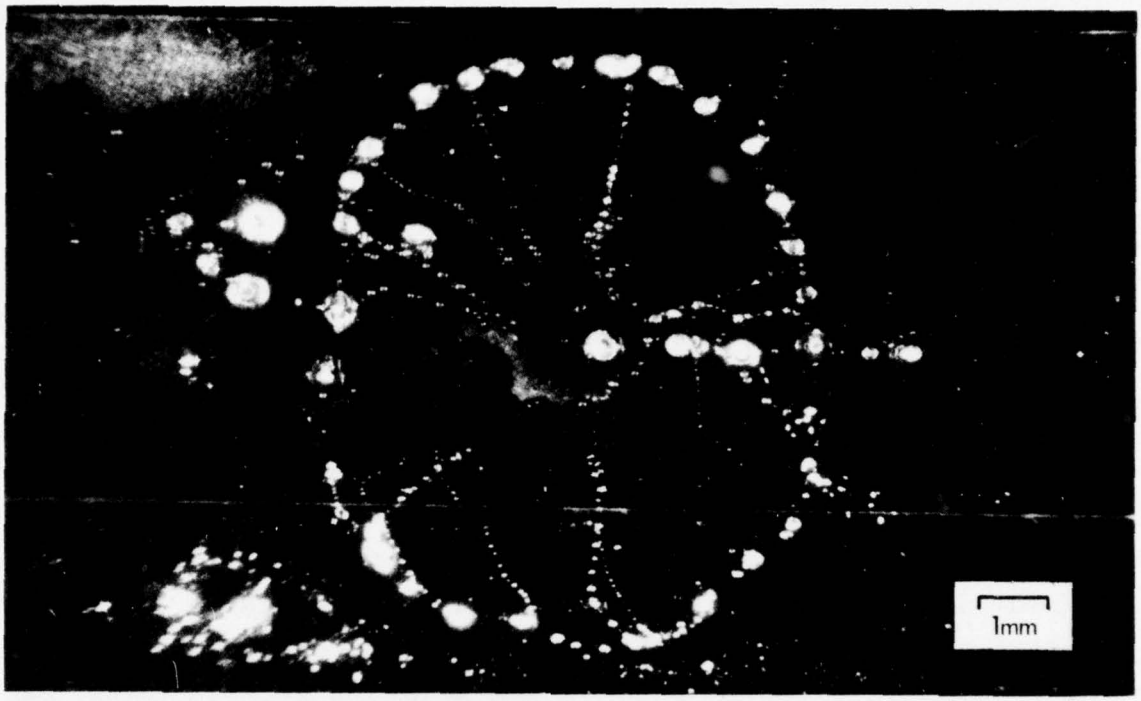

Figure 29a. Radial Splash pattern from a drop ~ 1.0 mm diameter. Splash products travel over 10 mm from the impact site. *Replica is removed from the central* initial impact area which gives the size of the original drop.

(b)

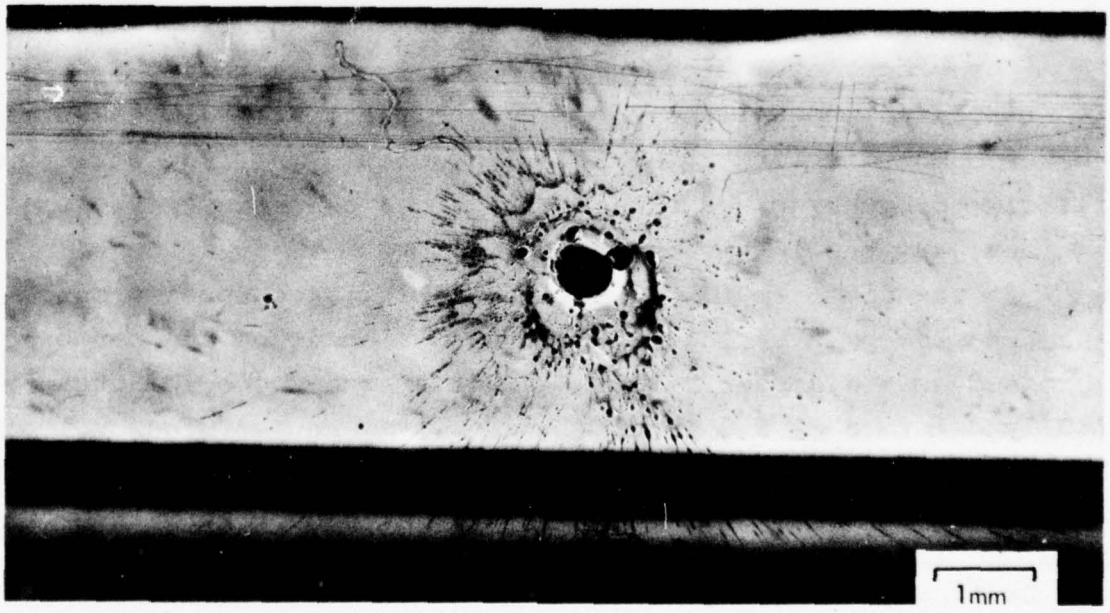

Figure 29b. Higher impact velocity gives more catastrophic *breakup.*

a considerable distance and be replicated several centimeters from the original impact point. As the splash drop retracts, under surface tension forces, a central jet may also form giving rise to several drops diameter $\sim$ 0.1 d which may be replicated nearby. The detail of drop breakup is influenced by the drop size and impact velocity (through the splash index or Weber Number, the ratio of kinetic to surface energy), the formvar solution thickness, and the formvar solution viscosity through its concentration and temperature. This breakup process takes place for drops even though they may be supercooled; splash patterns of this kind collected at air temperature well below 0°C gives good evidence for the presence of supercooled raindrops. The splash takes place in a time short (0.1 m s) compared with the time taken for such a drop to freeze (20 m s at -20°C). The physics of the splash process changes as the drop diameter significantly exceeds the solution depth. Drops smaller than this depth enter the solution without breakup providing the impact Reynolds' Number (characterized by its impact velocity and water kinematic viscosity) is less and about 3000 (Table I, page 67). This is a criterion consistent with that required for a water drop to enter a plane water surface and propagate as a non-turbulent, expanding and decelerating vortex ring (Christensen and Hallett - to be published). In all cases the Weber Number is large compared with unity. The drop will be more likely to break up and splash the larger the entry Reynolds' Number, and the larger the Weber Number.

The diameter to which an impacting drop spreads on impact has been investigated by several techniques and can be expressed as a diameter ratio. Raindrop size drops impacting almost fully deformed at 0.9 terminal velocity were measured by impacting drops on a cold plate and examination of the frozen remnants (Bari and Hallett, 1973)[17] to give a value between 0.18 and 0.2;

---

[17] Bari, S., and J. Hallett, 1973: Nucleation of Air Bubbles at a Growing Ice-Water Interface. J. Glaciology, 13, 489-520.

TABLE I.

1 drop diameter (d) cm	μm	2 Impact Velocity (V) cm s^{-1}	3 Kinematic Viscosity (ν) cm^2 s^{-1} (water)	($CHCl_3$)	4 Impact Reynolds' Number (water)	5 Impact Reynolds' Number (formvar)	6 Weber Number $\frac{dV^2}{1000}$ (a) air	(b) * $CHCl_3$
10^{-4}	1	10^4	0.01	2	100	0.5	10	50
10^{-3}	10	10^4	.01	2	10^3	5	100	500
10^{-2}	100	10^4	.01	2	10^4	50	10^3	10^3
10^{-1}	1000	10^4	.01	2	10^5	500	10^4	5.10^4

TABLE I. SPLASH INDEX Kinetic energy/Surface energy. $\frac{1/2\ 4/3\ \pi r^3\ \rho_L V^2}{4\ \pi r^2\ \sigma} \simeq \frac{(dV^2)}{(1000)}$ and impact Reynolds' number for water and formvar.

$2r = d$ = drop diameter

σ = surface tension air-water

* Increase assuming lower surface tension by X 0.2 for drop immersed in chloroform.

Langmuir (1961)[18] found a value of 0.17 for drops on soot at about 0.5 terminal velocity. This is to be compared with 0.86 found by May (1950)[19] for cloud drops in MgO and 0.8 for drops in formvar described earlier. These results are assembled in Figure 30.

(f) Droplet Coalescence and Rafting. Should droplets coalesce in the solution following almost simultaneous impact, no evidence remains in the dried formvar. This effect can be substantially reduced by ensuring a low areal coverage of drops and correcting the drop distribution for the probability of a simultaneous impact. With too great a solution depth, drops and crystals move around before drying is complete and give rise to agglomerates of drops which, with small numbers, are similar to those formed when small drops break on impact (Figure 31). With the present system this problem is reduced to a minimum by ensuring that the initial solution thickness does not exceed $\sim$ 50 μm. Under these conditions agglomerates are confined to splash effects.

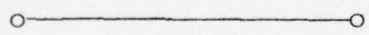

A summary of drop and crystal interactions is given in Figure 25.

---

[18] Langmuir, I., 1961: Mathematical Investigation of Water Droplet Trajectories. Collected Works, 11, 335-393.

[19] May, K.R., 1950: The Measurement of Airborne Droplets by the Magnesium Oxide Method. J. Sci. Instru., 27, 128-132.

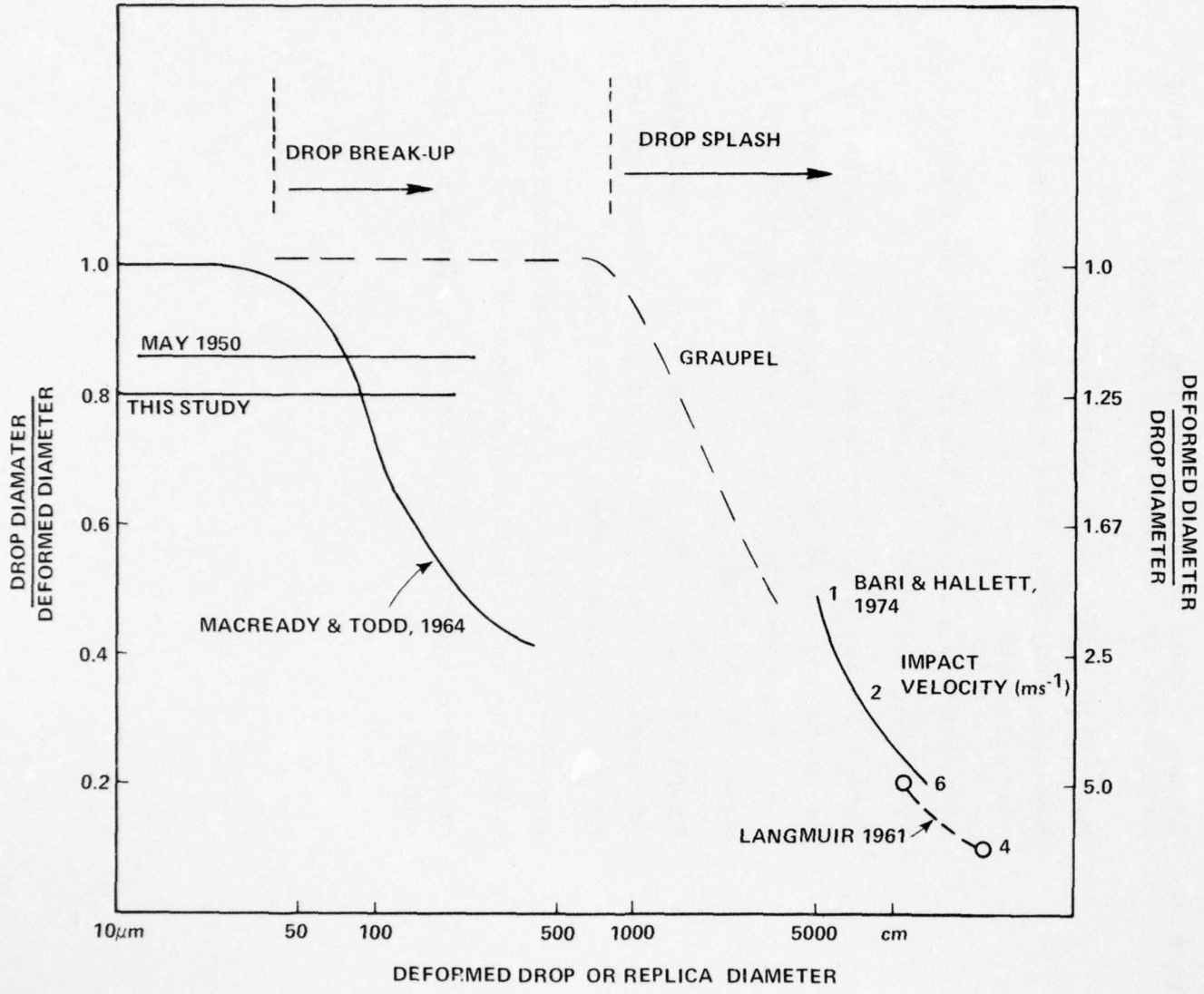

Figure 30. Summary of crater/drop calibration. Deformed drop or replica diameter.

Figure 30. Impact crater diameter related to original drop size found by various investigators.

May, 1950 - MgO, wide velocity range.

MacReady and Todd, 1964 - 60 μm formvar solution (6%), 25 m s^{-1}.

This study - page 45, 100 μm deep, 5% formvar solution, terminal velocity.

Bari & Hallett, 1974 - drops on copper plate at velocity indicated (m s^{-1}), diameter represents that of a coherent disc, the periphery of which shed smaller drops.

Drops diameter > 40 μm break up to a small number of comparable size drops; drops > 500 μm splash to give a large number of small drops.

Langmuir, 1961, 10, p. 255 - water on vaseline coated slide at velocity indicated (m s^{-1}).

Graupel - inferred calibration at 100 m s^{-1} impact velocity.

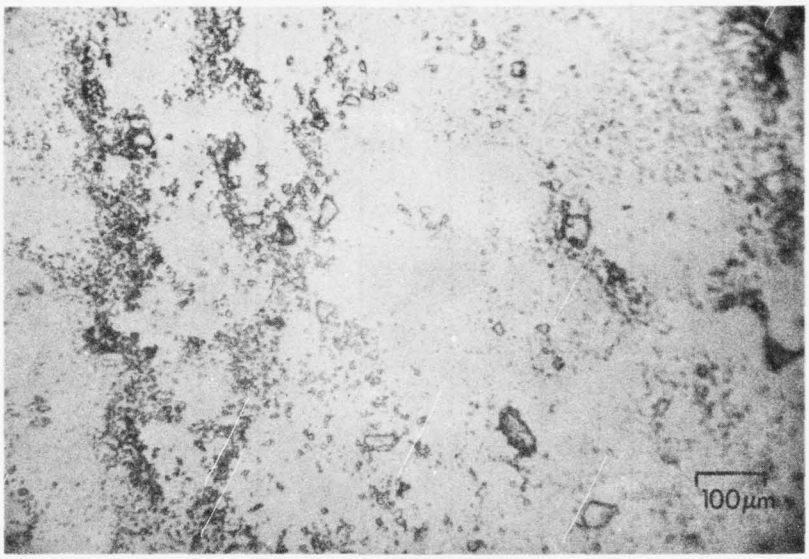

Figure 31. Fragments of ice crystals and cloud drops "rafting" by motion in a thick formvar film after collection.

IX. REPLICATOR SAMPLING STATISTICS

The concentration of particles collected on the film depend on the true air speed of the aircraft, the slot width and the speed of the film, as described on page 8. It is convenient to tabulate the volume sampled per frame and the linear flight path sampled per frame for typical flight conditions - Table II, page 72.

1	2	3	4	5	6	7	8
Film Speed #		in. per sec.	mm per sec.	frames per sec. (40 frames = 12")	Vol. per frame as projected* cm^3	Vol. cm^3 mm^{-2}	flight distance per frame (meters)
Low Speed	High Speed						
1		1.5	38	5	183	4.36	20
2	1	3	76	10	92	2.19	10
3		4.5	114	15	61	1.45	6.7
4	2	6	152	20	46	1.10	5
5		7.5	190	25	37	0.85	4
6	3	9	229	30	31	0.74	3.3
7		10.5	267	35	26	0.62	2.9
8	4	12	305	40	23	0.55	2.5
	5	15	381	50	18	0.43	2.0
	6	18	457	60	15	0.36	1.7
	7	21	533	70	13	0.31	1.4
	8	24	610	80	11.5	0.27	1.25

TABLE II. Approximate sample volume and flight path per 16 mm film frame under typical conditions.

Slot height: 6 mm
Slot width: 1.65 mm
} Area 0.1 cm^2

True air speed: 100 m s^{-1}

Volume swept out by slot 1000 cm^3 s^{-1} - 1 liter s^{-1}

For unit collection efficiency, the particles from 1 liter of air are spread out on the length of film of col. 4 and 6 mm wide.

* The actual frame width is 7.65 mm; approximately 0.65 mm is masked to give a projected area of 7 x 6, 42 mm^2.

As illustrated in Figure 1, larger atmospheric particles have in general lower concentrations. A sample of precipitating cloud may give 500 cm^{-3} cloud drops and perhaps ten mm raindrops or snow crystals per liter. Particles contained in 10 to 100 cm^3 of air will be spread over one frame (Table II, page 72, column 6) which might contain $\sim$ 5000 to 50,000 cloud drops and one mm particle on average per frame. For the large number of cloud drops (or classes of cloud drop size for a spectrum) the large number (N) of drops gives a standard deviation of $\pm \sqrt{N}$. To obtain a meaningful spectrum of drops, of 10 class intervals, it is practical to count from one frame sufficient drops to give 1000 per interval with a standard deviation of $\frac{\sqrt{1000}}{1000} \sim 3\%$. This will give a mean of particles over 2 to 20 meters of flight path depending on film speed, and is essentially the lower limit of spatial resolution of the instrument. For larger particles, with lower concentration, we must assume that particles are collected on each frame according to Poisson statistics,

$$P_n(a) = \frac{e^{-a}\, a^n}{n}$$

where a = average number of particles per frame, $P_n(a)$ is the probability of finding n particles (Table III). With one particle average per frame the most probable distribution, in 100 frames, would be: 37 empty, 37 will contain one particle, 18 two, 6 three, and 2 frames four. To obtain an estimate of number concentrations to the same level of significance as cloud drops, would require an average over a flight path of several kilometers. Conclusions regarding the homogeneity (or lack of it) of an area of precipitation must therefore take account of the statistics of collection.

Areal Coverage

For large concentrations of particles, interpretation problems may arise when two particles overlap. If two cloud drops impact almost simultaneously and coalesce in the solution, there is no possibility of detection of this process. It is necessary to limit the replica surface concentration such that

TABLE III. Probability of finding n particles with average number of particles, a, per frame.

a / n	1	2	3	4	5	average number of particles per frame
0	.37	.135	.05	.018	.007	
1	.37	.27	.15	.073	.030	
2	.18	.27	.22	.140	.080	
3	.06	.18	.22	.195	.140	
4	.02	.135	.168	.195	.176	
5		.016	.101	.156	.176	
6			.015	.104	.146	
7				.060	.104	
8					.065	

this probability is low. The overlapping of two ice particles is more easily detected, but the likelihood of this occurring with the lower concentration is much less. Langmuir (1961)[20] estimated that the areal coverage for the collection of cloud drops should be less than 3%. For drops diameter 25 μm, this is about 3000 per frame; drop numbers in excess of this will give a significant likelihood of coalescence in the solution and with an apparent increase of the number of larger drops.

X. ICE PARTICLE REPLICA INTERPRETATION

The concentration and size of atmospheric ice particles varies over an even wider range than that of water drops (Figure 1). At temperatures between about -40 and 0°C ice particle concentration is often less than cloud drop concentration by as much as 10^6; these particles grow quickly from the vapor in a supersaturation prescribed by the presence of cloud drops with linear growth velocity $\sim$ 0.1 to 1 μm s^{-1} to reach sizes one or two orders of magnitude larger than cloud drops, in periods 100 to 1000 seconds. At temperatures below -40°C, the liquid phase only exists as drops of supersaturated solution and all cloud water drops freeze. The supersaturation is now prescribed only by the cooling rate - from ascent rate or radiation - and the particles grow slowly and are mutually competitive. Ice particle size and concentration nucleated at these low temperatures is therefore comparable with cloud drops at temperatures above about -40°C. This situation is to be contrasted with ice nucleated by heterogeneous nucleation at temperatures above -40°C at sub-water saturation - concentration of these particles may be as low as the measurement limit - $\lesssim$ 0.1 per liter.

Replicas of mixed phase clouds usually contain a high (several hundred per cm^2) concentration of small (10 to 20 μm) cloud drops together with a low (few per liter) concentration of large (mm) ice particles. A further complication occurs

---

[20] Langmuir, I., 1961: Mathematical Investigation of Water Droplet Trajectories. Collected Works, 11, 335-393.

under conditions of ice crystal multiplication through the Hallett/Mossop process (1974)[21]. Here three classes of particles are present - high concentration of cloud drops, low concentration of graupel, and secondary ice particles which grow quickly under the ambient supersaturation and show distinct faceted structure. Visual examination of replica via a stop motion projector is ideal for rapid assessment of the presence of these particle classes.

Ice particles in the atmosphere can be characterized to give information on their gross physical property characteristics - size, density, mass, fall speed and also to give information on their origin and growth history - habit, degree of riming, single or polycrystalline. The classification of Magono and Lee is a convenient starting point. From the viewpoint of analysis of replica to yield this kind of information, several factors need to be considered (Figure 32).

(a) Ice particle sizes which are comparable with cloud drops give replicas in a similar way. A crystal submerged in solution (and maintained below 0°C) will gradually emerge as the solution thins to leave a cast with a thick surround and thin (0.01 μm) upper skin. This subsequently collapses as the ice evaporates and gives colored interference patterns at the base of the crater, as in the case of drops.

(b) Ice particles whose size is less than the dried formvar (thin plates) a hollow cast will remain - it will probably show thin film interference colors.

(c) A particle large compared with the initial solution depth will protrude and become rapidly covered by a thin solution layer. The solution dries and shrinks to leave a cast of the base; the fragile, thin film is lost.

---

[21] Hallett, J., and S.C. Mossop, 1974: Ice Crystal Concentration in Cumulus Clouds. Influence of the Drop Spectrum. Science, 186, 632-634.

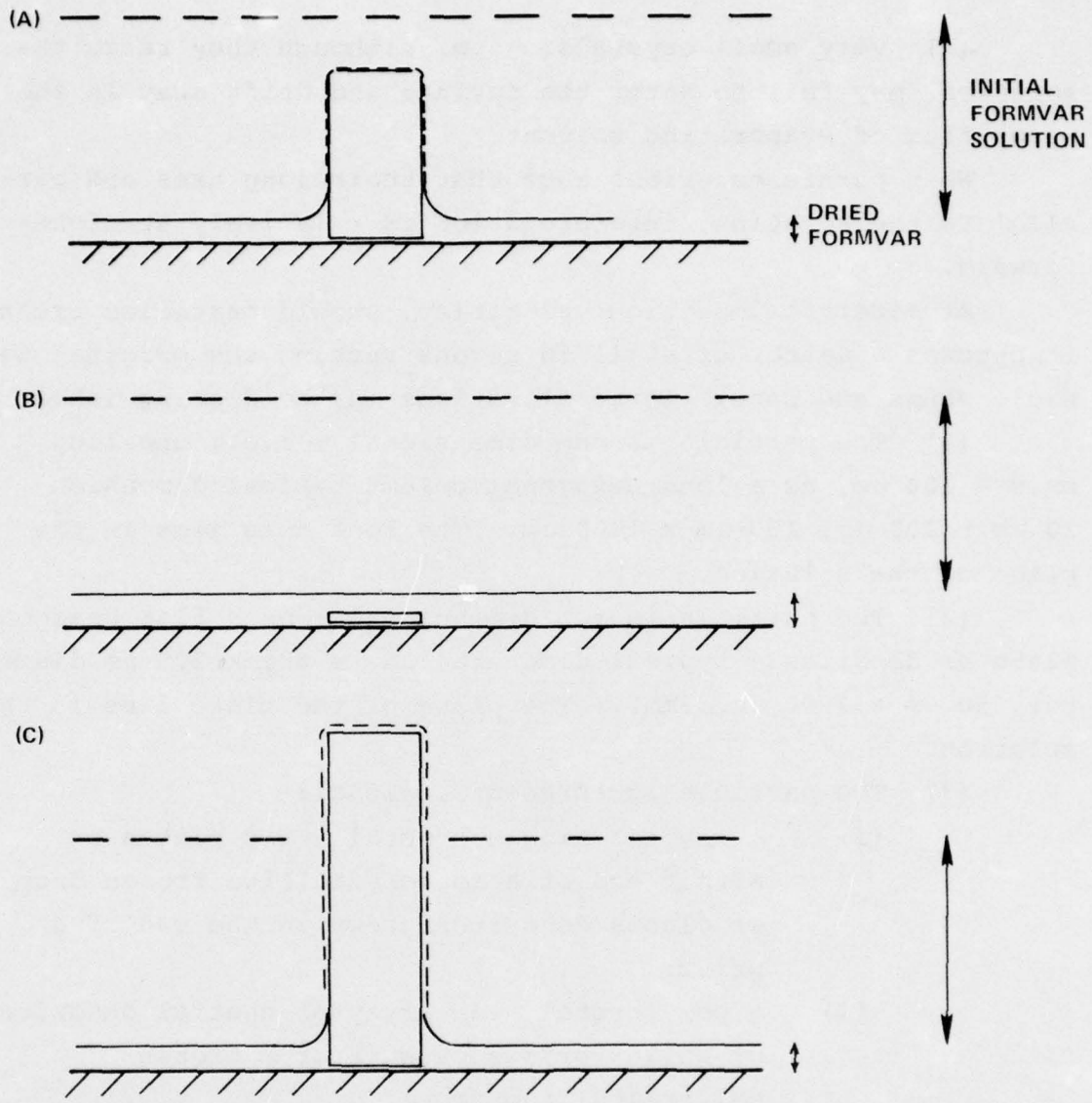

Figure 32. Replication of particles of different sizes.

(a) a particle almost immersed in the solution film retains a thin layer as drying occurs and the film shrinks; this subsequently collapses as the ice evaporates.

(b) a particle thinner than the dried film thickness leaves a cast which may partly collapse.

(c) a large particle is initially covered with a thin spreading film which collapses. In cases (a) and (c) a thicker layer of formvar occurs around the crystal base. The height of the top of this layer (measured by interferometry or depth of focus) will give the minimum crystal thickness.

(d) very small crystals, ~ μm, although they reach the solution, may fail to enter the surface and drift away in the vapor flux of evaporating solvent.

When particles orient such that their long axes are parallel to the solution, interpretation is relatively straightforward.

At aircraft impaction velocities, should particles break, it becomes a matter of skill in reconstructing the original particle shape and size. Three situations may be distinguished:

(1) The particle is one dimensional - i.e., one long axis > 100 μm, as a long hexagonal column typical dimension 20 μm x 200 μm; 100 μm x 1000 μm. The long axis lies in the plane of the solution.

(2) The particle is two-dimensional - as a flat hexagonal plate or dendrite - typical dimension 20 μm thick 200 μm diameter, 50 μm > 2000 μm (2mm). The plane of the plate lies in the solution.

(3) The particle is three-dimensional:

(i) a spatial single crystal - two plates on eitner end of a monocrystalline frozen drop or plates dendrites grown on the end of a prism;

(ii) a polycrystal - an array of spatial dendrites or hollow prisms grown from a frozen polycrystalline drop;

(iii) conical or spherical graupel;

(iv) frozen drizzle or raindrop.

Should the particle be replicated without fracture, the size and structure of one dimension columns can be readily obtained since these visually possess a six-fold symmetry axis in the long direction. The major dimension of a two-dimensional plate or dendrite is also readily obtained, although the thickness may be more difficult, unless the plate is thin and is completely encapsulated. Otherwise minimum thickness can be estimated by interference microscopy of replica edge as already described, or an

estimate based on direct field measurements (Ono, 1969;[22] Auer and Veale, 1970)[23] of comparable shaped crystals.

High density particles such as frozen drizzle drops do not shatter and leave an irregular circular replica which must be distinguished from spurious large air bubbles. Similarly, small ($\lesssim$ 500 μm) low density graupel particles may not shatter and their dimension can be determined directly; small conical graupel and hexagonal graupel formed on a plate can also be recognized.

Broken one or two dimensional crystals can usually be reconstructed. Broken three dimensional crystals and particles require interpretation; the following guidelines are suggested:

(a) Spatial dendrites, plates or prisms, and spatial single crystals often collapse as a two dimensional projection of their array on impact (Figure 23a,b).

(b) Low density ($\lesssim$ 0.4) graupel particles, diameter $>$ 500 μm, spread into a circular pattern on impact as does a large drop. As opposed to a large drop, there is no tendency for the particles to recombine by surface tension (p.60). The replica consists of a central clear spot, surrounded by broken graupel material in the form of a crater. (This effect can be readily observed on a car windshield when driving in graupel). (Figure 22). An estimate from the volume of replicated debris indicates an original particle size which is comparable with, or somewhat greater than, the central clear area. The relationship between original and debris diameter is approximately between 0.2 and 0.5; it appears to be influenced by both impact velocity and the graupel density. Spreading is somewhat less than occurs for drop impaction (page 66).

---

[22] Ono, A., 1969: The Shape and Riming Properties of Ice Crystals in Natural Clouds. J. Atmos. Sci., 26, 138-147.

[23] Auer, A.H., and D.L. Veale, 1970: The Dimension of Ice Crystals in Natural Clouds. J. Atmos. Sci., 27, 919-926.

Some calibration through simultaneous measurement with an optical array would be highly desirable. Results are summarized, together with drop deformation data, in Figure 30 .

Density of Particles

The mean density of particles can sometimes be estimated directly from the geometry - as a dendrite or hollow column; this enables a direct estimate to be made of particle mass. Alternatively measured values of density for different habit of crystals may be used - for example, Ono (1969-1970)[24]; Auer & Veal (1970)[25] and Ryan (1974)[26].

For graupel, a qualitative estimate of density can be made from the shape and packing of the drops of unshattered fragments and the presence (or absence) of vapor grown crystal faces, linear arrays of frozen drops, and the departure of each drop from spherical shape, after Macklin (1961)[27] and Zikmunda & Vali (1972)[28].

The following scheme (Chapter XI) enables mass to be determined graphically subject to this estimate of crystal density, and in addition, for a [2] particle, an estimate of crystal thickness. This can be obtained from measurements of Ono, Auer & Veal (1970) and Hobbs, Chang & Locatelli, (1974)[29] for plates and dendrites with thickness variation from 30 μm (100 μm diameter) to 75 μm (1000 μm diameter).

---

[24] Ono, A., 1970: Growth Mode of Ice Crystals in Natural Clouds. J. Atmos. Sci., 27, 649-658.

[25] Auer, A.H., and D.L. Veal, 1970: The Dimension of Ice Crystals in Natural Clouds. J. Atmos. Sci., 27, 919-926.

[26] Ryan, B.F., et al., 1974: The Densities and Growth Rates of Ice Crystals between -5°C and -9°C. J.Atmos.Sci.,31,2136-2141.

[27] Macklin, W.C., 1961: The Density and Structure of Ice Formed by Accretion. Q.J. Roy. Met. Soc., 88, 30-50.

[28] Zikmunda, J., and G. Vali, 1972: Fall Patterns and Fall Velocities of Rimed Ice Crystals. J. Atmos. Sci., 29, 1334-1347.

[29] Hobbs, P.V., S. Chang, and J.D. Locatelli, 1974: J. Geophys. Res., 79, 2199-2206.

XI. ESTIMATE OF MASS FROM CRYSTAL REPLICA

The method depends on an interpretation of crystal habit, and whether it is either essentially

(a) one dimensional crystal column or needle [1], or

(b) a plate sector or dendrite, two dimensional crystal [2], or

(c) a spatial dendrite, plate sector, or rosette; a graupel particle, three dimensional array [3].

Density is given in g cm^{-3}, Mg m^{-3}.

Replicator Analysis - Mass-Size Relationship

Estimate

(a) Columns, Needles [1] or

(b) Plates, Dendrites [2] or

(c) Hail, Graupel, Spatial arrays of columns, Plates, Dendrites [3].

Case a: [1] non-rimed | measure { length / width } from replica

if solid, density = 0.9

if hollow,

warm region, density = 0.8

cold region, density = 0.6

if diameter 75 μm - use curves

[1] for mass (Figure 33, page 85)

if diameter other - use overlay (1) Figure 34

Align axes with x - y and transpose to measured diameter on [3] curves (sphere, Figure 33)

rimed

lightly - same as non-rimed.

{ medium / heavy } As above, use density 0.4.

Case b: [2] If possible estimate thickness - for example from an end - on plate, otherwise

Measure diameter from replica and assume thickness.

to 100 μm diameter - assume 30 μm thickness.

100 to 1000 μm diameter - assume 75 μm thickness.

non-rimed

Use [2] curves from Figure 33 with densities:

0.4 dendrites

0.5 sectors

0.6 plates

Align x - y axes of overlay (Figure 34) and transpose to appropriate thickness on [3] curves (sphere, Figure 33).

rimed - lightly same as non-rimed

medium density 0.2 } If no thickness estimate, align [2] curves on overlay transposed to 200 μm thickness.

heavy 0.3 → 0.4 }

AD-A033 067 NEVADA UNIV RENO LAB OF ATMOSPHERIC PHYSICS F/G 4/2
MEASUREMENT OF SIZE, CONCENTRATION AND STRUCTURE OF ATMOSPHERIC--ETC(U)
JUL 76 J HALLETT F19628-72-C-0280
UNCLASSIFIED AFGL-TR-76-0149 NL

2 OF 2
AD
A033067

END
DATE
FILMED
1-77

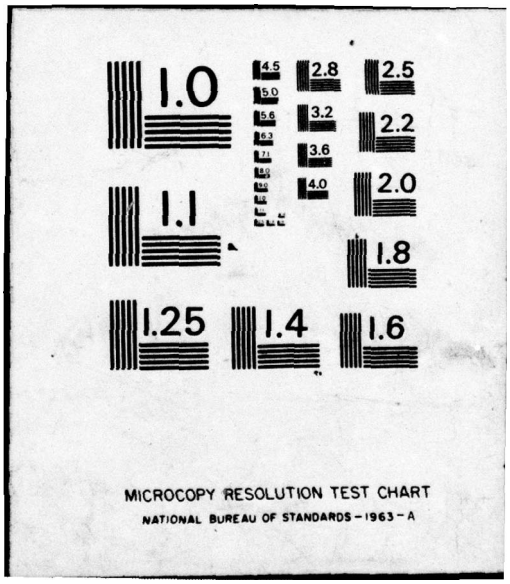
1.0
1.1
1.25
1.4
1.6
1.8
2.0
2.2
2.5
2.8
3.2
3.6
4.0
4.5
5.0
5.6
6.3
7.1
8.0
9.0
MICROCOPY RESOLUTION TEST CHART
NATIONAL BUREAU OF STANDARDS-1963-A

Case c: [3] Measure diameter d.

Use [3] curves on graph, Figure 33.

Density: non-rimed

Rosettes	Dendrites	Plates
.2 → .3	.3 → .4	.4 → .5

Medium rimed	Heavy rimed
.3 - .4	.4 - .5

Note

(i) If crater present use higher density.

(ii) If aggregates present measure individually for mass.

(iii) It may be desirable to make a plot of crystal number versus frame, where each frame is represented by 1/10" square on graph paper; crystals can be represented by appropriate symbols in each square. Note if melting is taking place; estimate mass from $\Sigma N \frac{\pi d^3}{6}$ with d corrected for splash dispersal.

(iv) For completely shattered ice crystal, measure area of parts and assume thickness = 75 μm.

(v) Interpolate densities where appropriate.

(vi) Particle form can be estimated by use of overlay (2), Figure 35.

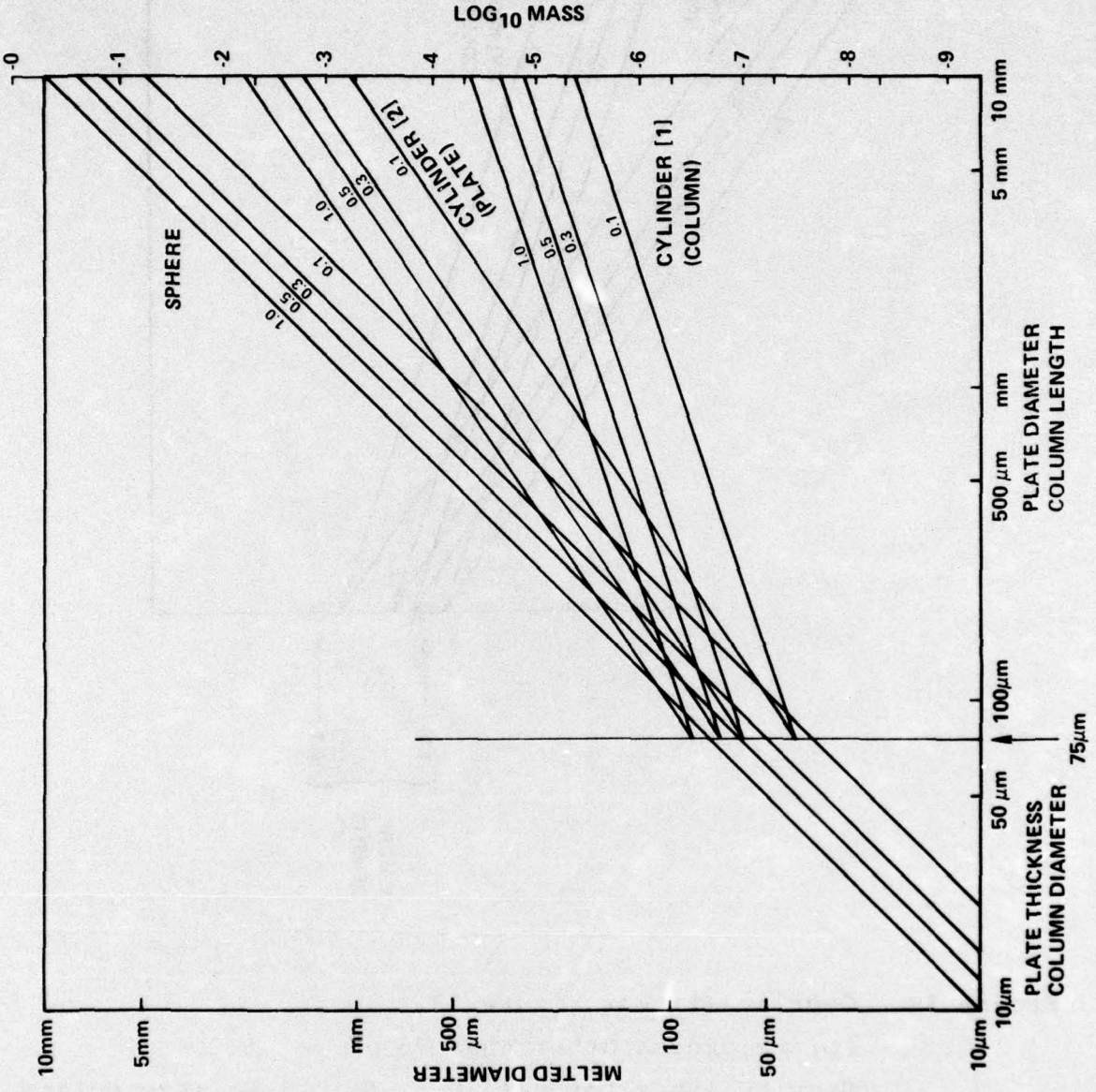

Figure 33. Mass-diameter relation for atmospheric ice particles. Ordinate is diameter for plate or dendrite or any three [3] dimensional array; length for a column or needle. Each set of lines is to be used for [1], [2] or [3] dimensions, with appropriate density, g cm^{-3} (Mg m^{-3}).

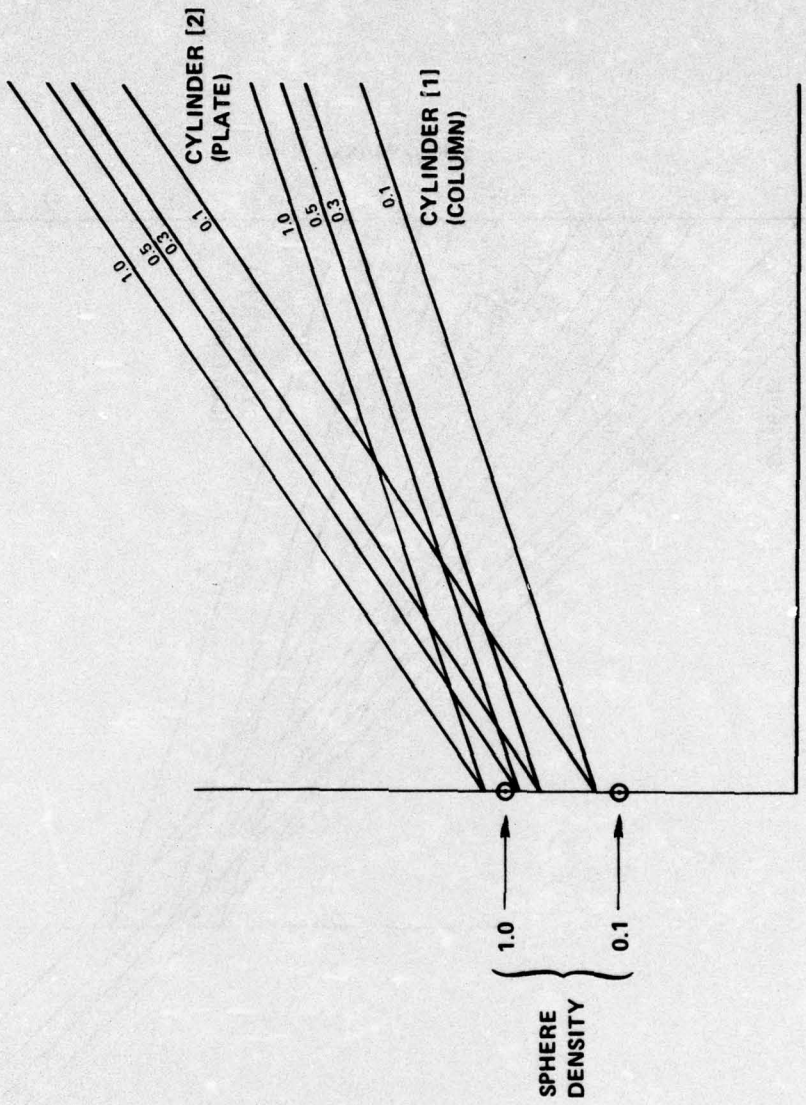

Figure 34. Overlay (1) For Figure 33.
For thickness other than 75 μm.
Density lines for 0.1, 0.3, 0.5, 1.0; interpolate for other densities.

(i) Align axes parallel to x - y on Figure 33 and transpose to appropriate measured or estimated thickness.

(ii) Estimate density.

(iii) Read mass on right hand axis of Figure 33.

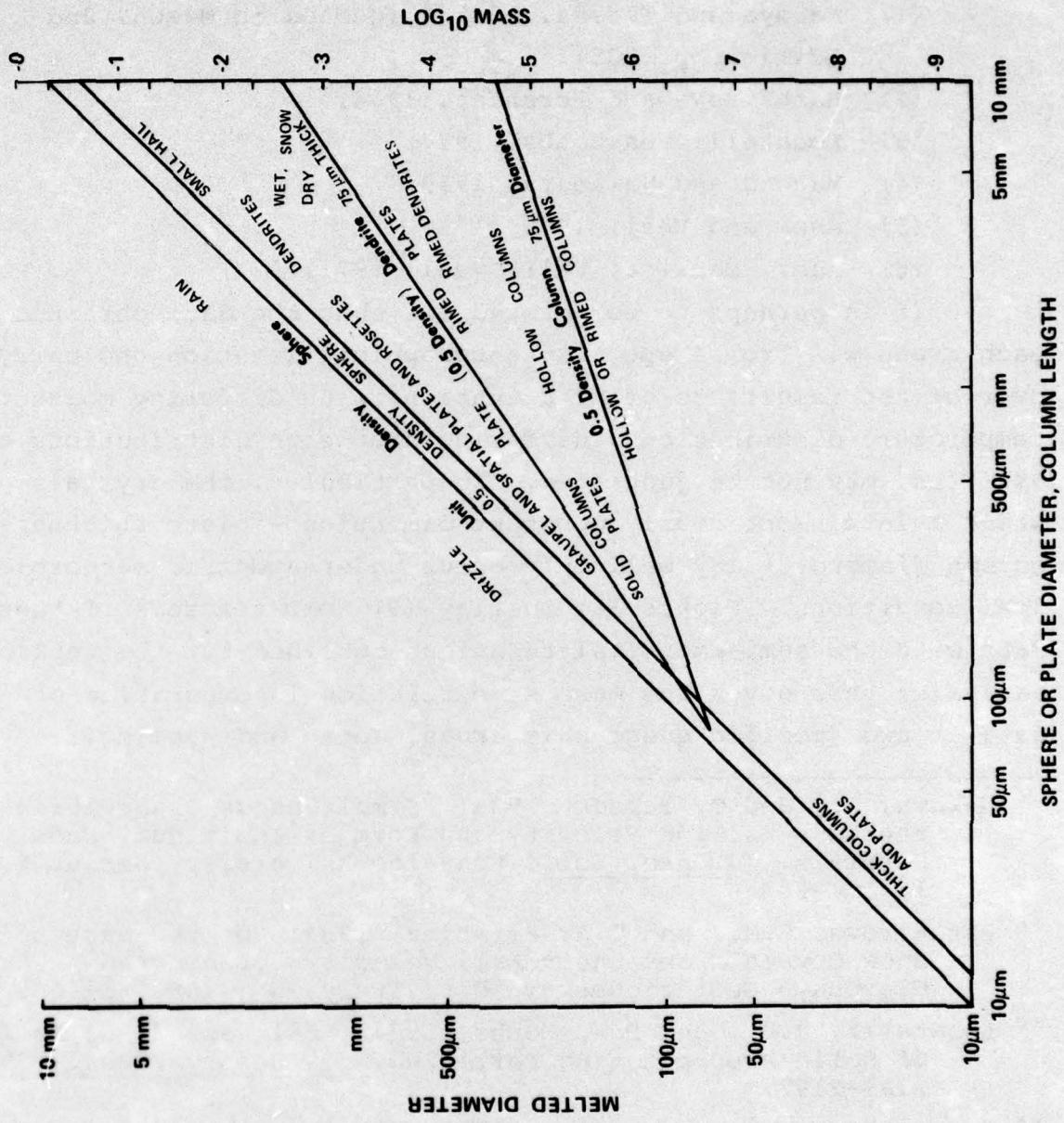

Figure 35. Overlay (2) For Figure 33.
Precipitation particle form related to particle dimension and mass.

An alternative approach to estimate of particle mass is to estimate the closest description of the particle and use the field measurements of other workers.

(1) Nakaya and Tereda, 1935[30] (quoted in Mason, 2nd Edition, p. 238).

(2) Bashkirova and Pershina, 1964.[31]

(3) Locatelli and Hobbs, 1974.[32]

(4) Magono and Nakamura, 1959.[33]

(5) Auer and Veal, 1970.[34]

(6) Auer, Marwitz, Vali, Veal, 1971.[35]

It is perhaps to be pointed out that the data obtained by each group was from a specific geographical location and carry-over of the results to other situations with differing moisture-temperature distributions, differing drop size distributions and updrafts, may not be justified. In particular, the crystals which maintain one nearly constant dimension - plate thickness or column diameter - may well only occur under specific meteorological conditions. Figure 36, overlay (3) compares some of these data with the semi-empirical technique outlined for the replica analysis; this gives the mass size relation incorporating data of two specific geographic areas, Japan and Wyoming.

---

[30] Nakaya, U., and T. Tereda, 1935: Simultaneous Observation of the Mass Falling Velocity and Form of Individual Snow Crystals. J. Fac. Sci., Hokkaido University, Series 2, 1, 191-201

[31] Bashkirova, G.M., and T.A. Pershina, 1964: On the Mass of Snow Crystals and their Fall Velocity. Leningrad Glavonaya Geofizicheskaya Obs. Trudy, No. 156, 83-100.

[32] Locatelli, J.D., and P.V. Hobbs, 1974: Fall Speed and Masses of Solid Precipitating Particles. J. Geophys. Res., 79, 2185-2197.

[33] Magono, C., and T. Nakamura, 1959: On the Behavior of Water Droplets During Collision with a Large Water Drop. J. Meteoro. Soc. of Japan, 37, 124-217.

[34] Auer, A.H., and D.L. Veal, 1970: The Dimension of Ice Crystals in Natural Clouds. J. Atmos. Sci., 27, 919-926.

[35] Auer, A.H., J.D. Marwitz, G. Vali and D.L. Veal, 1971: Final Report to NSF, Grant GA 1527, GA 19105, Department of Atmospheric Resources, Laramie, Wyoming.

Figure 36. Mass-size relation from Wyoming and Japan data (R.C. Cunningham, AFGL, private communication). Overlay (3).

REFERENCES

Auer, A.H., J.D. Marwitz, G. Vali and D.L. Veal, 1971: Final Report to NSF, Grant GA 1527, GA 19105, Department of Atmospheric Resources, Laramie, Wyoming.

Auer, A.H., and D.L. Veal, 1970: The Dimension of Ice Crystals in Natural Clouds. J. Atmos. Sci., 27, 919-926.

Bari, S., and J. Hallett, 1973: Nucleation of Air Bubbles at a Growing Ice-Water Interface. J. Glaciology, 13, 489-520.

Bashkirova, G.M., and T.A. Pershina, 1964: On the Mass of Snow Crystals and their Fall Velocity. Leningrad Glavonaya Geofizicheskaya Obs. Trudy, No. 156, 83-100.

Bentley, W.A., and W.J. Humphries, 1931. Snow Crystals. McGraw-Hill.

Davies, J.T., and E.K. Rideal, 1961: Interface Science, p. 22. Academic Press, New York.

Hallett, J., 1976: AFGL Report, Part I. Operating Manual, Part II, Service Manual.

Hallett, J., and S.C. Mossop, 1974: The Production of Secondary Ice Particles During the Riming Process, Nature, 249, 26-28.

Hallett, J., and S.C. Mossop, 1974: Ice Crystal Concentration in Cumulus Clouds: Influence of the Drop Spectrum. Science, 186, 632-634.

Heymsfield, A.T., and R.G. Knollenberg, 1972: Properties of Cirrus Generating Cells. J. Atmos. Sci., 29, 1358-1366.

Hindman, E.E., 1964: Continuous Sampler for Settling Particles. J. Rech. Atmos., 1, 29-35.

Hindman, E.E., and R.L. Rinker, 1967: Continuous Snowfall Replicator. J. Appl. Meteor., 6, 126-133.

Hobbs, P.V., S. Chang, and J.D. Locatelli, 1974: J. Geophys. Res., 79, 2199-2206.

Kajikawa, M., 1972: Measurement of Falling Velocity of Individual Snow Crystals, Journal Meteoro. Soc. of Japan, 50, 577-583, Series II.

Langmuir, I., 1961: Mathematical Investigation of Water Droplet Trajectories. Collected Works, 11, 335-393.

Locatelli, J.D., and P.V. Hobbs, 1974: Fall Speed and Masses of Solid Precipitating Particles. J. Geophys. Res., 79, 2185-2197.

MacCready, P.V., and C.J. Todd, 1964: Continuous Particle Sampler, J. Appl. Meteor., 3, 450-460.

Macklin, W.C., 1962: The Density and Structure of Ice Formed by Accretion. Q.J. Roy. Met. Soc., 88, 30-50.

Magono, C., and T. Nakamura, 1959: On the Behavior of Water Droplets During Collision with a Large Water Drop. J. Meteoro. Soc. of Japan, 37, 124-127.

May, K.R., 1950: The Measurement of Airborne Droplets by the Magnesium Oxide Method. J. Sci. Instru., 27, 128-132.

Nakaya, U., 1954: Snow Crystals, Natural and Artificial. Harvard University Press, Cambridge.

Nakaya, U., and T. Terada, 1935: Simultaneous Observation of the Mass Falling Velocity and Form of Individual Snow Crystals. J. Fac. Sci., Hokkaido University, Series 2, 1, 191-201.

Nielsen, K.W., 1969: An Experimental Inquiry into the Flow Around Two Continuous Particle Replicator Heads. Desert Research Institute, University of Nevada, Reno, Technical Report, No. 4, Physical Sciences.

Norment, H.G., 1974: Effects of Airplane Flow Fields on Hydrometeor Concentration Measurements. AFCRL-TR-74-0602.

Norment, H.G., 1975: Effects of Airplane Flow Fields on Cloud Water Content Measurements. AFCRL-TR-75-0231.

Ono, A., 1969: The Shape and Riming Properties of Ice Crystals in Natural Clouds. J. Atmos. Sci., 26, 138-147.

Ono, A., 1970: Growth Mode of Ice Crystals in Natural Clouds. J. Atmos. Sci., 27, 649-658.

Ryan, B.F., E.R. Wishart, and E.W. Holroyd, 1974: The Densities and Growth Rates of Ice Crystal Between -5°C and -9°C. J. Atmos. Sci., 31, 2136-2141.

Schaefer, V.J., 1941: A Method for Making Snowflake Replicas. Science, 93, 239-240.

Schaefer, V.J., 1946: The Production of Ice Crystals in a Cloud of Supercooled Water Droplets. Science, 104, 457.

Schaefer, V.J., 1962: The Vapor Method for Making Replicas of Liquid and Solid Aerosols. J. Appl. Met., 1, 413-418.

Speyers-Duran, P.A., and R.R. Braham, 1967: An Airborne Continuous Cloud Particle Replicator. J. Appl. Met., 6, 1108-1113.

Weickmann, H., 1944: The Ice Phase in the Atmosphere. Translation Volkenrade, 716, 95 pp, Ministry of Supply, London.

Zikmunda, J., and G. Vali, 1972: Fall Patterns and Fall Velocities of Rimed Ice Crystals. J. Atmos. Sci., 29, 1334-1347.